

# RICH performance in 2011/12

Malte Wilfert\*, Johannes Giarra†

COMPASS note 2017-6

## Contents

<b>1</b>	<b>Introduction</b>	<b>1</b>
1.1	Data selection . . . . .	1
1.1.1	$K^0$ and $\Lambda$ selection . . . . .	2
1.1.2	$\phi$ selection . . . . .	4
<b>2</b>	<b>RICH Particle Identification</b>	<b>5</b>
<b>3</b>	<b>Method</b>	<b>7</b>
<b>4</b>	<b>Calculation of the efficiencies and uncertainties</b>	<b>9</b>
<b>5</b>	<b>Results</b>	<b>10</b>
<b>6</b>	<b>Problems at high <math>z</math></b>	<b>23</b>
<b>7</b>	<b>PID using <math>\rho^0</math></b>	<b>24</b>
7.1	Data selection . . . . .	24
7.2	Results . . . . .	26
<b>8</b>	<b>Performance of the RICH detector in 2012</b>	<b>32</b>
8.1	Comparison of the efficiencies of 2011 to 2012 . . . . .	32
8.2	Conclusion . . . . .	36
	<b>Bibliography</b>	<b>37</b>
	<b>A Tables for the RICH efficiency in 2011 using the strict LH cuts</b>	
	<b>B Tables for the RICH efficiency in 2011 using the 2007 LH cuts</b>	
	<b>C Comparison of RICH efficiencies in 2011 and 2012</b>	

---

\*Institut für Kernphysik, Johannes-Gutenberg Universität Mainz

†Institut für Kernphysik, Johannes-Gutenberg Universität Mainz

# 1 Introduction

In this note the method and results of the evaluation of the RICH performance in 2011 and 2012 are presented. The identification and misidentification probabilities of kaons, pions and protons are evaluated as a function of the entrance angle  $\theta$  of the RICH and the particle momentum. The same method was already used in the determination of the RICH efficiency for the 2006 data described in Ref. [1]. A description on the calculation of the likelihood values for the different particles is explained in Ref. [2].

In previous analysis on the RICH particle identification efficiency, "exclusive"  $\phi$  mesons were used. These are  $\phi$  meson produced in an exclusive reaction. Therefore, only three particles are detected in the spectrometer. These are the scattered muon and the two kaons from the decay of the  $\phi$  meson. Such events do not represent typical events at COMPASS from deep inelastic scattering where also more than three particles are detected. Therefore, so called "inclusive"  $\phi$  mesons are used for the analysis. These are  $\phi$  mesons produced in deep inelastic scattering. Such events contain not only the scattered muon and the decay kaons from the  $\phi$  meson but might also contain additional particles.

At high  $z$ , problems were found in the separation between kaons and pions using likelihood values (see talks at the AM [3, 4]). This problem is not correctly taken into account using  $K^0$  mesons. Therefore, a first test on using  $\rho^0$  mesons instead is performed in order to determine the correct values for the identification and misidentification probabilities in this kinematic region.

## 1.1 Data selection

For the determination of the RICH efficiency, it is necessary to have a source of events where the true kind of the particle passing the RICH is known. That kind of events is obtained using two body particle decays, namely the decay of a  $K^0$  into two pions ( $K^0 \rightarrow \pi^+\pi^-$ ), the  $\phi$  decay into two kaons ( $\phi \rightarrow K^+K^-$ ), the  $\Lambda$  decay into a pion and a proton ( $\Lambda \rightarrow p\pi^-$ ). In order to select such events with such decays, deep inelastic scattering events with a scattered muon are selected. Therefore, the typical cuts are applied to the data:

1. Exclude bad spills
2. Select best primary vertex with incoming and scattered muon <sup>1</sup>
3. Check if primary vertex is inside one of the target cells (PaAlgo::InTarget)
4. Extrapolated track of the incoming muon should cross all target cells (PaAlgo::CrossCells)
5.  $0.1 \leq y \leq 0.9$

Different selection criteria have to be used for  $K^0$ ,  $\Lambda$  and  $\phi$  decays. In the case of  $K^0$  mesons and  $\Lambda$  baryons, the particles decay by the weak force. Therefore, the decay length is long enough to produce a secondary vertex, which can be separated from the primary one. The  $\phi$  mesons decays by the strong force. This results in a very short decay length and it is not possible to separate the secondary vertex from the primary one.

---

<sup>1</sup>Phast.7.136

### 1.1.1 $K^0$ and $\Lambda$ selection

For  $K^0$  mesons the decay into  $\pi^+$  and  $\pi^-$  with a branching ration of  $(69.20 \pm 0.05)\%$  [5] and in the case of  $\Lambda$  and  $\bar{\Lambda}$  baryons the decay into a proton and a pion with an branching ratio of  $(63.9 \pm 0.5)\%$  [5] is used. In both decays the reconstruction of the secondary vertex is possible. The following cuts are applied to select these decays:

1. Selection of good secondary vertex

- Loop over all vertices
- Vertex is not a primary one
- Exactly two oppositely charged outgoing particles
- The tracks should not be connected to any other primary vertex
- Primary and secondary vertex separated by more than  $2\sigma$

2. Select good hadron tracks

- Both particles should not have crossed more than 10 radiation length
- Last measured position ( $Z_{\text{Last}}$ ) behind SM1
- Transverse momentum with respect to the mother particle larger than 23 MeV to suppress electrons
- Check that the decaying particle is connected to the primary vertex ( $\theta \leq 0.01$ )

3. Additional cuts

- $p_h > 1 \text{ GeV}/c$
- Mass difference smaller than  $150 \text{ MeV}/c^2$  between the  $K^0/\Lambda$  mass and the invariant mass of the two decay hadrons assuming the correct masses

The same cuts except for the mass cuts are used for  $K^0$  and  $\Lambda$  candidates. For the selected candidates, the RICH likelihoods of the two decay particles are stored for further analysis. During the first selection step, good secondary vertices are selected with only two outgoing tracks. In order to ensure that the two tracks belong to this secondary vertex, the vertex is skipped if a track is assumed to originate from a primary vertex. In addition, the primary and secondary vertex should be separated from one another. Therefore, the distance between both should be larger than two times the reconstruction accuracy.

During the second selection step, good hadron tracks are selected. In order to suppress tracks from muons, tracks which have passed a large amount of material are rejected. In addition, only tracks with a measured momentum are selected. This is ensured by a last measured position behind the first spectrometer Magnet. In addition, it is ensured that the  $K^0$  meson or  $\Lambda$  baryon is produced in the primary vertex by comparing the angle  $\theta$  between their momentum vector and the vector connecting the primary and secondary vertex. Tracks from electrons are suppressed by removing particles with low transverse momenta with respect to the mother particle. This is shown in Figure 1. Here, the transverse momentum of a particle is shown as a function of the ratio of the longitudinal momentum ratio of two particles:

$$\alpha = \frac{p_{L,1} - p_{L,2}}{p_{L,1} + p_{L,2}} . \quad (1)$$

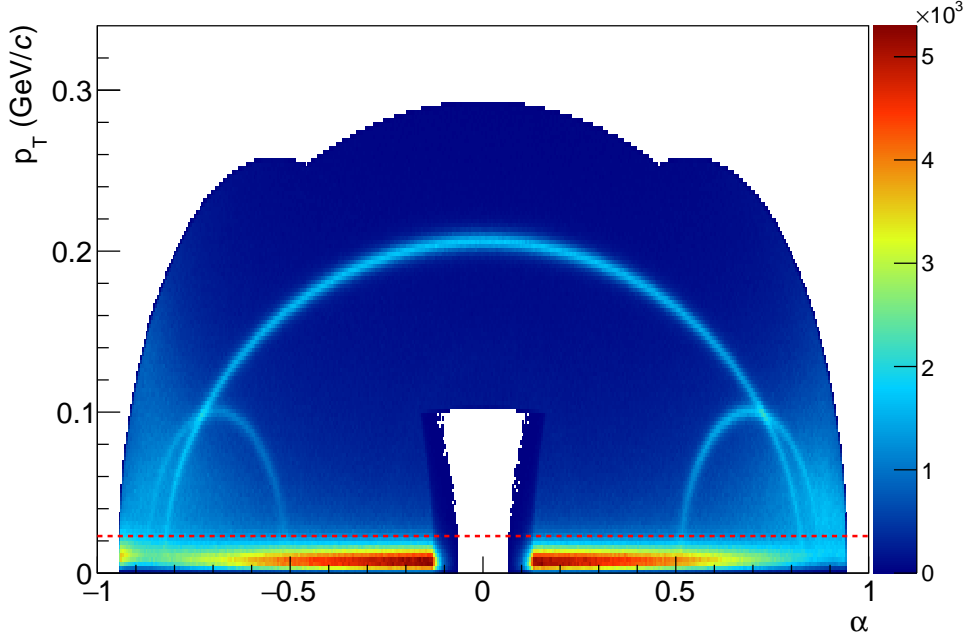


**Figure 1:** Armenteros plot showing the effect of the cut on the transverse momentum, which is illustrated by a red line.

The three visible arcs are produced by the decay of the  $K^0$  mesons and the  $\Lambda$  baryons. The decay of  $K^0$  mesons in two particles with the same mass results in the symmetric arc, whereas the decay of  $\Lambda$  baryons into two particles with different masses result in the two smaller arcs on the left and right side. The band at the bottom is produced by electrons from pair production. These are removed by the cut on the transverse momentum. This is also shown in Figure 2 for the transverse momentum of the particles from decays of  $K^0$  meson or  $\Lambda$  baryon candidates.

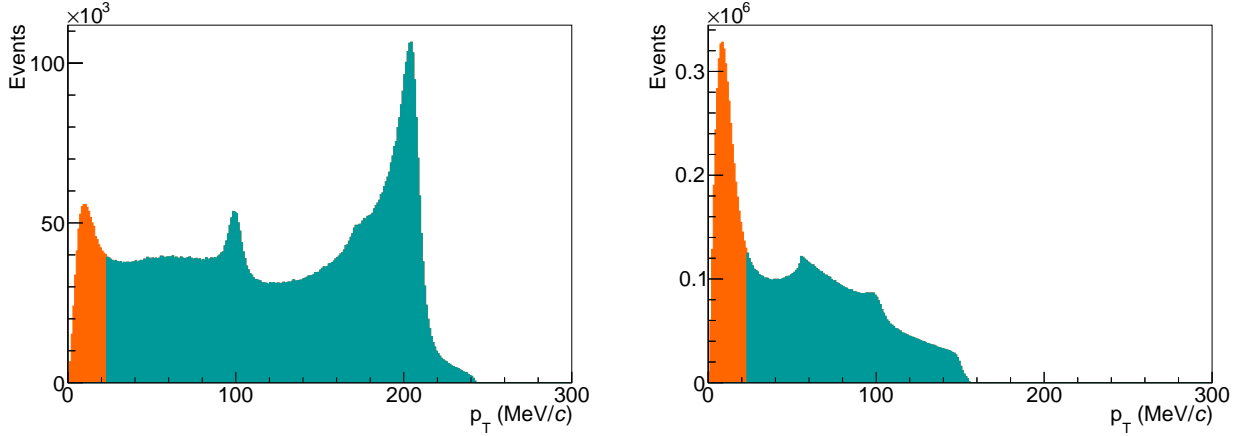


**Figure 2:** Distribution of the transverse momentum for  $K^0$  (left) and  $\Lambda$  (right) candidates. The orange area corresponds to the removed events.

During the third selection step, events, which will not be used in the later analysis, are removed. Therefore, a minimal momentum of the particle is required and only a mass range of  $150 \text{ MeV}/c^2$  around the  $K^0$  or  $\Lambda$  mass is selected.

The effect of the cuts on the invariant mass of the  $K^0$  and  $\Lambda$  candidates is shown in Figure 3

in the range of their mass. The strongest reduction is achieved by requiring the production of the  $K^0$  meson or  $\Lambda$  baryons at the primary vertex. In addition, also the effect of the Likelihood cuts for the particle identification, which are applied later one, is shown.

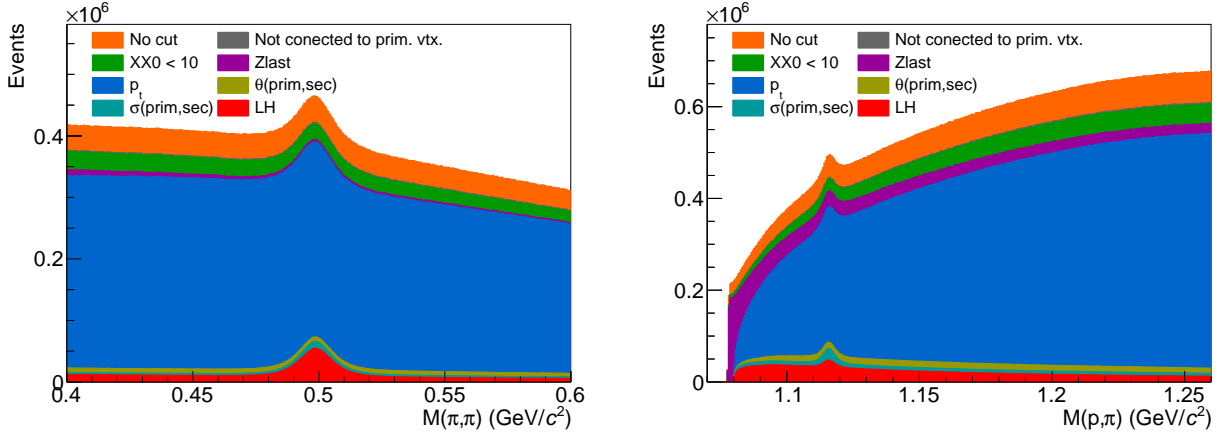


**Figure 3:** Invariant mass for  $K^0$  (left) and  $\Lambda$  (right) candidates after the application of various cuts.

### 1.1.2 $\phi$ selection

The  $\phi$  meson decay length is too short to separate the primary and decay vertex. Therefore, all outgoing particles from a primary vertex are taken into account for the search of possible  $\phi$  mesons. The branching ratio of the decay into two kaons is  $(48.9 \pm 0.5\%)$  [5].

#### 1. Select possible event with $\phi$ mesons

- At least 3 outgoing particles (includes scattered muon)
- Loop over all outgoing particles
- Oppositely charged pairs of hadrons (none is a muon)

#### 2. Select good hadron tracks

- Last measured position behind SM1
- Transverse momentum with respect to the mother particle larger than 23 MeV to suppress electrons

#### 3. Additional cuts

- $9 \text{ GeV}/c < p < 55 \text{ GeV}/c$
- Mass difference between the  $\phi$  mass and the invariant mass of the two hadrons smaller than  $120 \text{ MeV}/c^2$  assuming the kaon mass

The selection steps are similar the selection of the  $K^0/\Lambda$  candidates. In the first step, primary vertices with oppositely charged hadron pairs are selected. During the second selection step, only particles with a measured momentum are kept and possible electrons are removed by removing particles with a too low transverse momentum. During the third step additional cuts are applied to remove events, which will not be used in the later analysis. The effect of the various cuts is shown in Figure 4. The selection of  $\phi$  meson candidates results in a

large combinatorial background. During the selection the largest suppression is achieved by the removal of electrons. By also applying the Likelihood cuts to identify the kaons a large suppression can be achieved.

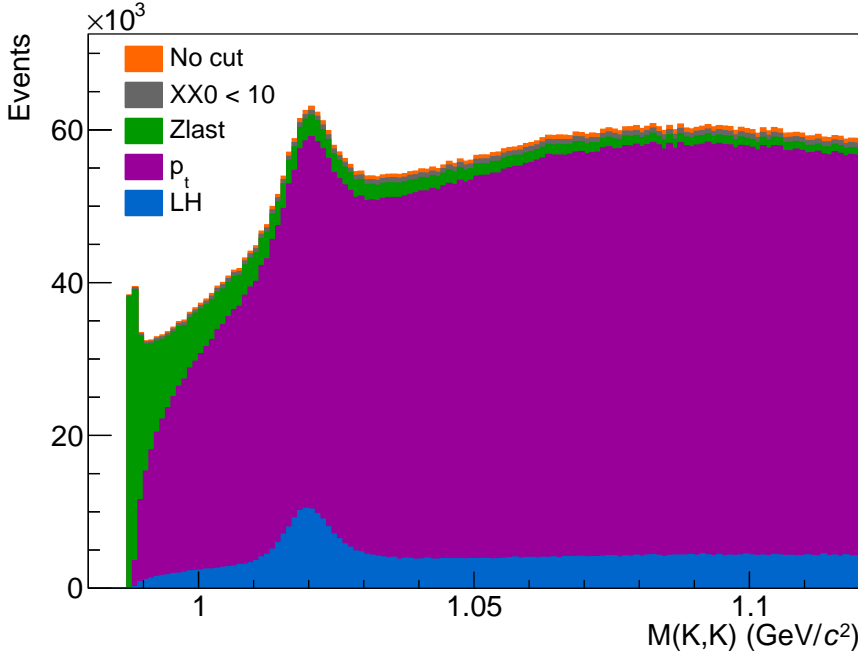


**Figure 4:** Invariant  $K^+K^-$  mass after the application of various cuts. Also the effect of the identification of one kaon is shown.

## 2 RICH Particle Identification

The goal of the selection is a clean pion and kaon sample. Due to the larger amount of pions compared to kaons stricter selection cuts are imposed for kaons. The identification of these particles is done using likelihood cuts. Using the likelihood values, the particle identification is done by comparing these values with one another. In the simplest case, the highest one determines the particle type. This method is used in the case of pions. In the case of kaons, stricter likelihood cuts are applied to suppress misidentified pions. These stricter cuts are an improvement compared to previous COMPASS analysis and are used in the multiplicity analysis. The likelihood cuts are listed in Table 1. Also less stricter likelihood cuts are used, which are listed in Table 2. Similar cuts were used in the analysis of the hadron asymmetries using 2007 data. A further improvement is the inclusion of protons in the RICH particle identification efficiency determination.

The RICH particle identification efficiency is studied in the momentum range of  $10 \text{ GeV}/c \leq p \leq 50 \text{ GeV}/c$ . In this range, pions and kaons are emitting Cherenkov light, while up to  $\sim 17 \text{ GeV}$  protons are still below the threshold of

$$p_{\text{thr},i} = m_i \cdot \frac{1}{\sqrt{n^2 - 1}} , \quad (2)$$

where  $n$  is the refractive index. This is shown in Figure 5 where the reconstructed Cherenkov angle is shown as a function of the hadron momentum. As the momentum range is restricted

**Table 1:** Likelihood cuts for pion, kaon and protons.

	PION	KAON	PROTON	
Momentum	$p > p_{\pi,\text{thr}}$	$p > p_{K,\text{thr}}$	$p \leq p_{p,\text{thr}}$	$p > p_{p,\text{thr}}$
Likelihood type $i$	$\pi$	$K$	bg	$p$
$\text{LH}(i)/\text{LH}(\pi)$	—	$> 1.08$	$> 1.0$	$> 1.0$
$\text{LH}(i)/\text{LH}(K)$	$> 1.0$	—	$> 1.0$	$> 1.0$
$\text{LH}(i)/\text{LH}(p)$	$> 1.0$	$> 1.00$	—	—
$\text{LH}(i)/\text{LH}(bg)$	$> 1.0$	$> 1.24$	—	$> 1.0$

**Table 2:** Less strict likelihood cuts for pion, kaon and protons.

	PION	KAON	PROTON	
Momentum	$p > p_{\pi,\text{thr}}$	$p > p_{K,\text{thr}}$	$p \leq p_{p,\text{thr}}$	$p > p_{p,\text{thr}}$
Likelihood type $i$	$\pi$	$K$	bg	$p$
$\text{LH}(i)/\text{LH}(\pi)$	—	$> 1.00$	$> 1.0$	$> 1.0$
$\text{LH}(i)/\text{LH}(K)$	$> 1.0$	—	$> 1.0$	$> 1.0$
$\text{LH}(i)/\text{LH}(p)$	$> 1.0$	$> 1.00$	—	—
$\text{LH}(i)/\text{LH}(bg)$	$> 1.0$	$> 1.07$	—	$> 1.0$

to momenta larger than  $10 \text{ GeV}/c$ , no electron rejection can be performed. In this momentum range the Cherenkov angle for pions and electrons are too close to one another. Muons can also be not rejected using likelihood cuts as the Cherenkov angle for muon and pion is too close to one another. But they are identified using cuts on the radiation length passed by a particle. The identification of pions, kaons and protons above the momentum threshold is done by comparing the likelihood values with one another. The likelihood cuts for protons require its likelihood to be the largest one. These cuts are also given in Table 1. Below the momentum threshold, protons do not emit Cherenkov light. Therefore, the likelihood values are used to test whether the detected light is consistent with random noise in the detector (background). In order to avoid possible problems due to the uncertainty on the reconstructed momentum or the uncertainty of the refractive index of the RICH gas, a region of  $\pm 5 \text{ GeV}/c$  around the

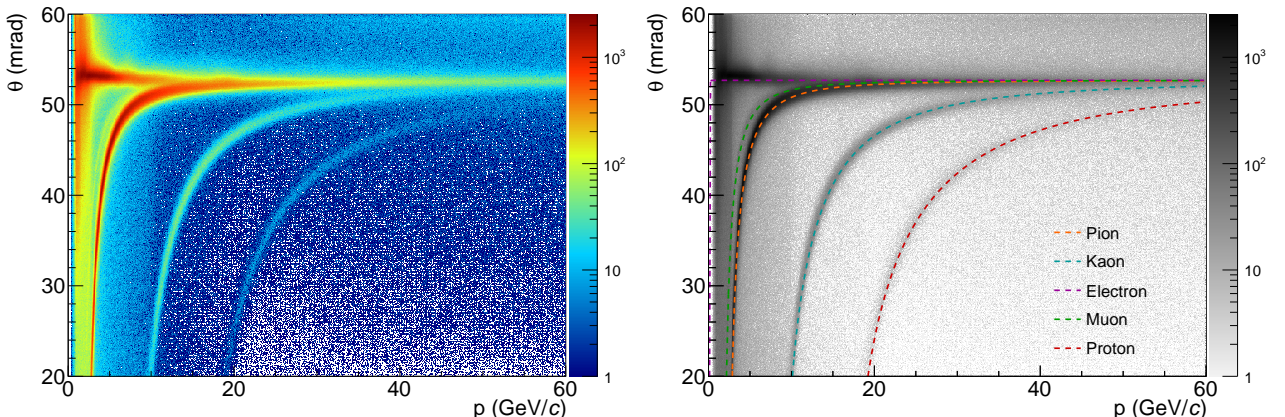


**Figure 5:** Left: Reconstructed Cherenkov angle as a function of the momentum. Right: Comparison with the calculated Cherenkov angle for each particle type using the refractive index of the RICH gas.

proton threshold is used, where both hypothesis are applied for proton identification.

### 3 Method

The particle identification efficiency of the RICH is studied as a function of the hadron phase space, which is given by the hadron momentum and the polar angle at the entrance of the RICH. This was already studied before, for example in References [6] and [7]. The binning used for this study is similar to a previous analysis described in Reference [1]. A fine binning is used for the momentum dependence since the Cherenkov effect depends on this variable. For the dependence on the polar angle, a coarse binning is used, since only a weak dependence is observed. The binning is given by:

- Momentum  $p(\text{GeV}/c) = (10, 11, 12, 13, 15, 17, 19, 22, 25, 27, 30, 35, 40, 50)$
- Angle  $\theta(\text{rad}) = (0.0, 0.01, 0.04, 0.12, 0.3)$

For each bin, the elements of the efficiency matrix  $M_{\text{RICH}}$  are determined separately for positive and negative particles. The elements of this matrix contain the probability for a particle  $i$  to be identified as a particle of type  $j$ , for example a pion that is correctly identified as pion or wrongly as a kaon. The full matrix is given by:

$$M_{\text{RICH}} = \begin{pmatrix} \epsilon(\pi \rightarrow \pi) & \epsilon(\pi \rightarrow K) & \epsilon(\pi \rightarrow p) & \epsilon(\pi \rightarrow \text{noID}) \\ \epsilon(K \rightarrow \pi) & \epsilon(K \rightarrow K) & \epsilon(K \rightarrow p) & \epsilon(K \rightarrow \text{noID}) \\ \epsilon(p \rightarrow \pi) & \epsilon(p \rightarrow K) & \epsilon(p \rightarrow p) & \epsilon(p \rightarrow \text{noID}) \end{pmatrix} \quad (3)$$

The different elements are determined by  $\epsilon(i \rightarrow j) = N(i \rightarrow j)/N(i)$  where  $N(i)$  is the total number of particles  $i$  and  $N(i \rightarrow j)$  is the number of particles  $i$ , which are identified as particle  $j$ . These numbers are evaluated using samples, where the particle type is known, as in the case of the selected decays.

In the case of positive pions, the events from the  $K^0$  sample are used where the negative hadron is identified as a pion using the likelihood cuts shown in Table 1. Therefore, the second particle has to be a pion too, if the decaying particle was a  $K^0$ . Using the RICH, the particle type is determined for the second particle, which results in the number  $N(\pi^+ \rightarrow j)$ . An equivalent procedure is used for positive kaons and protons using the  $\phi$  and  $\Lambda$  samples.

In order to obtain these numbers for the negative particles, the same samples are used but this time performing the identification of the positive particle in the first place.

The numbers  $N(i \rightarrow j)$  are extracted using a fit, which is described here for the  $K^0$  sample, where the negative pion is already identified. The events are put into five different groups, depending on the particle type determined by the RICH:

1. All events (RICH not used for second particle)
2. Events where  $\pi^+$  is identified as  $\pi^+$
3. Events where  $\pi^+$  is identified as  $K^+$
4. Events where  $\pi^+$  is identified as  $p$
5. Events where  $\pi^+$  is not identified

**Table 3:** Functional form for the description of the mass spectra for  $K^0$ ,  $\phi$  and  $\Lambda$  candidates. The symbol  $G$  represents a Gaussian distribution and the symbol  $BW$  a Breit-Wigner distribution.

SAMPLE	SIGNAL	BACKGROUND
$K^0$	$\delta G(\mu, \sigma_1) + (1 - \delta)G(\mu, \sigma_2)$	$1 + ax + b(2x^2 - 1) + c(4x^3 - 3x)$
$\phi$	$BW(\mu, \sigma_1) \otimes G(\mu, \sigma_2)$	$(x - t)^n \cdot \exp(-a(x - t))$ with $t = 2 \cdot m_K$
$\Lambda$	$\delta G(\mu, \sigma_1) + (1 - \delta)G(\mu, \sigma_2)$	$(x - t)^n \cdot \exp(-a(x - t))$ with $t = m_p + m_\pi$

For each of these groups, the invariant  $K^0$  mass spectra are shown in Figure 6, for example, and the number of events in the peak and the background are determined by a simultaneous fit of all five spectra. These spectra are described using two Gaussian distributions with the same mean for the signal,  $f_{\text{Sig}}$ , and a polynomial to describe the background,  $f_{\text{BG}}$ . Their expressions are given in Table 3. The two Gaussian distributions account for the different resolutions of the two spectrometer stages. The fitted function for each of the groups is given by:

$$f(x) = N_{\text{Sig}} \cdot f_{\text{Sig}} + N_{\text{BG}} \cdot f_{\text{BG}}, \quad (4)$$

where  $N_{\text{Sig}}$  is the amount of  $K^0$  and  $N_{\text{BG}}$  the amount of background events. Here, the same width,  $\sigma_1$  and  $\sigma_2$ , of the two Gaussian distributions was used for all five spectra. Also the ratio  $\delta$  of the amount of events in both Gaussian distributions is the same. The shape of the background is the same for all spectra except the one where the pion is identified as a proton. In this case, a possible background contribution due to decays from  $\Lambda$  baryons decaying in a pion and an proton can be enriched. This results in a slightly different background shape. The integral of the background remains a independent parameter in all five cases. In order to ensure

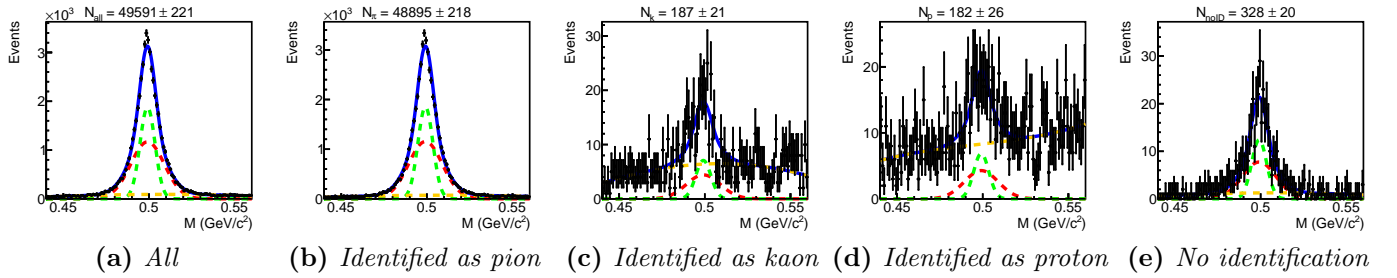


**Figure 6:** Mass spectra for  $K^0$  candidates with an identified  $\pi^-$  for various hypothesis for the second hadron. The momentum of the positive hadron is in the range of  $(25 \text{ GeV}/c^2 < p < 27 \text{ GeV}/c^2)$  and the angle in the range of  $(0.01 < \theta < 0.04)$ .

that the sum of all efficiencies ( $\epsilon(\pi^+ \rightarrow \pi^+) + \epsilon(\pi^+ \rightarrow K^+) + \epsilon(\pi^+ \rightarrow p) + \epsilon(\pi^+ \rightarrow \text{noID})$ ) is 100%, an additional constraint is introduced to the fit.

$$N^{\text{all}}(K^0) = N^\pi(K^0) + N^K(K^0) + N^p(K^0) + N^{\text{noID}}(K^0), \quad (5)$$

where  $N^i(K^0)$  ( $i = \pi, K, p, \text{noID}$ ) is the number of  $K^0$  obtained from the histogram where the pion is identified as  $i$ . This results in 16 free parameters of the fit. The same method is used in the case of kaons and protons. The main difference between those fits and the one for the  $K^0$  sample is the description of the signal and the background. The functions describing both are also given in Table 3. Again the parameters describing the shape are the same in all five spectra and the fit parameters describing the integrals of the functions are used as free

parameters, except for the parameter of the mass spectrum including all events. This results in 15 free parameters for the fit of the  $\phi$  sample and in 15 free parameters for the fit of the  $\Lambda$  sample.

Examples of the fits performed for the  $\phi$  and  $\Lambda$  samples are shown in Figures 7 and 8. The fits show the results for one momentum bin ( $25 \text{ GeV}/c^2 < p < 27 \text{ GeV}/c^2$ ) and angular bin ( $0.01 < \theta < 0.04$ ), which was also shown for the  $K^0$  sample.

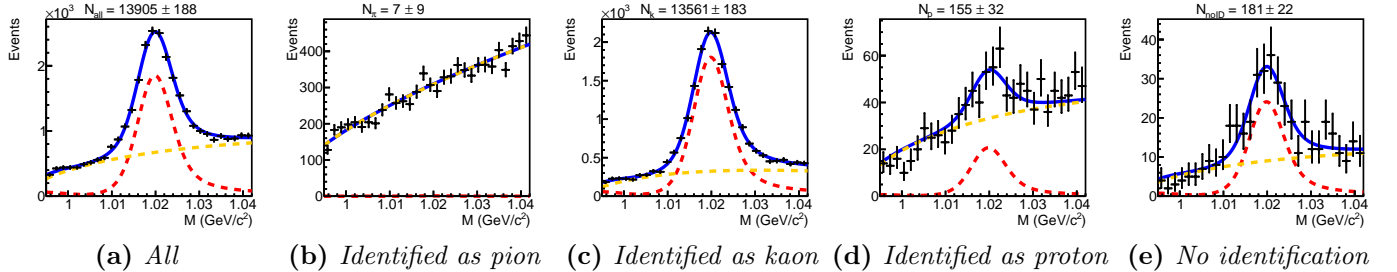


**Figure 7:** Mass spectra for  $\phi$  candidates with an identified  $K^-$  for various hypothesis for the second hadron. The momentum of the positive hadron is in the range of ( $25 \text{ GeV}/c^2 < p < 27 \text{ GeV}/c^2$ ) and the angle in the range of ( $0.01 < \theta < 0.04$ ).

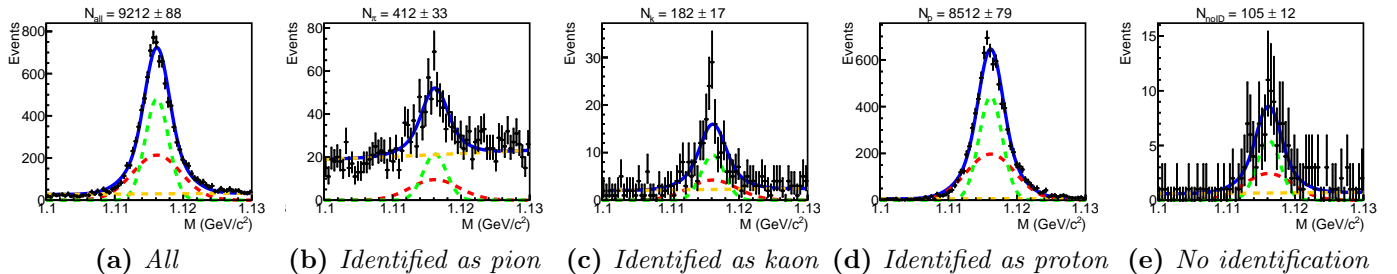


**Figure 8:** Mass spectra for  $\Lambda$  candidates with an identified  $\pi^-$  for various hypothesis for the second hadron. The momentum of the positive hadron is in the range of ( $25 \text{ GeV}/c^2 < p < 27 \text{ GeV}/c^2$ ) and the angle in the range of ( $0.01 < \theta < 0.04$ ).

## 4 Calculation of the efficiencies and uncertainties

The elements of the efficiency matrix  $M_{\text{RICH}}$  are determined from fitted numbers of signal events,

$$\epsilon(i \rightarrow j) = N(i \rightarrow j)/N(i) . \quad (6)$$

Here,  $N(i)$  is given by the sum of all  $N(i \rightarrow j)$ . As the nominator and denominator are correlated, the uncertainty can be determined via error propagation taking into account the covariance matrix of the fit,

$$\Delta\epsilon = \sqrt{\sum_{j=1}^m \left( \frac{\partial\epsilon}{\partial N(i \rightarrow j)} \right)^2 \cdot u_j + 2 \sum_{j=1}^{m-1} \sum_{k=j+1}^m \left( \frac{\partial\epsilon}{\partial N(i \rightarrow j)} \frac{\partial\epsilon}{\partial N(i \rightarrow k)} \cdot u(j, k) \right)} . \quad (7)$$

Here,  $u_j$  are the diagonal elements of the covariance matrix,  $u(j, k)$  are the off diagonal elements and  $\epsilon$  is one of the elements of the efficiency matrix. The summations are done over all possible particle types, which are pion, kaon, proton and no identification in this case.

## 5 Results

The result for the RICH particle identification efficiency is shown in Figures 9 to 14 for the various particles and their charges using the stricter likelihood cuts. In each figure, the momentum dependence for the various angular bins are shown. The weak dependence on the angle as well as the strong dependence on the momentum especially near the threshold is visible. The RICH performs a correct identification of pions in more than 95% of the cases for momenta below  $30 \text{ GeV}/c^2$  and the probability for a misidentification of a pion as a kaon is below  $\sim 1\%$ . For kaons, near the threshold a strong dependence on the momentum is visible. At higher momenta the correct identification is given in  $\sim 95\%$  of the cases. For protons, the momentum dependence at the threshold is even stronger. Below the threshold, protons are identified correctly in about 50% of the cases. Above the threshold, the efficiency rises up to  $\sim 95\%$ . For the future analysis of hadron asymmetries, the inverse of the efficiency matrix will be needed. Similar results are obtained using the less strict likelihood cuts. These results are shown in Figures 15 to 20. The correct identification of pions below  $30 \text{ GeV}/c^2$  is performed in more than 95% of the cases. Due to the less strict likelihood cuts the misidentification of pions as kaons is a little bit larger but still below 3% for momenta below  $30 \text{ GeV}/c^2$ . For larger momenta a larger fraction is misidentified as kaons, which got no identification in the case of the stricter likelihood cuts. For kaons and protons similar results are obtained as in the case of the stricter cuts. The probability for the correct identification of kaons is a little bit lower than in the case of the stricter cuts but still above 95%.

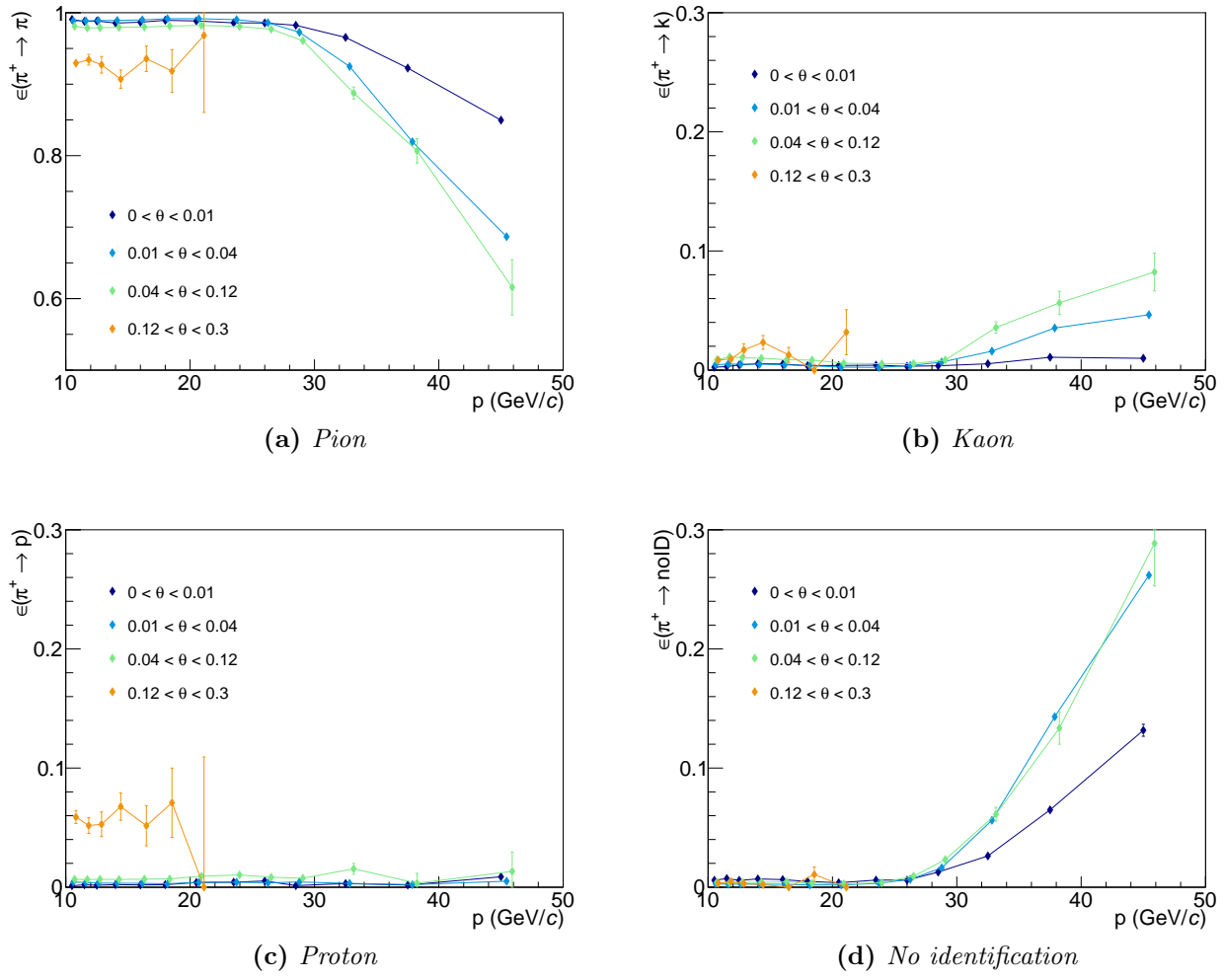


**Figure 9:** Identification probabilities  $\epsilon(\pi^+ \rightarrow j)$  for positive pions. The results for the different  $\theta$  bins are slightly shifted to the right to avoid an overlap.

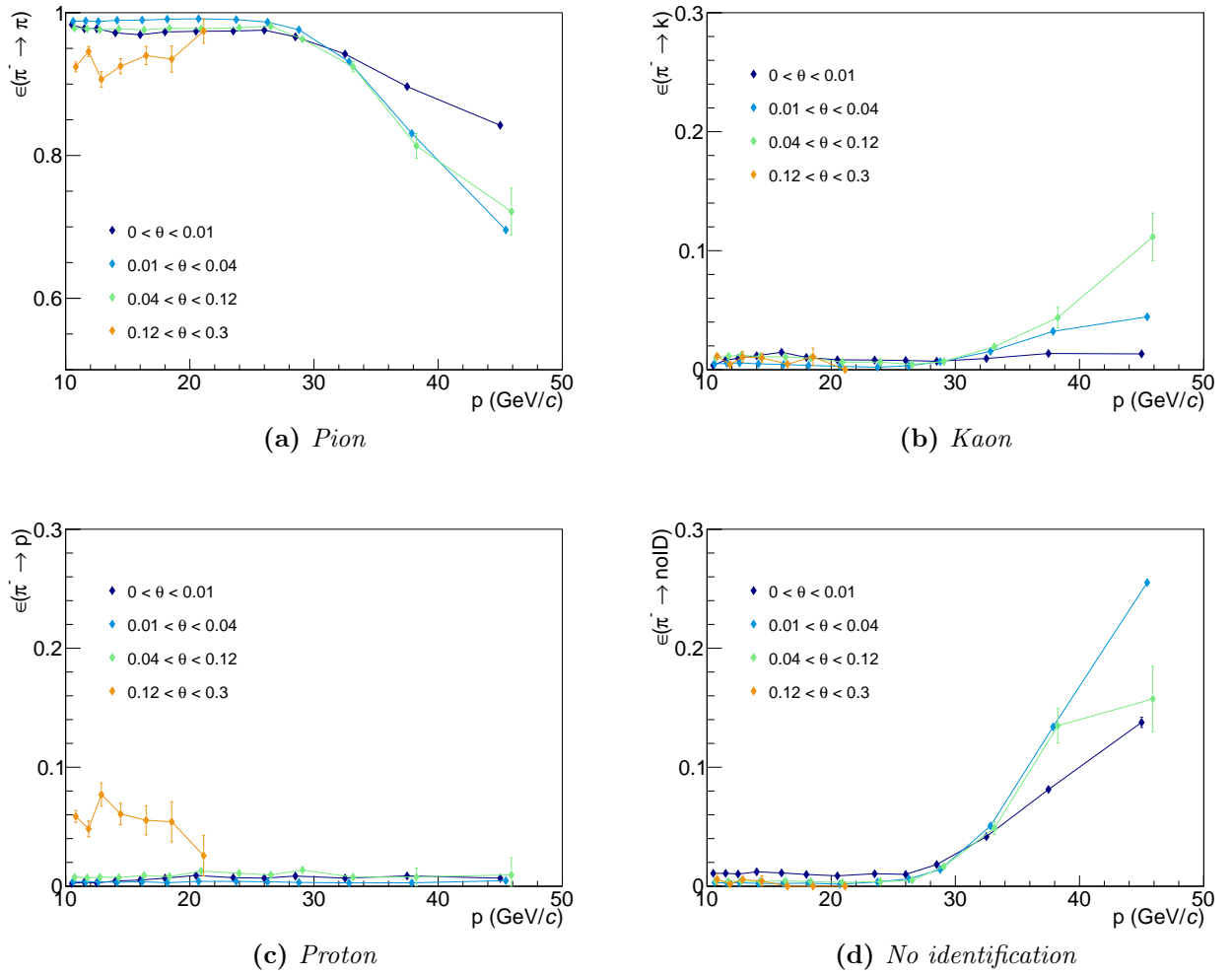


**Figure 10:** Identification probabilities  $\epsilon(\pi^- \rightarrow j)$  for negative pions. The results for the different  $\theta$  bins are slightly shifted to the right to avoid an overlap.

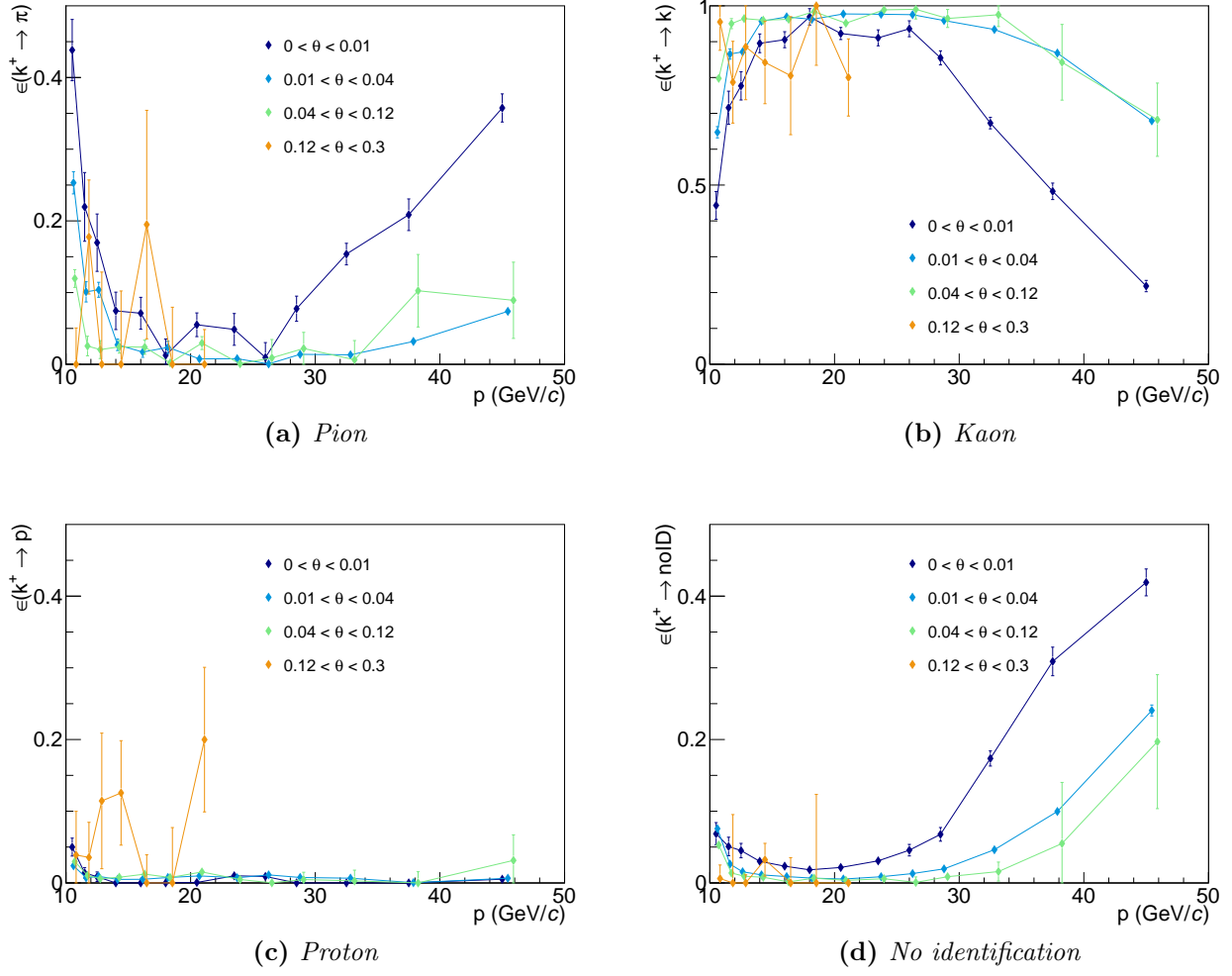


**Figure 11:** Identification probabilities  $\epsilon(K^+ \rightarrow j)$  for positive kaons. The results for the different  $\theta$  bins are slightly shifted to the right to avoid an overlap.

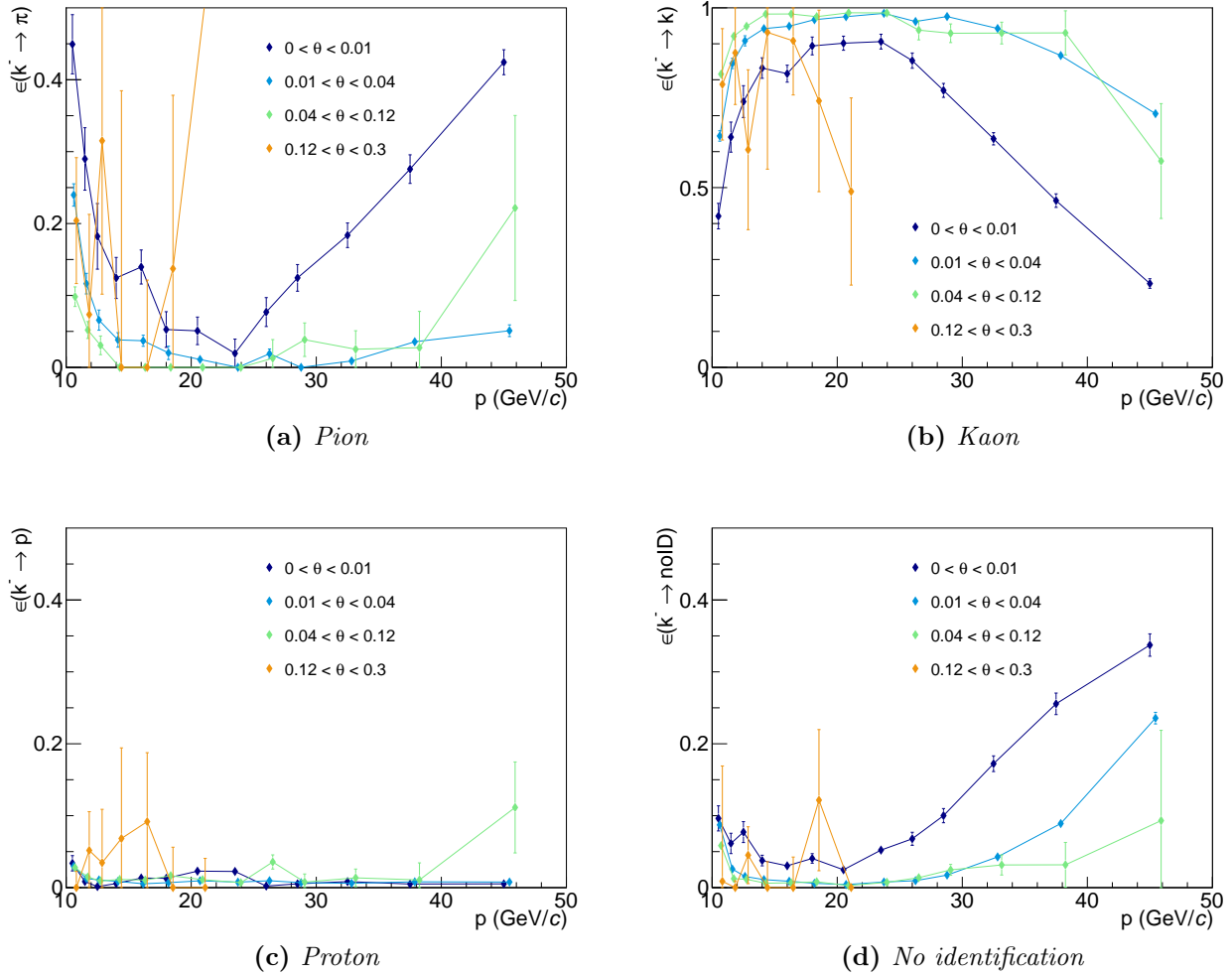


**Figure 12:** Identification probabilities  $\epsilon(K^- \rightarrow j)$  for negative pions. The results for the different  $\theta$  bins are slightly shifted to the right to avoid an overlap.

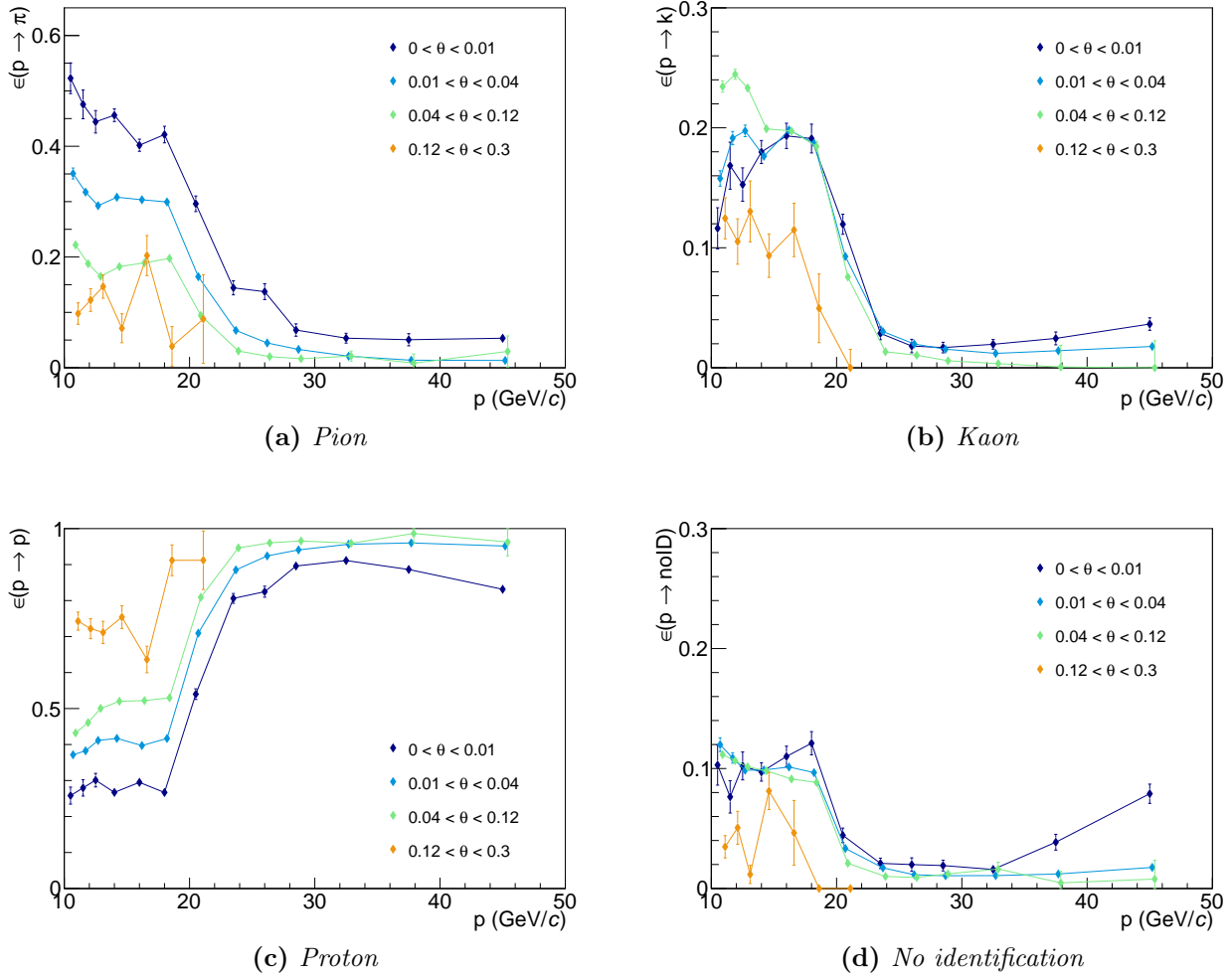


**Figure 13:** Identification probabilities  $\epsilon(p \rightarrow j)$  for protons. The results for the different  $\theta$  bins are slightly shifted to the right to avoid an overlap.

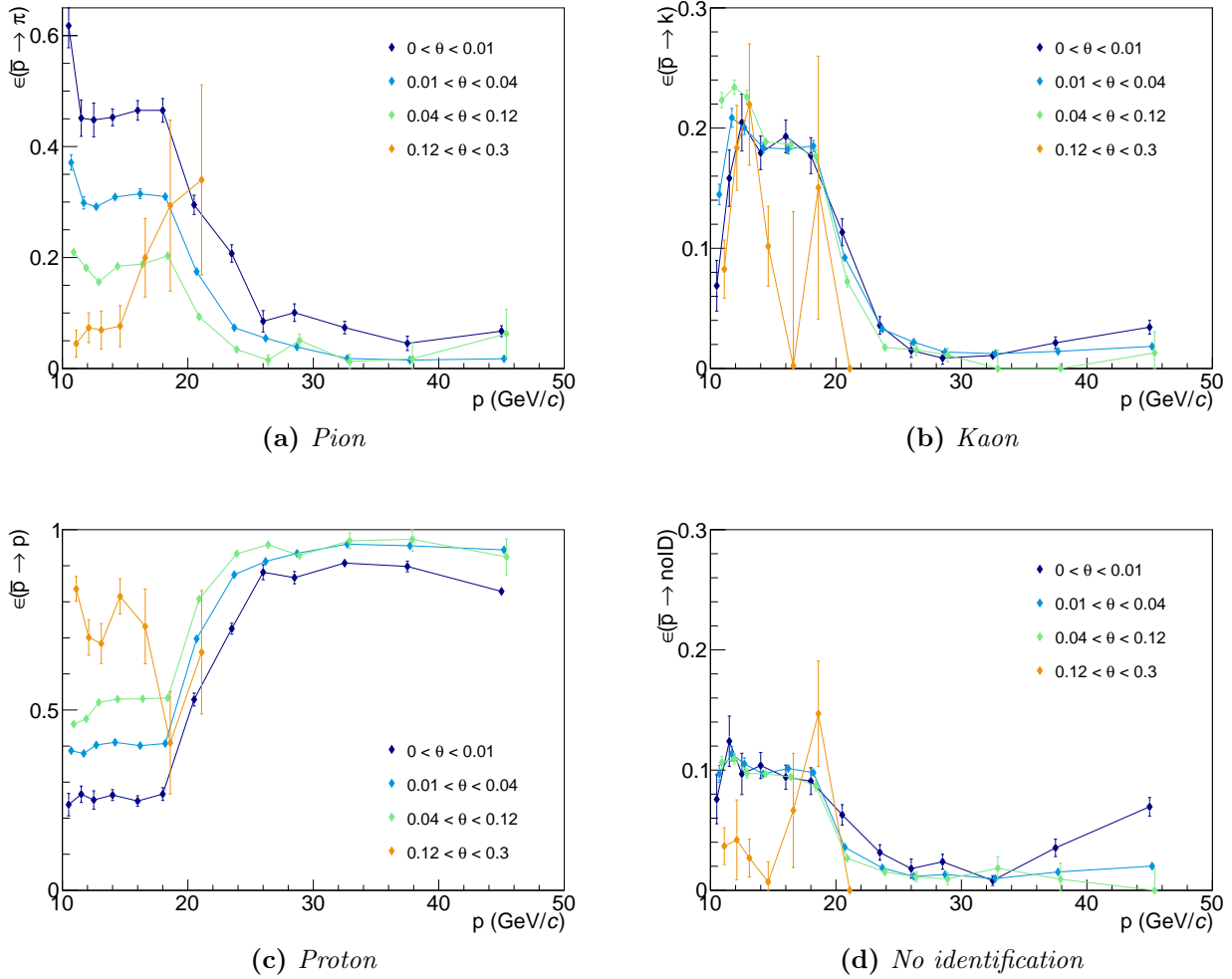


**Figure 14:** Identification probabilities  $\epsilon(\bar{p} \rightarrow j)$  for antiprotons. The results for the different  $\theta$  bins are slightly shifted to the right to avoid an overlap.

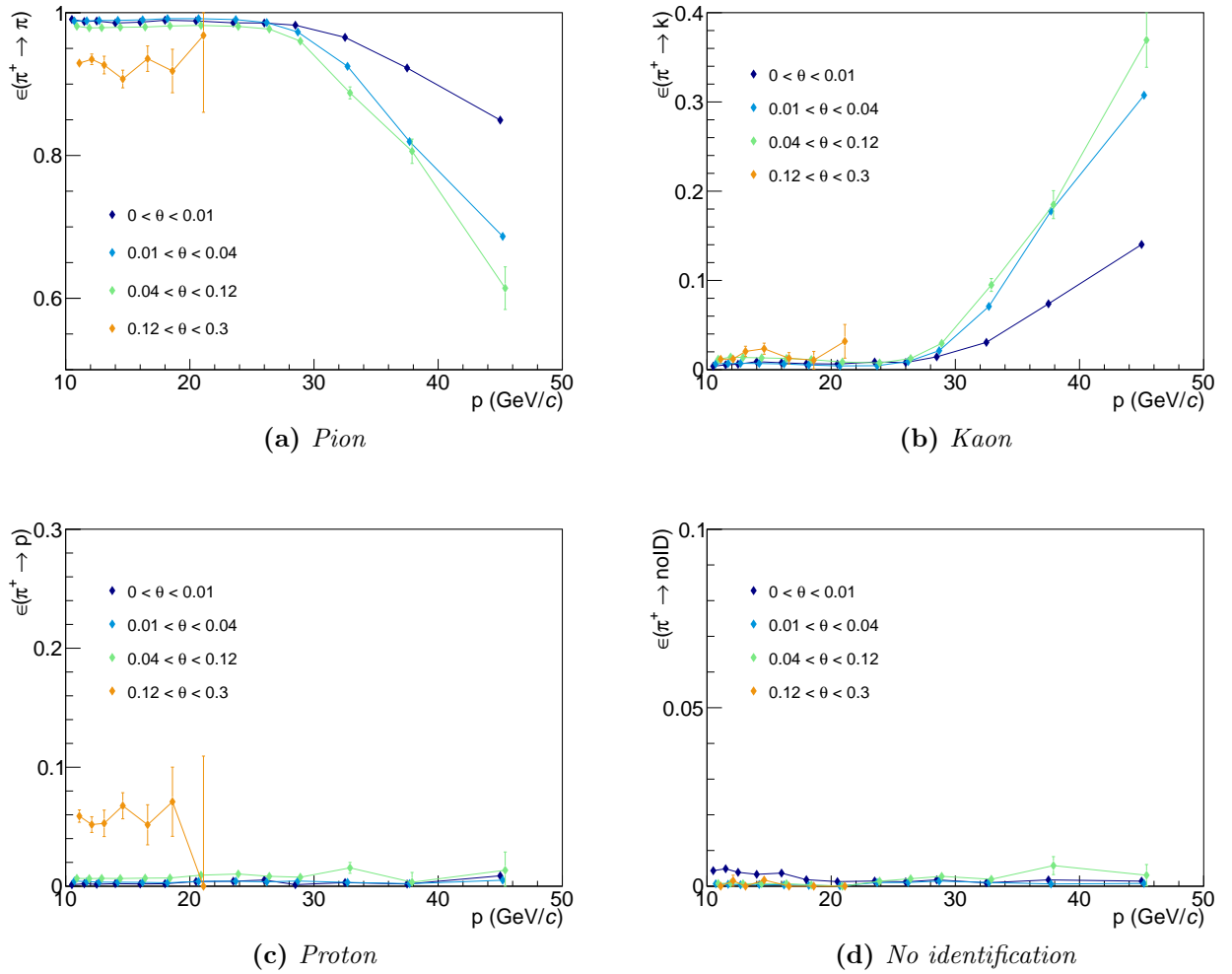


**Figure 15:** Identification probabilities  $\epsilon(\pi^+ \rightarrow j)$  for positive pions using the 2007 likelihood cuts. The results for the different  $\theta$  bins are slightly shifted to the right to avoid an overlap.

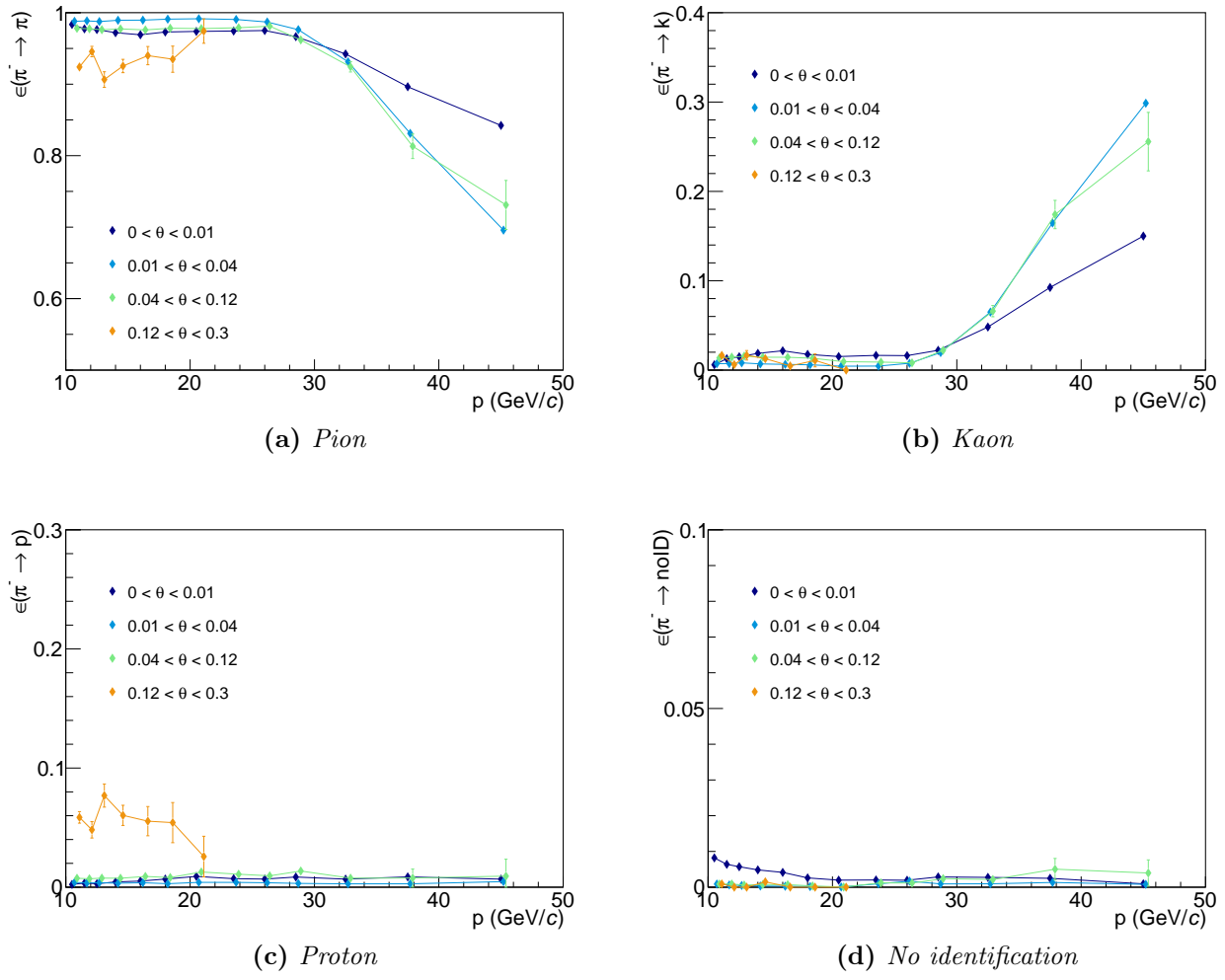


**Figure 16:** Identification probabilities  $\epsilon(\pi^- \rightarrow j)$  for negative pions using the 2007 likelihood cuts. The results for the different  $\theta$  bins are slightly shifted to the right to avoid an overlap.

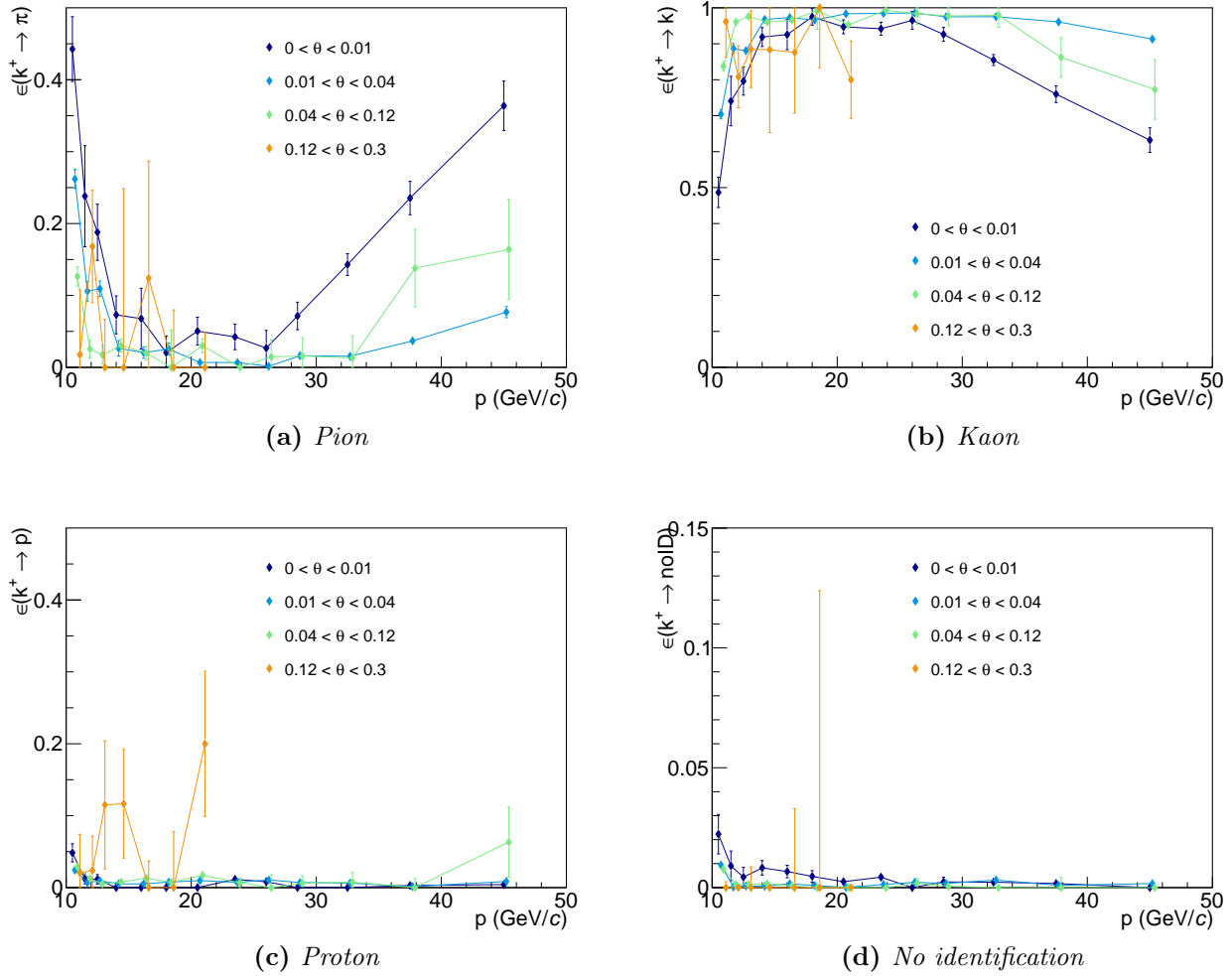


**Figure 17:** Identification probabilities  $\epsilon(K^+ \rightarrow j)$  for positive kaons using the 2007 likelihood cuts. The results for the different  $\theta$  bins are slightly shifted to the right to avoid an overlap.

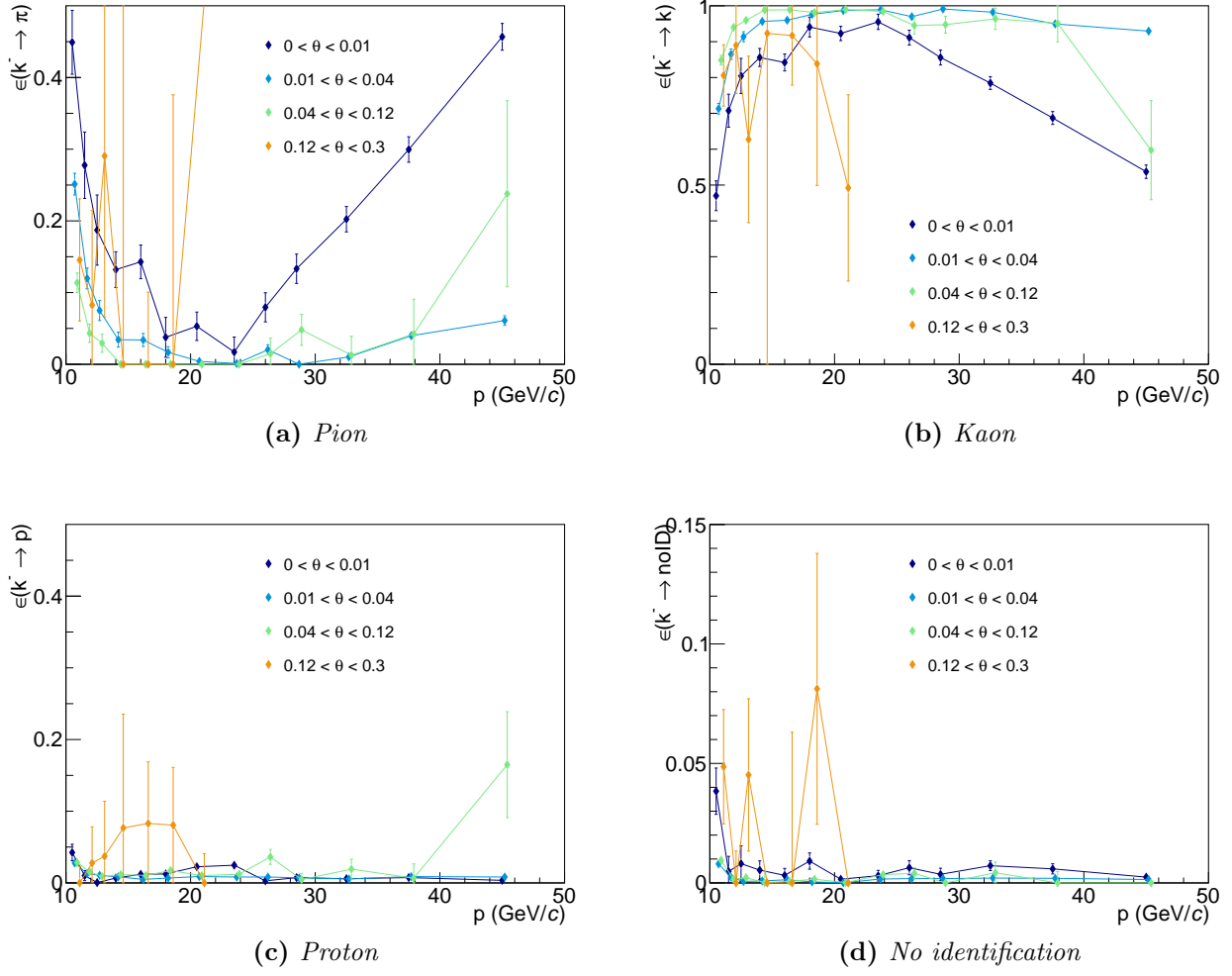


**Figure 18:** Identification probabilities  $\epsilon(K^- \rightarrow j)$  for negative pions using the 2007 likelihood cuts. The results for the different  $\theta$  bins are slightly shifted to the right to avoid an overlap.

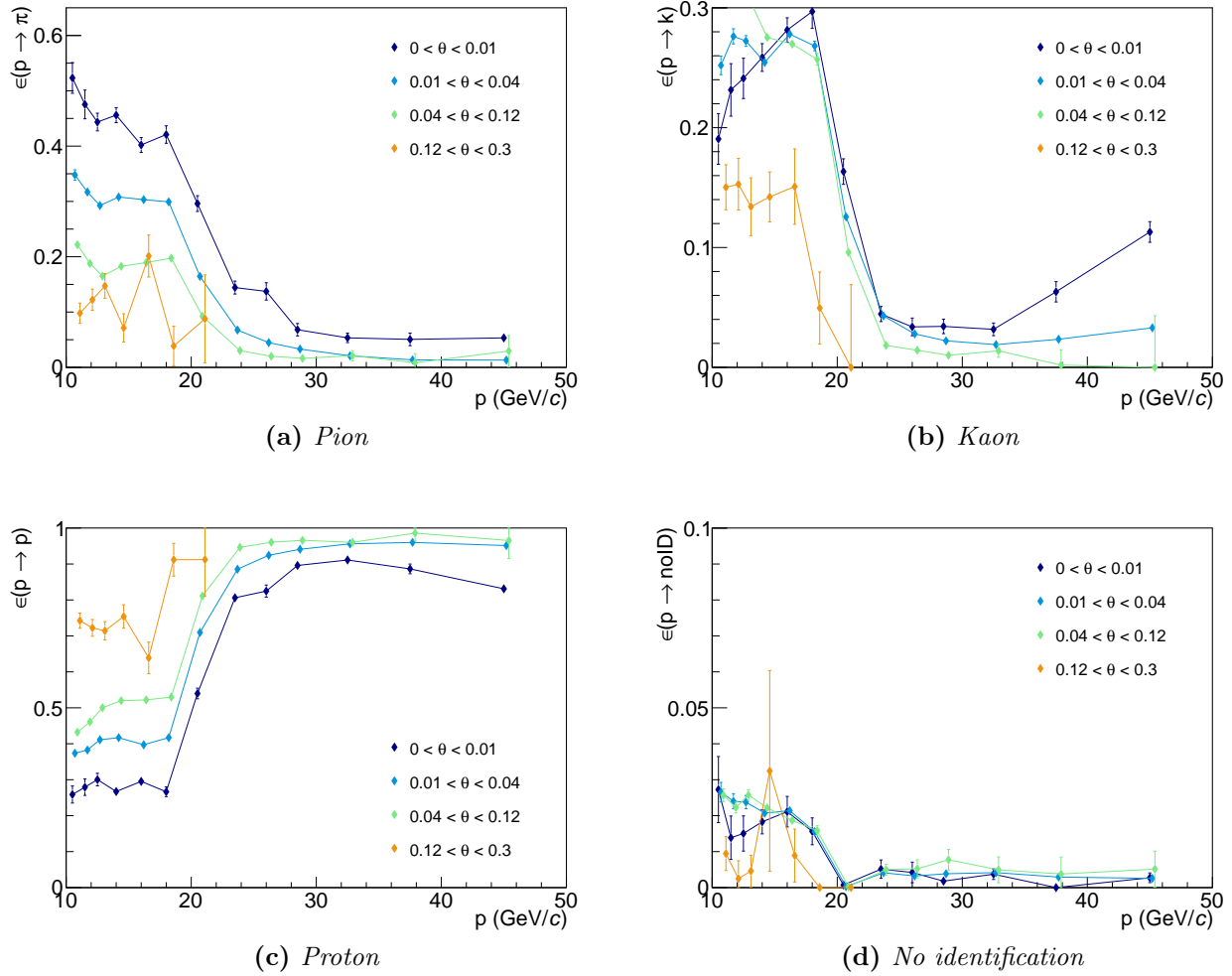


**Figure 19:** Identification probabilities  $\epsilon(p \rightarrow j)$  for protons using the 2007 likelihood cuts. The results for the different  $\theta$  bins are slightly shifted to the right to avoid an overlap.

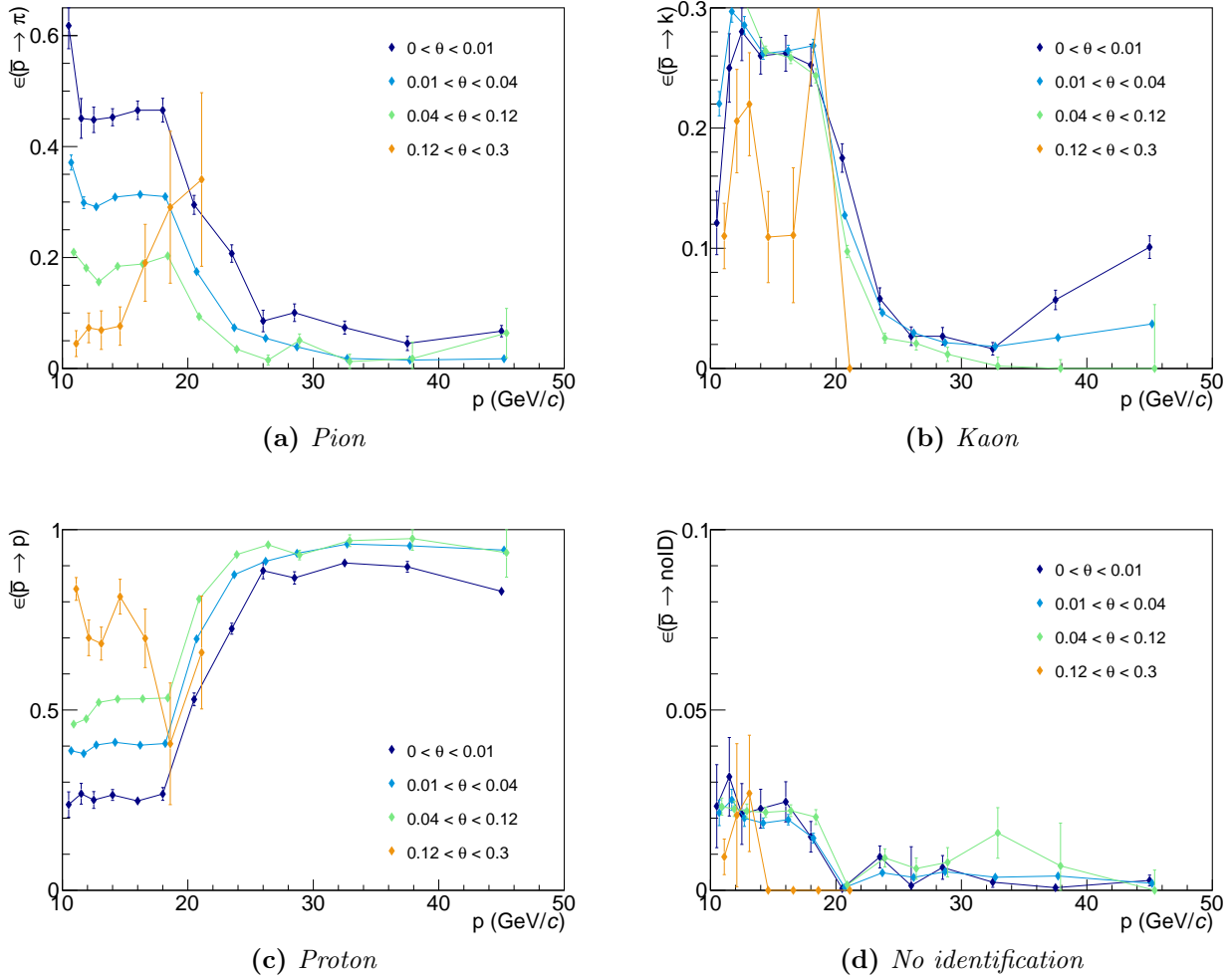


**Figure 20:** Identification probabilities  $\epsilon(\bar{p} \rightarrow j)$  for antiprotons using the 2007 likelihood cuts. The results for the different  $\theta$  bins are slightly shifted to the right to avoid an overlap.

## 6 Problems at high $z$

Marcin Stolarski discovered in a particular kinematic region ( $35 \text{ GeV} < p < 40 \text{ GeV}$ ,  $z > 0.7$ ) that non-linearities exist between the likelihood values for kaons and pions (see e.g. Ref. [3, 4]) in the 2006 data. The effect is shown in Figure 21. Instead of the expected separation

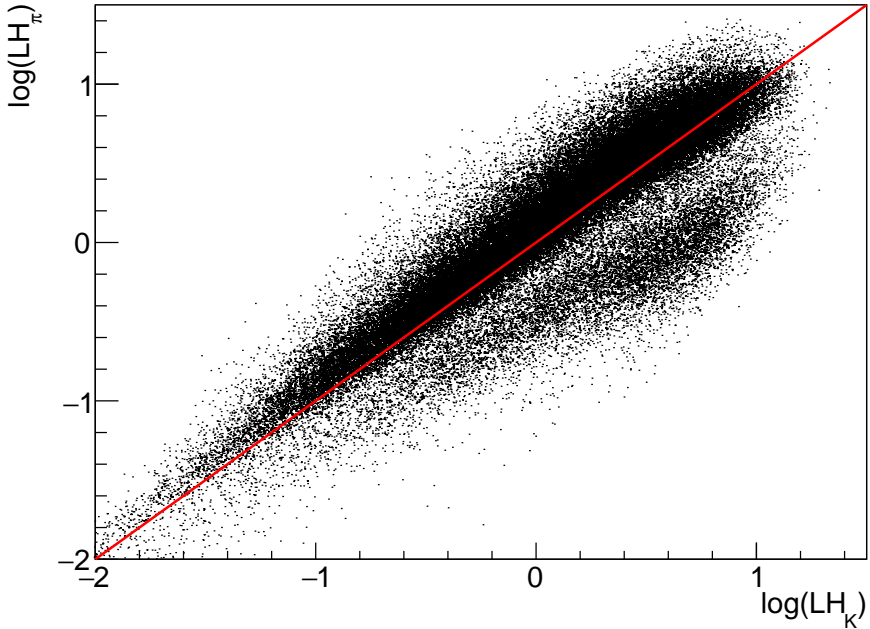


**Figure 21:** Likelihood for pions as a function of the likelihood for kaons using 2006 data.

between pions and kaons at  $LH_\pi = LH_k$ , pions are found at  $LH_\pi < LH_k$ . The amount is larger for high likelihood values. This behaviour was also found in the 2007 and 2011 data as shown in Figure 22. For the 2006 data, Marcin Stolarski showed that the probability for

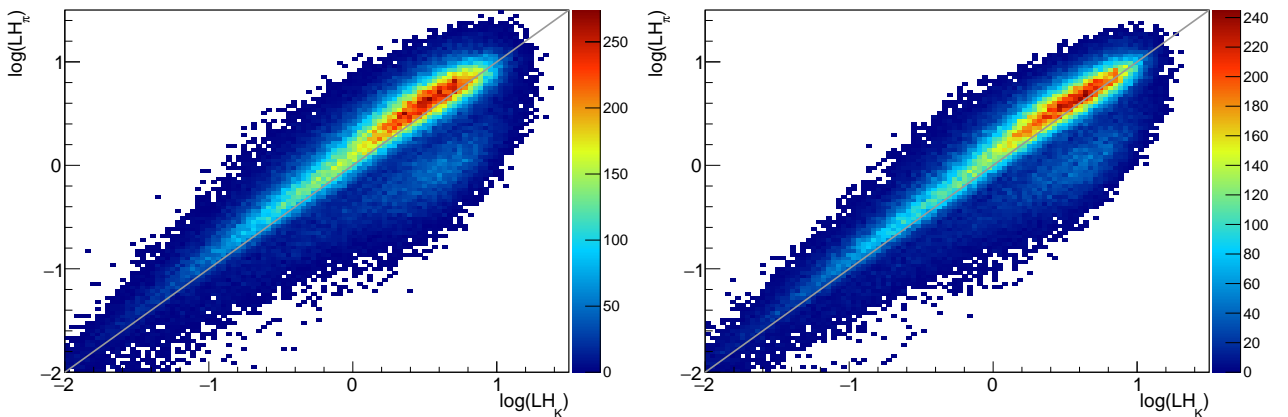


**Figure 22:** Likelihood for pions as a function of the likelihood for kaons using 2007 data (left) and 2011 data (right).

the misidentification of pions as kaons differs from the value given in the RICH tables in this kinematic region using the  $p_T$  spectra (see Ref. [3]). In order to see if the non-linearities are taken correctly into account in the RICH tables, the likelihood values for pions and kaons are

compared using the  $K^0$  sample for high momenta and high  $z$ . This comparison is shown in Figure 23. It shows that the problematic kinematic region is not covered by the  $K^0$  sample and therefore the RICH tables are not valid in this kinematic region due to the non-linearities. In order to obtain the correct values for the RICH tables and to cross check the results from

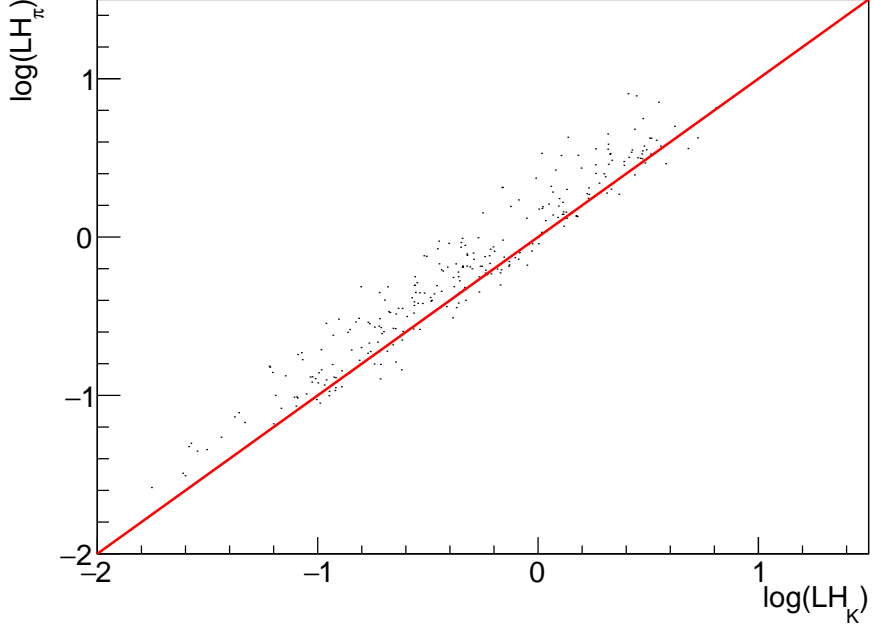


**Figure 23:** Likelihood for pions as a function of the likelihood for kaons using the 2011  $K^0$  sample.

Marcin Stolarski, a different sample for pions is needed. This new sample was obtained using the  $\rho^0$  decay into two pions. This sample contains, in contrast to the  $K^0$  sample, events at high momenta and high  $z$ , which cover high likelihood values. The sample also shows the same behaviour as seen before in the SIDIS sample. The correlation between pion and kaon likelihood values is shown in Figure 24 for the  $\rho^0$  sample in the mass range of the  $\rho^0$  at high momenta and high  $z$ .

## 7 PID using $\rho^0$

In order to calculate the RICH tables at high momenta and high  $z$ , a sample of  $\rho^0$  candidates decaying into two charged pions is used. The selection is described in the following.

### 7.1 Data selection

The  $\rho^0$  meson decay length is too short to separate the primary and decay vertex. Therefore, all outgoing particles from a primary vertex are taken into account for the search of possible  $\rho^0$  mesons. This results in a large combinatorial background like in the case of the selection of  $\phi$  mesons. branching ratio of the decay into two pions is  $\sim 100\%$  [5].

1. Select possible event with  $\rho^0$  mesons
  - At least 3 outgoing particles (includes scattered muon)

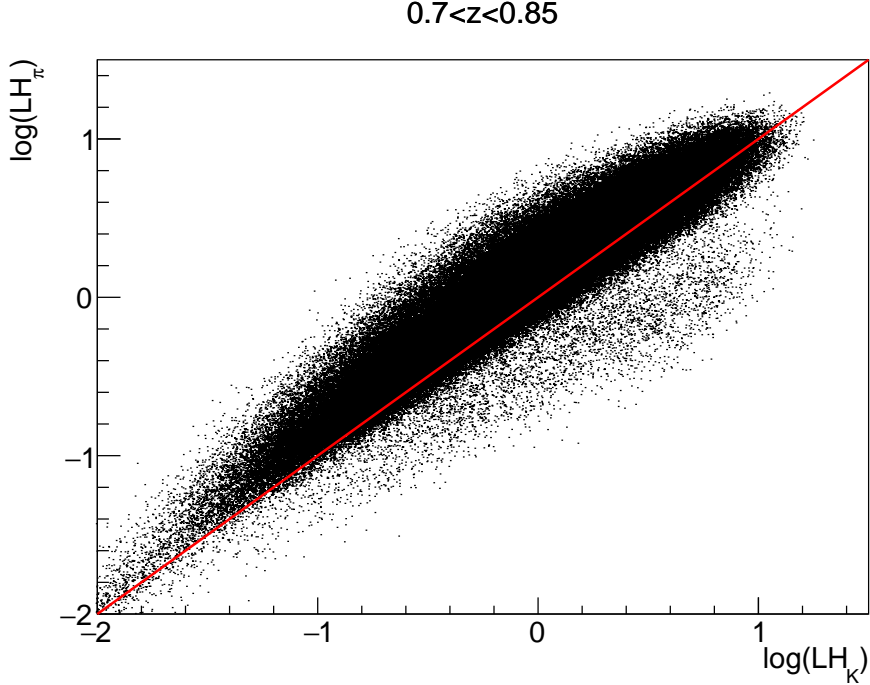


**Figure 24:** Likelihood for pions as a function of the likelihood for kaons using the 2006  $\rho^0$  sample.

- Loop over all outgoing particles
  - Oppositely charged pairs of hadrons (none is a muon)
2. Select good hadron tracks
    - First measured position in front of SM1
    - Last measured position behind SM1
    - Skip possible muon candidates with last measured positions  $> 3300$  cm or  $X/X_0 > 10$
    - Transverse momentum with respect to the mother particle larger than 23 MeV to suppress electrons
    - Good reconstructed track with  $\chi^2/\text{NDF} < 10$
  3. Additional cuts
    - $p > 1 \text{ GeV}/c$
    - Mass difference between  $\rho^0$  mass and the invariant mass of the two hadrons smaller than  $250 \text{ MeV}/c^2$  assuming the pion mass
    - Invariant mass of the two hadrons smaller than  $1.04 \text{ MeV}/c^2$  assuming the kaon mass in order to suppress  $\phi$  mesons

The selection steps are similar to the selection of the  $\phi$  candidates. In the first step, primary vertices with oppositely charged hadron pairs are selected. During the second selection step, only particles with a measured momentum are kept and possible electrons are removed by removing particles with a low transverse momentum. Also possible muon candidates are removed. During the third step, additional cuts are applied to remove events, which will not be used in the later analysis. Similar to the selection of  $\phi$  meson candidates, also a large combinatorial background is obtained.

## 7.2 Results

In order to calculate the RICH efficiencies for the identification or misidentification of pions, the same method as described before is used (see Section 3). The functional forms used to fit the various mass spectra are the same ones as used in the case of  $K^0$  mesons (see Table 3). In the case of the misidentification of pions as kaons from the  $\rho^0$  sample, an additional background contribution from  $K^*$  mesons ( $K^* \rightarrow (K\pi)^\pm$ , BR  $(99.900 \pm 0.009\%)$  [5]) arises, which can appear as an additional peak in the  $\rho^0$  mass spectra and also moves beneath the  $\rho^0$  peak (see e.g. grey line and shifted peak position in Figure 25c). In order to deal with this additional background contribution, the amount of  $K^*$  mesons in the  $\rho^0$  mass range for the case of a misidentification of the pion as kaon has to be determined. This is done by an additional fit of the invariant  $\pi K$  mass spectra (see Figure 25f). This mass spectra is obtained using the same events in which the second pion is misidentified as an kaon (e.g. the ones in Figure 25c) but instead of using the pion mass, the kaon mass is assigned to the second particle. The fit of the  $\pi K$  mass spectra is performed before the simultaneous fit of all  $\pi\pi$  mass spectra. In the simultaneous fit, an additional background contribution is added to the functional form of the background in the case of a misidentification as a kaon. The additional component is given by a Gaussian, which accounts for the  $K^*$  mesons (grey line in Figure 25c). The result from such a fit is shown in Figure 25.

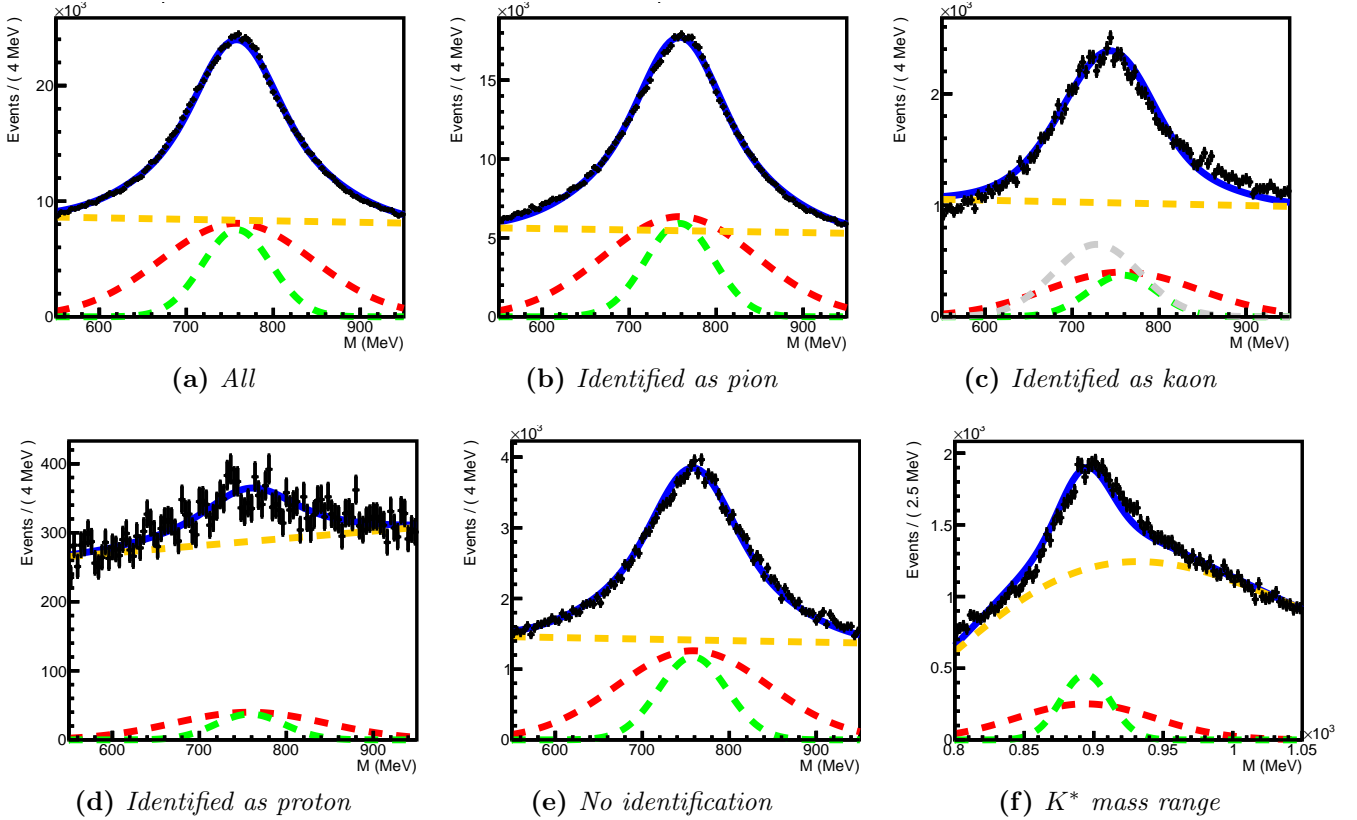


**Figure 25:** Mass spectra for  $\rho^0$  candidates with an identified  $\pi^+$  for various hypothesis for the second hadron. The momentum of the negative hadron is in the range of  $(35 \text{ GeV}/c^2 \leq p < 40 \text{ GeV}/c^2)$  and the angle in the range of  $(0.01 \leq \theta < 0.04)$ .

In a future analysis, the functional shape of the  $K^*$  background beneath the  $\rho^0$  peak has to be improved as it is not given by a simple Gaussian distribution. Also a preliminary version of the

fit was developed, in which the fit of the  $\rho^0$  and  $K^*$  mass spectra is performed simultaneously. This simultaneous method still needs further improvements of the model in order to be used and is not shown in this note.

Using the  $\rho^0$  sample and the simple model of an additional Gaussian in the background description, the  $z$  dependence of the RICH efficiency is determined using 2006 data. In this test, only one particular momentum and angular bin was used, which is given by the momentum range of  $35 \text{ GeV}/c \leq p < 40 \text{ GeV}/c$  and the angular range of  $0.01 \leq \theta < 0.04$ . In this kinematic range, the misidentification probability of a pion as a kaon is  $(3.2 \pm 0.2)\%$ , which was determined using the  $K^0$  sample. Using the  $\rho^0$  sample, a  $z$  dependence of the misidentification probability was found. These values are listed in Table 4 for positively and negatively charged pions. The corresponding fits of the  $\rho^0$  mass are shown in Figures 26 to 29. The problem with the additional background contribution can be seen at large  $z$ . Here for example, an additional background contribution arises beneath the  $K^*$  peak, which results in a worse fit. Also a shift of the position of the peak in the  $\rho^0$  mass spectra for identified kaons is visible.

**Table 4:** Probability for a correct identification of a pion as a pion and the misidentification probabilities as a kaon using the  $\rho^0$  sample ( $35 \text{ GeV}/c \leq p < 40 \text{ GeV}/c, 0.01 \leq \theta < 0.04$ ).

	$P(\pi^- \rightarrow \pi^-)$	$P(\pi^+ \rightarrow \pi^+)$	$P(\pi^- \rightarrow K^-)$	$P(\pi^+ \rightarrow K^+)$
$0.1 \leq z < 0.3$	$(75.4 \pm 1.5)\%$	$(71.6 \pm 1.4)\%$	$(2.8 \pm 1.5)\%$	$(2.4 \pm 1.3)\%$
$0.3 \leq z < 0.5$	$(76.6 \pm 0.4)\%$	$(73.7 \pm 1.1)\%$	$(5.7 \pm 0.4)\%$	$(4.7 \pm 0.4)\%$
$0.5 \leq z < 0.7$	$(78.4 \pm 0.2)\%$	$(74.0 \pm 0.2)\%$	$(6.3 \pm 0.1)\%$	$(8.6 \pm 0.1)\%$
$0.7 \leq z < 1.0$	$(80.4 \pm 0.2)\%$	$(76.8 \pm 0.2)\%$	$(4.4 \pm 0.1)\%$	$(5.6 \pm 0.1)\%$

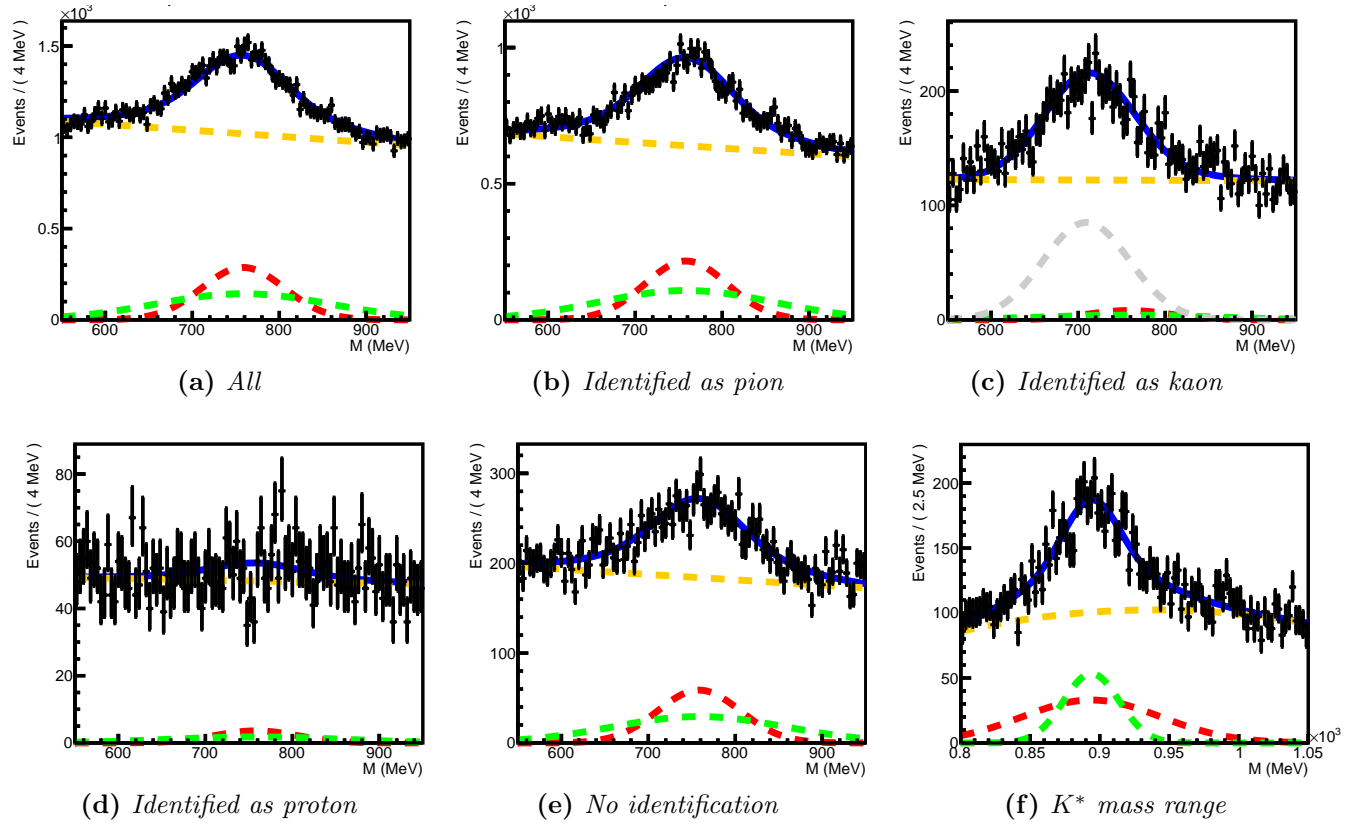


**Figure 26:** Mass spectra for  $\rho^0$  candidates with an identified  $\pi^+$  for various hypothesis for the second hadron. The momentum of the negative hadron is in the range of  $(35 \text{ GeV}/c^2 \leq p < 40 \text{ GeV}/c^2)$  and the angle in the range of  $(0.01 \leq \theta < 0.04)$ . In addition  $z$  is restricted to the range of  $0.1 \leq z < 0.3$ .

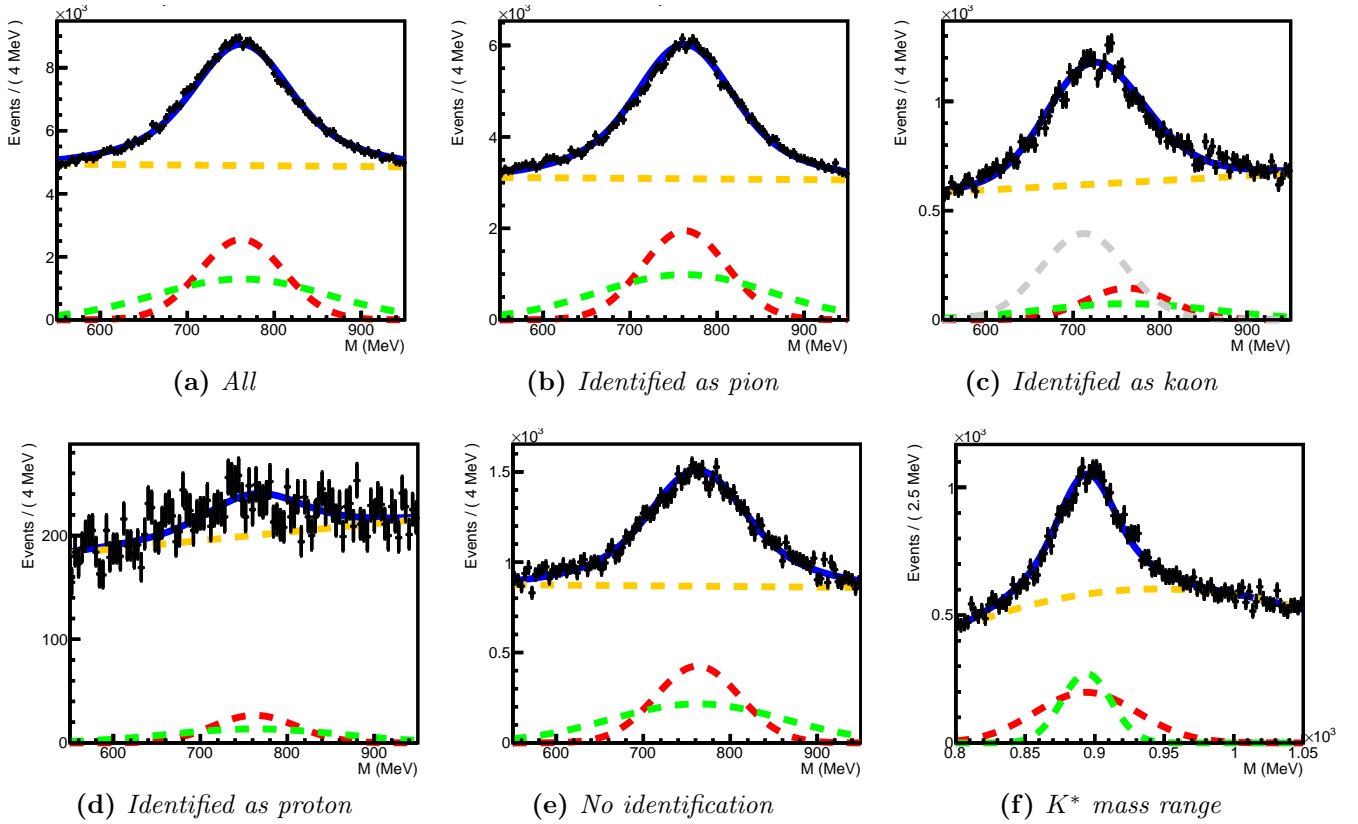


**Figure 27:** Mass spectra for  $\rho^0$  candidates with an identified  $\pi^+$  for various hypothesis for the second hadron. The momentum of the negative hadron is in the range of  $(35 \text{ GeV}/c^2 \leq p < 40 \text{ GeV}/c^2)$  and the angle in the range of  $(0.01 \leq \theta < 0.04)$ . In addition  $z$  is restricted to the range of  $0.3 \leq z < 0.5$ .

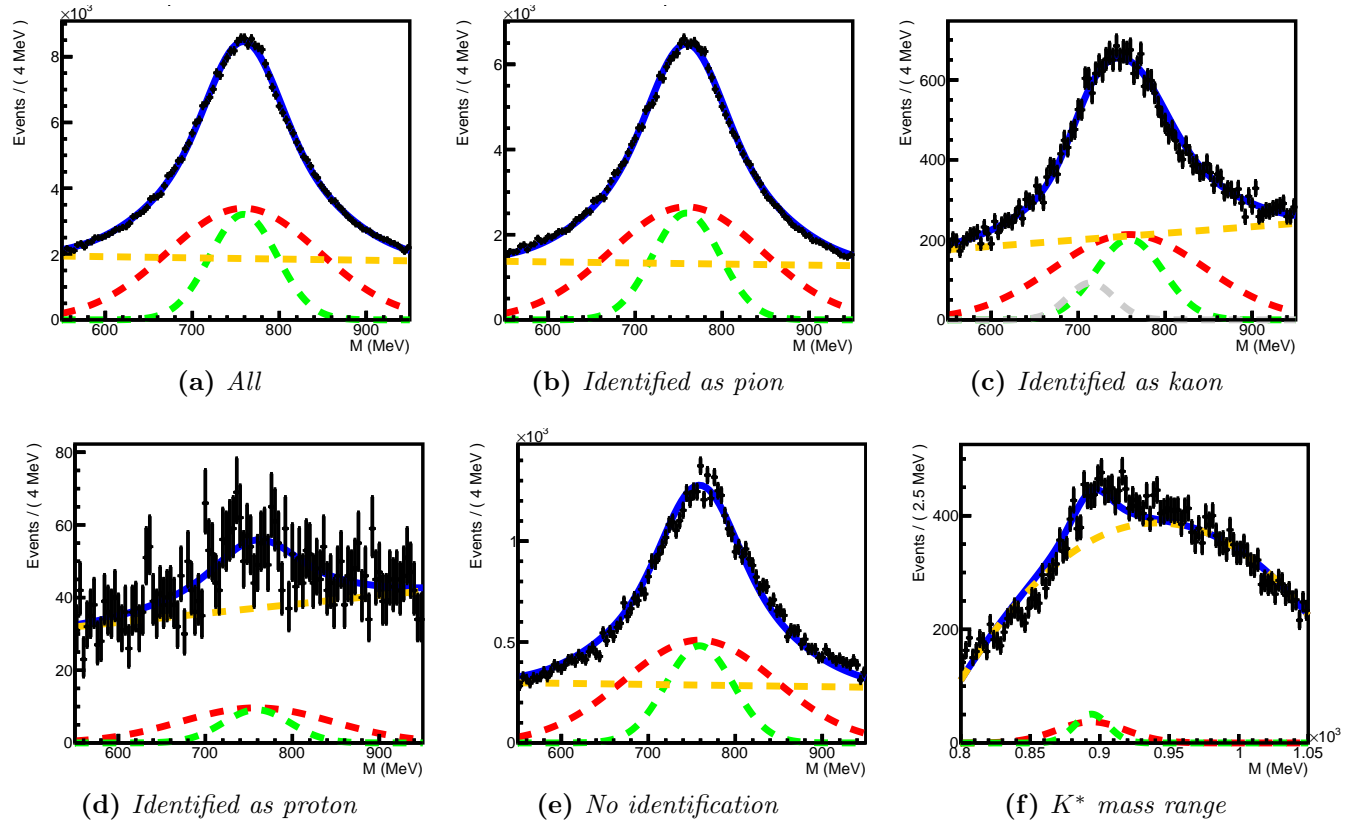


**Figure 28:** Mass spectra for  $\rho^0$  candidates with an identified  $\pi^+$  for various hypothesis for the second hadron. The momentum of the negative hadron is in the range of  $(35\text{ GeV}/c^2 \leq p < 40\text{ GeV}/c^2)$  and the angle in the range of  $(0.01 \leq \theta < 0.04)$ . In addition  $z$  is restricted to the range of  $0.5 \leq z < 0.7$ .

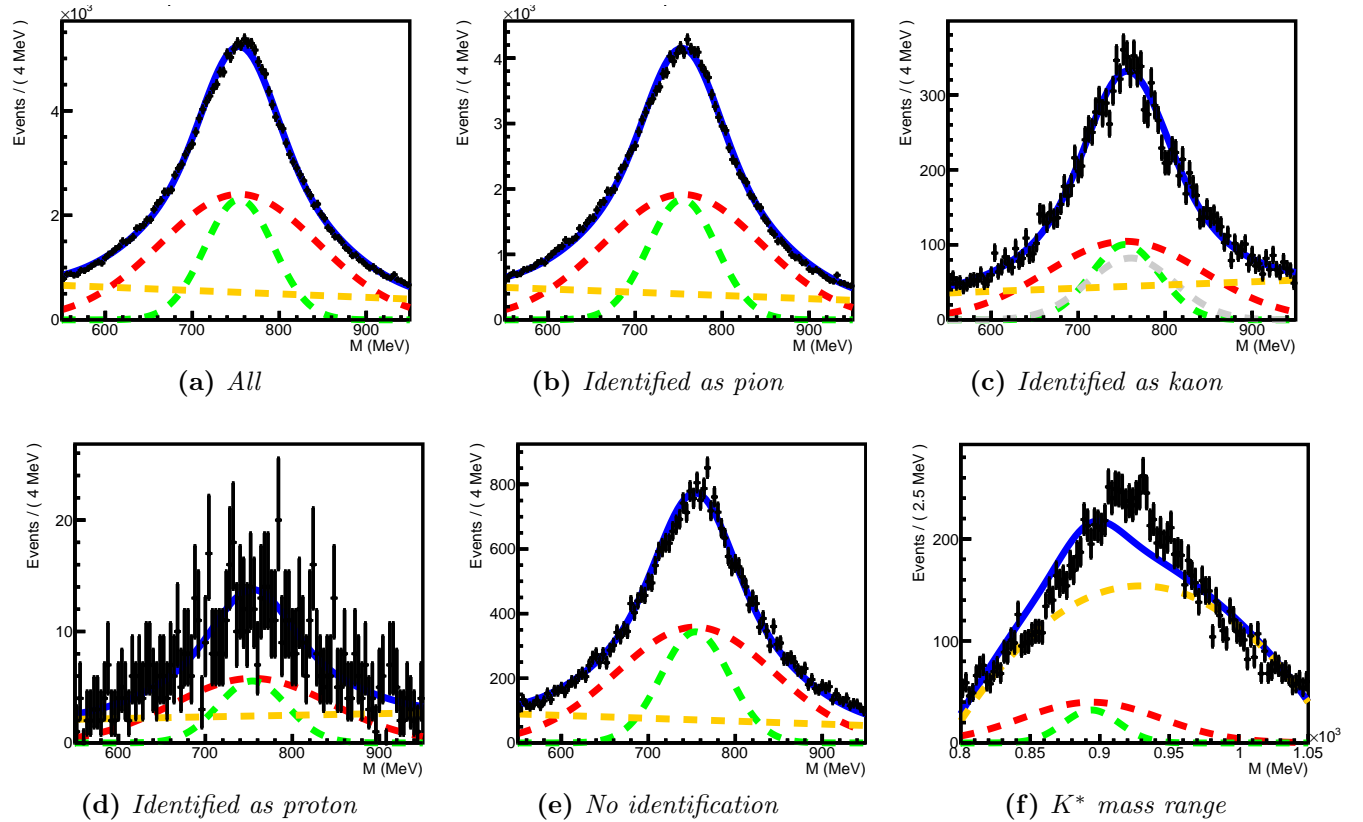


**Figure 29:** Mass spectra for  $\rho^0$  candidates with an identified  $\pi^+$  for various hypothesis for the second hadron. The momentum of the negative hadron is in the range of  $(35 \text{ GeV}/c^2 \leq p < 40 \text{ GeV}/c^2)$  and the angle in the range of  $(0.01 \leq \theta < 0.04)$ . In addition  $z$  is restricted to the range of  $0.7 \leq z < 1.0$ .

## 8 Performance of the RICH detector in 2012

In 2012 a DVCS test run was performed, resulting in five weeks of data taking (W44-W48). The data can be found at [/castor/cern.ch/compass/data/2012/oracle\\_dst](http://castor/cern.ch/compass/data/2012/oracle_dst). To determine the RICH efficiency a  $K_0$ ,  $\Lambda_0/\bar{\Lambda}_0$  and  $\Phi_0$  sample was selected, following the procedure described in section 1.1. To determine the probability of identify pions, kaons and protons correctly by the RICH the method of section 3 is applied.

As mentioned before the efficiencies are mostly depending on the momentum and angle of the particle crossing the fiducial volume of the detector. The probability is plotted as a function of the momentum (using the binning mentioned in section 3) for each angle interval. Because of the smaller dataset in 2012 compared to the dataset of 2011 the the last angle bin cannot be used, so only three bins are left (0.0, 0.01, 0.04, 0.12 rad). Even then there is no sufficient amount of statistics to determine the efficiencies properly for momenta larger than  $27\text{ GeV}/c$  in the last angle bin.

In the following the probabilities for identifying each particle (pion, kaon, (anti)proton) as a pion, kaon or proton and the probability that the particle can not be identified as one of these are shown in comparison to the results of 2011.

### 8.1 Comparison of the efficiencies of 2011 to 2012

The figures 30, 31 and 32 show the comparison of the identification probability for negative charged pions for each angle bin. One can see that there is a good agreement for the full momentum range and each angle bin. Even for the largest angles they agree very well until particle momenta of  $27\text{ GeV}/c$ . For larger momenta there are too few events in 2012 to do a proper prediction of the probabilities. One can also observe some deviations e.g. at very small angles ( $< 0.01\text{ rad}$ ) and high particle momenta ( $> 35\text{ GeV}/c$ ). This deviation is caused by a few events ( $< 3$  events) for which the uncertainties seems to be underestimated.

Also if one compares the probabilities of the identification of a positive charged pion for 2011 and 2012 one observes (see appendix figures 33, 34 and 35) that there is also a very good agreement.

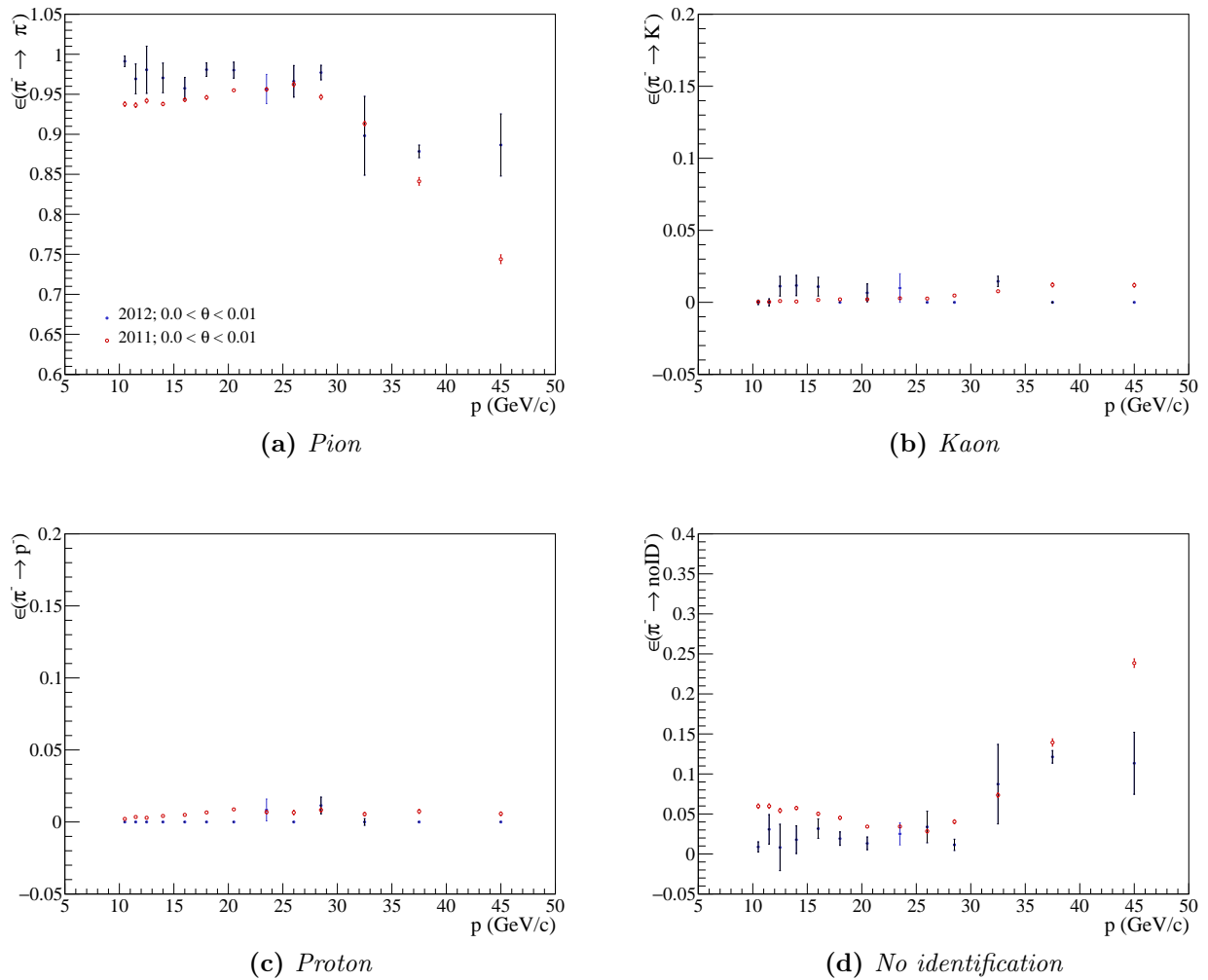


**Figure 30:** Comparison of the probability to identify negatively charged pions with angles between 0.0 and 0.01 rad for 2011 (red) and 2012 (blue).

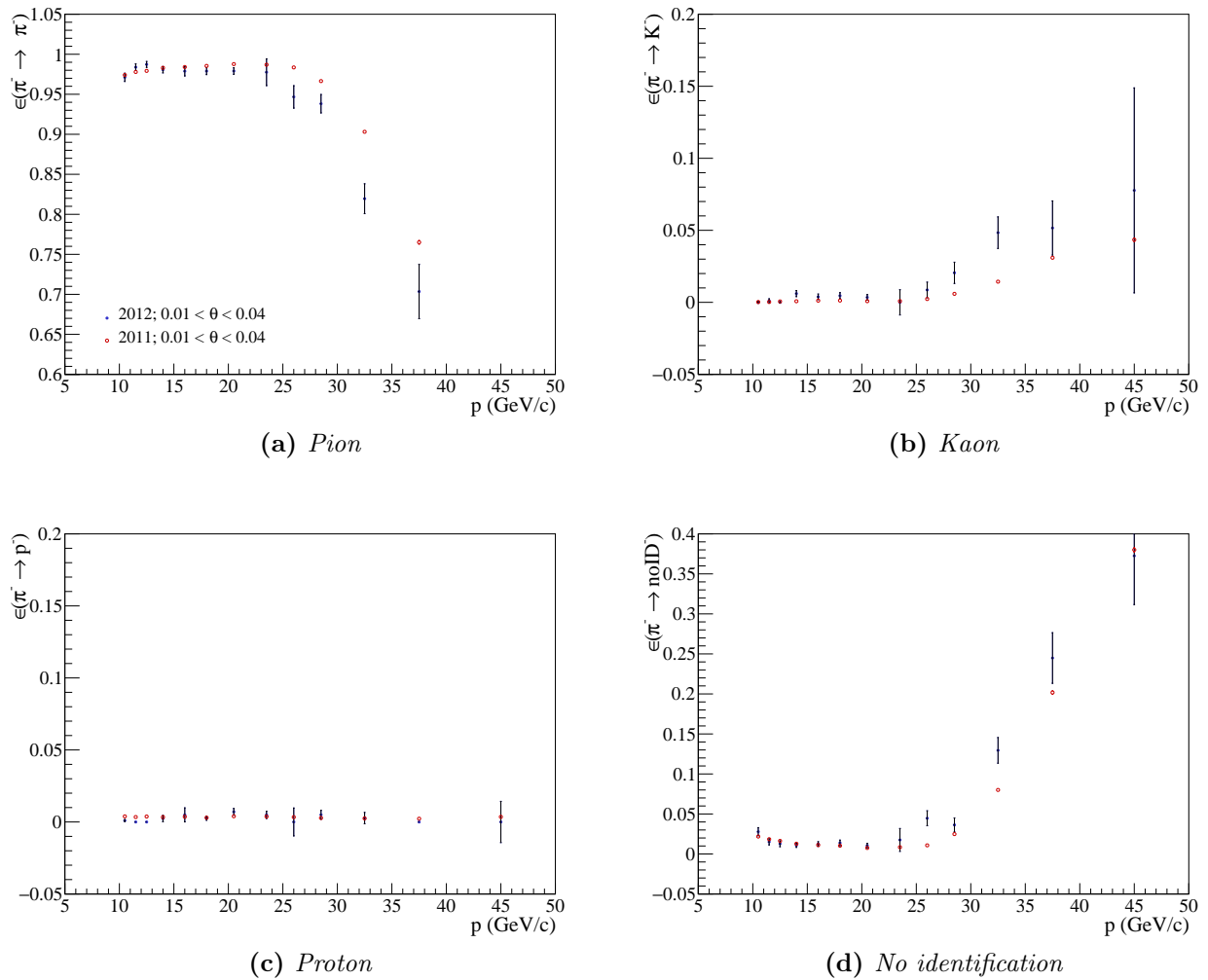


**Figure 31:** Comparison of the probability to identify negatively charged pions with angles between 0.01 and 0.04 rad for 2011 (red) and 2012 (blue).

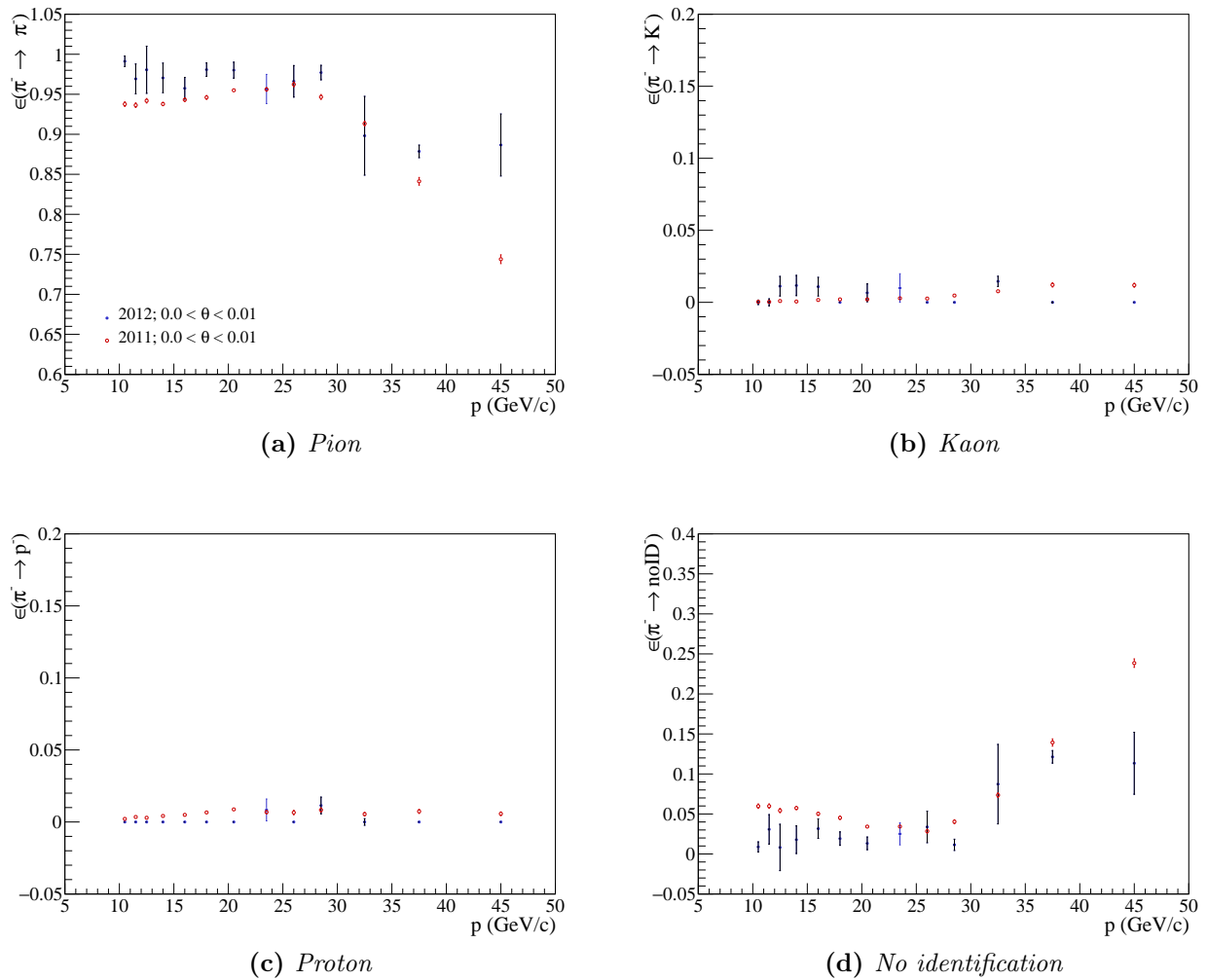


**Figure 32:** Comparison of the probability to identify negatively charged pions with angles between 0.04 and 0.12 rad for 2011 (red) and 2012 (blue).

The same is true for identifying negatively and positively charged kaons (see figures 36 - 41 in the appendix), as well as for antiprotons and protons (see figures 42 - 47 in the appendix). The efficiencies one gets for the 2012 data are showing a very good agreement with the 2011 data sample. All deviations are caused by single events. Because of the larger errors it is obvious that the data sample of the kaons and (anti)protons has even less statistics than the one of the pions.

## 8.2 Conclusion

In summary the RICH shows a stable performance during all the years. In 2012 the accuracy of the determinated efficiencies is limited by the small amount of data, but due to the good agreement within the errors with the 2011 efficiencies, they can also be used for the extraction of results from the 2012 data.

## References

- [1] Q. Curiel et al. (2013), COMPASS Note 2013-3.
- [2] P. Schiavon (2011), progress report, URL <http://wwwcompass.cern.ch/compass/detector/rich/like500.ps.gz>.
- [3] M. Stolarski (2016), talk at the October analysis meeting, URL [http://wwwcompass.cern.ch/compass/software/analysis/transparencies/2016/am\\_161013/talks/stolarski\\_161013.pdf](http://wwwcompass.cern.ch/compass/software/analysis/transparencies/2016/am_161013/talks/stolarski_161013.pdf).
- [4] M. Wilfert (2016), talk at the October analysis meeting, URL [http://wwwcompass.cern.ch/compass/software/analysis/transparencies/2016/am\\_161013/talks/wilfert\\_161013.pdf](http://wwwcompass.cern.ch/compass/software/analysis/transparencies/2016/am_161013/talks/wilfert_161013.pdf).
- [5] K. A. Olive et al. (Particle Data Group), Chin. Phys. **C38**, 090001 (2014).
- [6] F. Sozzi, Ph.D. thesis, Trieste U. (2007), URL <https://cds.cern.ch/record/1493519>.
- [7] Q. M. Curiel Garcia, Ph.D. thesis, U. Paris-Sud (2014).

## A Tables for the RICH efficiency in 2011 using the strict LH cuts













## B Tables for the RICH efficiency in 2011 using the 2007 LH cuts



**Table 12:** *RICH efficiency tables for  $k^+$ .*

RANGE	$\epsilon(k^+ \rightarrow \pi^+)$	$\epsilon(k^+ \rightarrow k^+)$	$\epsilon(k^+ \rightarrow p)$	$\epsilon(k^+ \rightarrow \text{NO ID})$
$0.00 \leq \theta < 0.01$				
$10\text{GeV}/c^2 \leq p < 11\text{GeV}/c^2$	$0.443 \pm 0.045$	$0.487 \pm 0.042$	$0.048 \pm 0.013$	$0.0223 \pm 0.0083$
$11\text{GeV}/c^2 \leq p < 12\text{GeV}/c^2$	$0.238 \pm 0.070$	$0.741 \pm 0.069$	$0.0122 \pm 0.0069$	$0.0091 \pm 0.0062$
$12\text{GeV}/c^2 \leq p < 13\text{GeV}/c^2$	$0.188 \pm 0.039$	$0.796 \pm 0.039$	$0.0115 \pm 0.0066$	$0.0043 \pm 0.0041$
$13\text{GeV}/c^2 \leq p < 15\text{GeV}/c^2$	$0.073 \pm 0.026$	$0.919 \pm 0.026$	$0.0000 \pm 0.0013$	$0.0082 \pm 0.0030$
$15\text{GeV}/c^2 \leq p < 17\text{GeV}/c^2$	$0.068 \pm 0.042$	$0.926 \pm 0.042$	$0.0000 \pm 0.0012$	$0.0067 \pm 0.0026$
$17\text{GeV}/c^2 \leq p < 19\text{GeV}/c^2$	$0.020 \pm 0.023$	$0.975 \pm 0.023$	$0.0000 \pm 0.0014$	$0.0047 \pm 0.0024$
$19\text{GeV}/c^2 \leq p < 22\text{GeV}/c^2$	$0.050 \pm 0.019$	$0.947 \pm 0.019$	$0.0000 \pm 0.0013$	$0.0025 \pm 0.0015$
$22\text{GeV}/c^2 \leq p < 25\text{GeV}/c^2$	$0.042 \pm 0.018$	$0.942 \pm 0.018$	$0.0115 \pm 0.0045$	$0.0043 \pm 0.0016$
$25\text{GeV}/c^2 \leq p < 27\text{GeV}/c^2$	$0.027 \pm 0.025$	$0.965 \pm 0.025$	$0.0081 \pm 0.0058$	$0.0000 \pm 0.0012$
$27\text{GeV}/c^2 \leq p < 30\text{GeV}/c^2$	$0.071 \pm 0.019$	$0.926 \pm 0.019$	$0.0000 \pm 0.0023$	$0.0024 \pm 0.0020$
$30\text{GeV}/c^2 \leq p < 35\text{GeV}/c^2$	$0.143 \pm 0.015$	$0.855 \pm 0.015$	$0.0000 \pm 0.0011$	$0.0022 \pm 0.0011$
$35\text{GeV}/c^2 \leq p < 40\text{GeV}/c^2$	$0.235 \pm 0.023$	$0.760 \pm 0.023$	$0.0029 \pm 0.0044$	$0.0017 \pm 0.0012$
$40\text{GeV}/c^2 \leq p < 50\text{GeV}/c^2$	$0.364 \pm 0.034$	$0.632 \pm 0.034$	$0.0042 \pm 0.0037$	$0.0000 \pm 0.0011$
$0.01 \leq \theta < 0.04$				
$10\text{GeV}/c^2 \leq p < 11\text{GeV}/c^2$	$0.262 \pm 0.013$	$0.704 \pm 0.013$	$0.0243 \pm 0.0032$	$0.0094 \pm 0.0019$
$11\text{GeV}/c^2 \leq p < 12\text{GeV}/c^2$	$0.106 \pm 0.014$	$0.887 \pm 0.014$	$0.0069 \pm 0.0024$	$0.00024 \pm 0.00063$
$12\text{GeV}/c^2 \leq p < 13\text{GeV}/c^2$	$0.109 \pm 0.011$	$0.881 \pm 0.011$	$0.0095 \pm 0.0020$	$0.00065 \pm 0.00066$
$13\text{GeV}/c^2 \leq p < 15\text{GeV}/c^2$	$0.026 \pm 0.011$	$0.968 \pm 0.011$	$0.0052 \pm 0.0014$	$0.00056 \pm 0.00045$
$15\text{GeV}/c^2 \leq p < 17\text{GeV}/c^2$	$0.0205 \pm 0.0077$	$0.9728 \pm 0.0078$	$0.0051 \pm 0.0013$	$0.00158 \pm 0.00044$
$17\text{GeV}/c^2 \leq p < 19\text{GeV}/c^2$	$0.0255 \pm 0.0082$	$0.9661 \pm 0.0082$	$0.0076 \pm 0.0013$	$0.00085 \pm 0.00036$
$19\text{GeV}/c^2 \leq p < 22\text{GeV}/c^2$	$0.0068 \pm 0.0060$	$0.9834 \pm 0.0061$	$0.0098 \pm 0.0016$	$0.00011 \pm 0.00011$
$22\text{GeV}/c^2 \leq p < 25\text{GeV}/c^2$	$0.0067 \pm 0.0054$	$0.9847 \pm 0.0056$	$0.0073 \pm 0.0019$	$0.00129 \pm 0.00038$
$25\text{GeV}/c^2 \leq p < 27\text{GeV}/c^2$	$0.0014 \pm 0.0013$	$0.9858 \pm 0.0027$	$0.0106 \pm 0.0023$	$0.00221 \pm 0.00057$
$27\text{GeV}/c^2 \leq p < 30\text{GeV}/c^2$	$0.0162 \pm 0.0060$	$0.9750 \pm 0.0062$	$0.0070 \pm 0.0019$	$0.00172 \pm 0.00053$
$30\text{GeV}/c^2 \leq p < 35\text{GeV}/c^2$	$0.0154 \pm 0.0056$	$0.9752 \pm 0.0058$	$0.0062 \pm 0.0017$	$0.00314 \pm 0.00054$
$35\text{GeV}/c^2 \leq p < 40\text{GeV}/c^2$	$0.0368 \pm 0.0063$	$0.9608 \pm 0.0066$	$0.0015 \pm 0.0020$	$0.00091 \pm 0.00053$
$40\text{GeV}/c^2 \leq p < 50\text{GeV}/c^2$	$0.0769 \pm 0.0078$	$0.9130 \pm 0.0081$	$0.0085 \pm 0.0024$	$0.00165 \pm 0.00044$
$0.04 \leq \theta < 0.12$				
$10\text{GeV}/c^2 \leq p < 11\text{GeV}/c^2$	$0.126 \pm 0.013$	$0.837 \pm 0.013$	$0.0286 \pm 0.0032$	$0.0077 \pm 0.0015$
$11\text{GeV}/c^2 \leq p < 12\text{GeV}/c^2$	$0.026 \pm 0.013$	$0.961 \pm 0.013$	$0.0125 \pm 0.0026$	$0.00123 \pm 0.00090$
$12\text{GeV}/c^2 \leq p < 13\text{GeV}/c^2$	$0.017 \pm 0.013$	$0.976 \pm 0.013$	$0.0052 \pm 0.0028$	$0.00131 \pm 0.00092$
$13\text{GeV}/c^2 \leq p < 15\text{GeV}/c^2$	$0.0303 \pm 0.0090$	$0.9604 \pm 0.0092$	$0.0077 \pm 0.0021$	$0.00164 \pm 0.00071$
$15\text{GeV}/c^2 \leq p < 17\text{GeV}/c^2$	$0.0199 \pm 0.0094$	$0.9664 \pm 0.0097$	$0.0131 \pm 0.0025$	$0.00069 \pm 0.00065$
$17\text{GeV}/c^2 \leq p < 19\text{GeV}/c^2$	$0.000 \pm 0.052$	$0.993 \pm 0.052$	$0.0075 \pm 0.0033$	$0.00000 \pm 0.00029$
$19\text{GeV}/c^2 \leq p < 22\text{GeV}/c^2$	$0.0300 \pm 0.0096$	$0.953 \pm 0.010$	$0.0171 \pm 0.0043$	$0.000000 \pm 0.000098$
$22\text{GeV}/c^2 \leq p < 25\text{GeV}/c^2$	$0.0001 \pm 0.0028$	$0.9932 \pm 0.0074$	$0.0067 \pm 0.0067$	$0.00000 \pm 0.00047$
$25\text{GeV}/c^2 \leq p < 27\text{GeV}/c^2$	$0.015 \pm 0.023$	$0.984 \pm 0.030$	$0.000 \pm 0.018$	$0.0018 \pm 0.0021$
$27\text{GeV}/c^2 \leq p < 30\text{GeV}/c^2$	$0.016 \pm 0.025$	$0.977 \pm 0.027$	$0.0063 \pm 0.0100$	$0.0005 \pm 0.0017$
$30\text{GeV}/c^2 \leq p < 35\text{GeV}/c^2$	$0.013 \pm 0.031$	$0.979 \pm 0.033$	$0.007 \pm 0.014$	$0.0000 \pm 0.0012$
$35\text{GeV}/c^2 \leq p < 40\text{GeV}/c^2$	$0.138 \pm 0.054$	$0.862 \pm 0.055$	$0.000 \pm 0.012$	$0.0000 \pm 0.0042$
$40\text{GeV}/c^2 \leq p < 50\text{GeV}/c^2$	$0.164 \pm 0.070$	$0.773 \pm 0.083$	$0.063 \pm 0.049$	$0.0 \pm 0.0$
$0.12 \leq \theta < 0.30$				
$10\text{GeV}/c^2 \leq p < 11\text{GeV}/c^2$	$0.018 \pm 0.090$	$0.962 \pm 0.099$	$0.021 \pm 0.054$	$0.0000 \pm 0.0024$
$11\text{GeV}/c^2 \leq p < 12\text{GeV}/c^2$	$0.168 \pm 0.078$	$0.808 \pm 0.086$	$0.024 \pm 0.048$	$0.0 \pm 0.0$
$12\text{GeV}/c^2 \leq p < 13\text{GeV}/c^2$	$0.000 \pm 0.067$	$0.88 \pm 0.11$	$0.115 \pm 0.089$	$0.0000 \pm 0.0086$
$13\text{GeV}/c^2 \leq p < 15\text{GeV}/c^2$	$0.00 \pm 0.25$	$0.88 \pm 0.23$	$0.117 \pm 0.076$	$0.0 \pm 0.0$
$15\text{GeV}/c^2 \leq p < 17\text{GeV}/c^2$	$0.12 \pm 0.16$	$0.88 \pm 0.17$	$0.000 \pm 0.037$	$0.000 \pm 0.033$
$17\text{GeV}/c^2 \leq p < 19\text{GeV}/c^2$	$0.000 \pm 0.080$	$1.00 \pm 0.17$	$0.000 \pm 0.078$	$0.00 \pm 0.12$
$19\text{GeV}/c^2 \leq p < 22\text{GeV}/c^2$	$0.000 \pm 0.048$	$0.80 \pm 0.11$	$0.20 \pm 0.10$	$0.0 \pm 0.0$





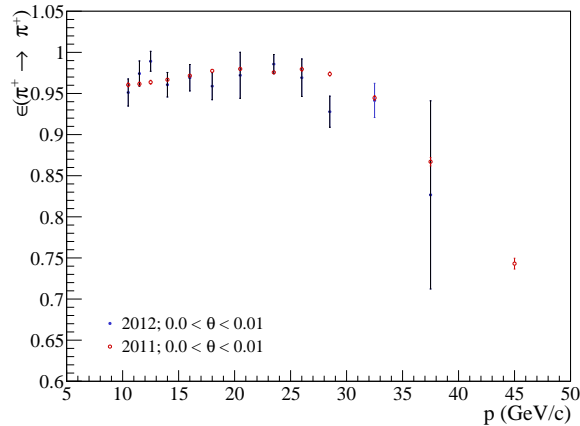
**Table 15:** *RICH efficiency tables for  $k^-$ .*

RANGE	$\epsilon(k^- \rightarrow \pi^-)$	$\epsilon(k^- \rightarrow k^-)$	$\epsilon(k^- \rightarrow \bar{p})$	$\epsilon(k^- \rightarrow \text{no ID})$
$0.00 \leq \theta < 0.01$				
$10\text{GeV}/c^2 \leq p < 11\text{GeV}/c^2$	$0.449 \pm 0.045$	$0.470 \pm 0.042$	$0.042 \pm 0.011$	$0.0384 \pm 0.0097$
$11\text{GeV}/c^2 \leq p < 12\text{GeV}/c^2$	$0.278 \pm 0.046$	$0.707 \pm 0.046$	$0.0102 \pm 0.0070$	$0.0048 \pm 0.0063$
$12\text{GeV}/c^2 \leq p < 13\text{GeV}/c^2$	$0.187 \pm 0.049$	$0.804 \pm 0.049$	$0.0004 \pm 0.0041$	$0.0081 \pm 0.0075$
$13\text{GeV}/c^2 \leq p < 15\text{GeV}/c^2$	$0.132 \pm 0.025$	$0.856 \pm 0.025$	$0.0068 \pm 0.0043$	$0.0054 \pm 0.0039$
$15\text{GeV}/c^2 \leq p < 17\text{GeV}/c^2$	$0.143 \pm 0.023$	$0.842 \pm 0.024$	$0.0120 \pm 0.0043$	$0.0032 \pm 0.0029$
$17\text{GeV}/c^2 \leq p < 19\text{GeV}/c^2$	$0.038 \pm 0.028$	$0.941 \pm 0.028$	$0.0125 \pm 0.0042$	$0.0091 \pm 0.0034$
$19\text{GeV}/c^2 \leq p < 22\text{GeV}/c^2$	$0.053 \pm 0.020$	$0.923 \pm 0.020$	$0.0225 \pm 0.0045$	$0.0015 \pm 0.0014$
$22\text{GeV}/c^2 \leq p < 25\text{GeV}/c^2$	$0.017 \pm 0.021$	$0.955 \pm 0.021$	$0.0247 \pm 0.0057$	$0.0030 \pm 0.0022$
$25\text{GeV}/c^2 \leq p < 27\text{GeV}/c^2$	$0.079 \pm 0.020$	$0.911 \pm 0.021$	$0.0029 \pm 0.0050$	$0.0064 \pm 0.0030$
$27\text{GeV}/c^2 \leq p < 30\text{GeV}/c^2$	$0.133 \pm 0.020$	$0.856 \pm 0.021$	$0.0074 \pm 0.0046$	$0.0036 \pm 0.0025$
$30\text{GeV}/c^2 \leq p < 35\text{GeV}/c^2$	$0.202 \pm 0.018$	$0.785 \pm 0.018$	$0.0059 \pm 0.0034$	$0.0072 \pm 0.0020$
$35\text{GeV}/c^2 \leq p < 40\text{GeV}/c^2$	$0.300 \pm 0.018$	$0.687 \pm 0.018$	$0.0074 \pm 0.0040$	$0.0059 \pm 0.0021$
$40\text{GeV}/c^2 \leq p < 50\text{GeV}/c^2$	$0.457 \pm 0.019$	$0.537 \pm 0.019$	$0.0036 \pm 0.0032$	$0.0024 \pm 0.0015$
$0.01 \leq \theta < 0.04$				
$10\text{GeV}/c^2 \leq p < 11\text{GeV}/c^2$	$0.251 \pm 0.015$	$0.713 \pm 0.015$	$0.0277 \pm 0.0033$	$0.0079 \pm 0.0019$
$11\text{GeV}/c^2 \leq p < 12\text{GeV}/c^2$	$0.120 \pm 0.015$	$0.865 \pm 0.014$	$0.0130 \pm 0.0022$	$0.00236 \pm 0.00088$
$12\text{GeV}/c^2 \leq p < 13\text{GeV}/c^2$	$0.075 \pm 0.014$	$0.914 \pm 0.014$	$0.0106 \pm 0.0022$	$0.00062 \pm 0.00072$
$13\text{GeV}/c^2 \leq p < 15\text{GeV}/c^2$	$0.034 \pm 0.010$	$0.956 \pm 0.010$	$0.0085 \pm 0.0014$	$0.00082 \pm 0.00042$
$15\text{GeV}/c^2 \leq p < 17\text{GeV}/c^2$	$0.0339 \pm 0.0091$	$0.9599 \pm 0.0091$	$0.0050 \pm 0.0012$	$0.00132 \pm 0.00041$
$17\text{GeV}/c^2 \leq p < 19\text{GeV}/c^2$	$0.0167 \pm 0.0079$	$0.9761 \pm 0.0080$	$0.0067 \pm 0.0013$	$0.00042 \pm 0.00035$
$19\text{GeV}/c^2 \leq p < 22\text{GeV}/c^2$	$0.0040 \pm 0.0019$	$0.9870 \pm 0.0024$	$0.0089 \pm 0.0015$	$0.00006 \pm 0.00011$
$22\text{GeV}/c^2 \leq p < 25\text{GeV}/c^2$	$0.00111 \pm 0.00092$	$0.9891 \pm 0.0020$	$0.0082 \pm 0.0017$	$0.00163 \pm 0.00040$
$25\text{GeV}/c^2 \leq p < 27\text{GeV}/c^2$	$0.0202 \pm 0.0069$	$0.9697 \pm 0.0072$	$0.0082 \pm 0.0020$	$0.00181 \pm 0.00065$
$27\text{GeV}/c^2 \leq p < 30\text{GeV}/c^2$	$0.00000 \pm 0.00025$	$0.9911 \pm 0.0021$	$0.0071 \pm 0.0019$	$0.00181 \pm 0.00059$
$30\text{GeV}/c^2 \leq p < 35\text{GeV}/c^2$	$0.0103 \pm 0.0062$	$0.9822 \pm 0.0066$	$0.0055 \pm 0.0016$	$0.00203 \pm 0.00049$
$35\text{GeV}/c^2 \leq p < 40\text{GeV}/c^2$	$0.0397 \pm 0.0064$	$0.9495 \pm 0.0066$	$0.0088 \pm 0.0019$	$0.00192 \pm 0.00058$
$40\text{GeV}/c^2 \leq p < 50\text{GeV}/c^2$	$0.0609 \pm 0.0067$	$0.9294 \pm 0.0070$	$0.0082 \pm 0.0022$	$0.00141 \pm 0.00069$
$0.04 \leq \theta < 0.12$				
$10\text{GeV}/c^2 \leq p < 11\text{GeV}/c^2$	$0.114 \pm 0.014$	$0.848 \pm 0.013$	$0.0283 \pm 0.0030$	$0.0094 \pm 0.0015$
$11\text{GeV}/c^2 \leq p < 12\text{GeV}/c^2$	$0.043 \pm 0.013$	$0.940 \pm 0.013$	$0.0154 \pm 0.0023$	$0.00155 \pm 0.00080$
$12\text{GeV}/c^2 \leq p < 13\text{GeV}/c^2$	$0.029 \pm 0.013$	$0.959 \pm 0.013$	$0.0090 \pm 0.0025$	$0.00218 \pm 0.00073$
$13\text{GeV}/c^2 \leq p < 15\text{GeV}/c^2$	$0.0000 \pm 0.0035$	$0.9883 \pm 0.0062$	$0.0116 \pm 0.0020$	$0.0001 \pm 0.0046$
$15\text{GeV}/c^2 \leq p < 17\text{GeV}/c^2$	$0.00000 \pm 0.00033$	$0.9889 \pm 0.0023$	$0.0104 \pm 0.0022$	$0.00068 \pm 0.00059$
$17\text{GeV}/c^2 \leq p < 19\text{GeV}/c^2$	$0.0000 \pm 0.0011$	$0.9811 \pm 0.0033$	$0.0173 \pm 0.0030$	$0.00155 \pm 0.00075$
$19\text{GeV}/c^2 \leq p < 22\text{GeV}/c^2$	$0.0000 \pm 0.0040$	$0.9897 \pm 0.0056$	$0.0102 \pm 0.0040$	$0.00014 \pm 0.00022$
$22\text{GeV}/c^2 \leq p < 25\text{GeV}/c^2$	$0.0000 \pm 0.0043$	$0.9844 \pm 0.0080$	$0.0122 \pm 0.0065$	$0.0035 \pm 0.0016$
$25\text{GeV}/c^2 \leq p < 27\text{GeV}/c^2$	$0.015 \pm 0.022$	$0.945 \pm 0.024$	$0.036 \pm 0.010$	$0.0040 \pm 0.0024$
$27\text{GeV}/c^2 \leq p < 30\text{GeV}/c^2$	$0.048 \pm 0.022$	$0.947 \pm 0.023$	$0.0046 \pm 0.0088$	$0.0000 \pm 0.0013$
$30\text{GeV}/c^2 \leq p < 35\text{GeV}/c^2$	$0.013 \pm 0.026$	$0.964 \pm 0.030$	$0.019 \pm 0.014$	$0.0043 \pm 0.0045$
$35\text{GeV}/c^2 \leq p < 40\text{GeV}/c^2$	$0.042 \pm 0.049$	$0.951 \pm 0.052$	$0.007 \pm 0.020$	$0.0000 \pm 0.0047$
$40\text{GeV}/c^2 \leq p < 50\text{GeV}/c^2$	$0.24 \pm 0.13$	$0.60 \pm 0.14$	$0.165 \pm 0.074$	$0.0 \pm 0.0$
$0.12 \leq \theta < 0.30$				
$10\text{GeV}/c^2 \leq p < 11\text{GeV}/c^2$	$0.146 \pm 0.085$	$0.806 \pm 0.086$	$0.000 \pm 0.023$	$0.049 \pm 0.024$
$11\text{GeV}/c^2 \leq p < 12\text{GeV}/c^2$	$0.08 \pm 0.13$	$0.89 \pm 0.13$	$0.028 \pm 0.050$	$0.000 \pm 0.013$
$12\text{GeV}/c^2 \leq p < 13\text{GeV}/c^2$	$0.29 \pm 0.22$	$0.63 \pm 0.23$	$0.037 \pm 0.077$	$0.045 \pm 0.032$
$13\text{GeV}/c^2 \leq p < 15\text{GeV}/c^2$	$0.0 \pm 1.1$	$0.92 \pm 1.00$	$0.08 \pm 0.16$	$0.0 \pm 0.0$
$15\text{GeV}/c^2 \leq p < 17\text{GeV}/c^2$	$0.00 \pm 0.10$	$0.92 \pm 0.14$	$0.083 \pm 0.086$	$0.000 \pm 0.063$
$17\text{GeV}/c^2 \leq p < 19\text{GeV}/c^2$	$0.00 \pm 0.38$	$0.84 \pm 0.34$	$0.081 \pm 0.080$	$0.081 \pm 0.057$
$19\text{GeV}/c^2 \leq p < 22\text{GeV}/c^2$	$0.51 \pm 0.26$	$0.49 \pm 0.26$	$0.000 \pm 0.041$	$0.0 \pm 0.0$

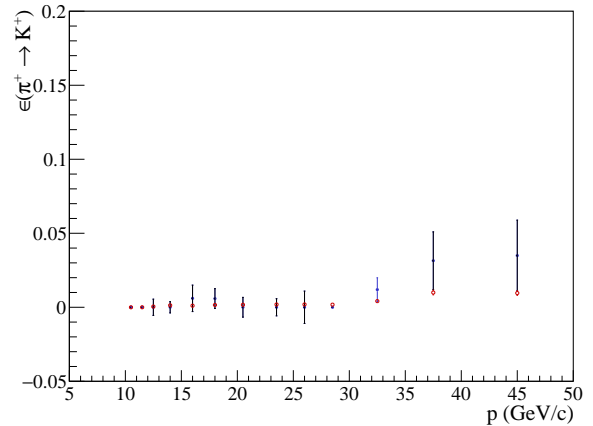
**Table 16:** *RICH efficiency tables for  $\bar{p}$ .*

RANGE	$\epsilon(\bar{p} \rightarrow \pi^-)$	$\epsilon(\bar{p} \rightarrow k^-)$	$\epsilon(\bar{p} \rightarrow \bar{p})$	$\epsilon(\bar{p} \rightarrow \text{no ID})$
$0.00 \leq \theta < 0.01$				
$10\text{GeV}/c^2 \leq p < 11\text{GeV}/c^2$	$0.618 \pm 0.042$	$0.121 \pm 0.026$	$0.238 \pm 0.035$	$0.023 \pm 0.012$
$11\text{GeV}/c^2 \leq p < 12\text{GeV}/c^2$	$0.451 \pm 0.036$	$0.250 \pm 0.028$	$0.268 \pm 0.029$	$0.031 \pm 0.011$
$12\text{GeV}/c^2 \leq p < 13\text{GeV}/c^2$	$0.448 \pm 0.023$	$0.280 \pm 0.024$	$0.250 \pm 0.023$	$0.0212 \pm 0.0084$
$13\text{GeV}/c^2 \leq p < 15\text{GeV}/c^2$	$0.453 \pm 0.015$	$0.260 \pm 0.015$	$0.264 \pm 0.015$	$0.0226 \pm 0.0054$
$15\text{GeV}/c^2 \leq p < 17\text{GeV}/c^2$	$0.465 \pm 0.017$	$0.262 \pm 0.015$	$0.248 \pm 0.012$	$0.0245 \pm 0.0056$
$17\text{GeV}/c^2 \leq p < 19\text{GeV}/c^2$	$0.466 \pm 0.021$	$0.252 \pm 0.017$	$0.267 \pm 0.018$	$0.0148 \pm 0.0042$
$19\text{GeV}/c^2 \leq p < 22\text{GeV}/c^2$	$0.295 \pm 0.017$	$0.175 \pm 0.012$	$0.529 \pm 0.018$	$0.0005 \pm 0.0012$
$22\text{GeV}/c^2 \leq p < 25\text{GeV}/c^2$	$0.207 \pm 0.016$	$0.0581 \pm 0.0090$	$0.725 \pm 0.015$	$0.0093 \pm 0.0030$
$25\text{GeV}/c^2 \leq p < 27\text{GeV}/c^2$	$0.086 \pm 0.019$	$0.0269 \pm 0.0077$	$0.886 \pm 0.022$	$0.001 \pm 0.011$
$27\text{GeV}/c^2 \leq p < 30\text{GeV}/c^2$	$0.101 \pm 0.016$	$0.0268 \pm 0.0073$	$0.866 \pm 0.017$	$0.0063 \pm 0.0033$
$30\text{GeV}/c^2 \leq p < 35\text{GeV}/c^2$	$0.074 \pm 0.012$	$0.0164 \pm 0.0052$	$0.908 \pm 0.013$	$0.0022 \pm 0.0014$
$35\text{GeV}/c^2 \leq p < 40\text{GeV}/c^2$	$0.045 \pm 0.013$	$0.0570 \pm 0.0081$	$0.897 \pm 0.015$	$0.0007 \pm 0.0013$
$40\text{GeV}/c^2 \leq p < 50\text{GeV}/c^2$	$0.067 \pm 0.010$	$0.1010 \pm 0.0095$	$0.829 \pm 0.013$	$0.0027 \pm 0.0015$
$0.01 \leq \theta < 0.04$				
$10\text{GeV}/c^2 \leq p < 11\text{GeV}/c^2$	$0.371 \pm 0.014$	$0.220 \pm 0.010$	$0.387 \pm 0.012$	$0.0215 \pm 0.0035$
$11\text{GeV}/c^2 \leq p < 12\text{GeV}/c^2$	$0.299 \pm 0.011$	$0.2970 \pm 0.0089$	$0.3792 \pm 0.0097$	$0.0251 \pm 0.0029$
$12\text{GeV}/c^2 \leq p < 13\text{GeV}/c^2$	$0.2915 \pm 0.0068$	$0.2855 \pm 0.0073$	$0.4030 \pm 0.0078$	$0.0200 \pm 0.0023$
$13\text{GeV}/c^2 \leq p < 15\text{GeV}/c^2$	$0.3090 \pm 0.0055$	$0.2620 \pm 0.0048$	$0.4104 \pm 0.0054$	$0.0187 \pm 0.0014$
$15\text{GeV}/c^2 \leq p < 17\text{GeV}/c^2$	$0.3137 \pm 0.0060$	$0.2643 \pm 0.0046$	$0.4024 \pm 0.0052$	$0.0196 \pm 0.0014$
$17\text{GeV}/c^2 \leq p < 19\text{GeV}/c^2$	$0.3098 \pm 0.0066$	$0.2686 \pm 0.0053$	$0.4071 \pm 0.0061$	$0.0144 \pm 0.0014$
$19\text{GeV}/c^2 \leq p < 22\text{GeV}/c^2$	$0.1745 \pm 0.0047$	$0.1274 \pm 0.0035$	$0.6972 \pm 0.0052$	$0.00079 \pm 0.00030$
$22\text{GeV}/c^2 \leq p < 25\text{GeV}/c^2$	$0.0736 \pm 0.0040$	$0.0464 \pm 0.0025$	$0.8752 \pm 0.0046$	$0.00487 \pm 0.00080$
$25\text{GeV}/c^2 \leq p < 27\text{GeV}/c^2$	$0.0546 \pm 0.0050$	$0.0296 \pm 0.0027$	$0.9123 \pm 0.0056$	$0.00358 \pm 0.00099$
$27\text{GeV}/c^2 \leq p < 30\text{GeV}/c^2$	$0.0389 \pm 0.0043$	$0.0215 \pm 0.0021$	$0.9345 \pm 0.0048$	$0.0052 \pm 0.0010$
$30\text{GeV}/c^2 \leq p < 35\text{GeV}/c^2$	$0.0180 \pm 0.0035$	$0.0183 \pm 0.0020$	$0.9601 \pm 0.0040$	$0.00362 \pm 0.00072$
$35\text{GeV}/c^2 \leq p < 40\text{GeV}/c^2$	$0.0151 \pm 0.0040$	$0.0257 \pm 0.0028$	$0.9552 \pm 0.0049$	$0.00396 \pm 0.00099$
$40\text{GeV}/c^2 \leq p < 50\text{GeV}/c^2$	$0.0176 \pm 0.0037$	$0.0371 \pm 0.0033$	$0.9435 \pm 0.0049$	$0.00193 \pm 0.00068$
$0.04 \leq \theta < 0.12$				
$10\text{GeV}/c^2 \leq p < 11\text{GeV}/c^2$	$0.2096 \pm 0.0067$	$0.3065 \pm 0.0068$	$0.4607 \pm 0.0060$	$0.0232 \pm 0.0024$
$11\text{GeV}/c^2 \leq p < 12\text{GeV}/c^2$	$0.1812 \pm 0.0061$	$0.3208 \pm 0.0066$	$0.4755 \pm 0.0072$	$0.0226 \pm 0.0021$
$12\text{GeV}/c^2 \leq p < 13\text{GeV}/c^2$	$0.1560 \pm 0.0062$	$0.3010 \pm 0.0056$	$0.5210 \pm 0.0068$	$0.0220 \pm 0.0019$
$13\text{GeV}/c^2 \leq p < 15\text{GeV}/c^2$	$0.1842 \pm 0.0040$	$0.2639 \pm 0.0043$	$0.5303 \pm 0.0049$	$0.0216 \pm 0.0014$
$15\text{GeV}/c^2 \leq p < 17\text{GeV}/c^2$	$0.1883 \pm 0.0040$	$0.2585 \pm 0.0049$	$0.5311 \pm 0.0054$	$0.0221 \pm 0.0016$
$17\text{GeV}/c^2 \leq p < 19\text{GeV}/c^2$	$0.2030 \pm 0.0060$	$0.2434 \pm 0.0059$	$0.5332 \pm 0.0056$	$0.0203 \pm 0.0021$
$19\text{GeV}/c^2 \leq p < 22\text{GeV}/c^2$	$0.0935 \pm 0.0059$	$0.0973 \pm 0.0051$	$0.8077 \pm 0.0073$	$0.00149 \pm 0.00054$
$22\text{GeV}/c^2 \leq p < 25\text{GeV}/c^2$	$0.0347 \pm 0.0062$	$0.0253 \pm 0.0040$	$0.9310 \pm 0.0076$	$0.0090 \pm 0.0025$
$25\text{GeV}/c^2 \leq p < 27\text{GeV}/c^2$	$0.0151 \pm 0.0090$	$0.0208 \pm 0.0055$	$0.958 \pm 0.011$	$0.0060 \pm 0.0030$
$27\text{GeV}/c^2 \leq p < 30\text{GeV}/c^2$	$0.051 \pm 0.012$	$0.0118 \pm 0.0059$	$0.930 \pm 0.013$	$0.0078 \pm 0.0041$
$30\text{GeV}/c^2 \leq p < 35\text{GeV}/c^2$	$0.012 \pm 0.013$	$0.0020 \pm 0.0074$	$0.970 \pm 0.016$	$0.0159 \pm 0.0070$
$35\text{GeV}/c^2 \leq p < 40\text{GeV}/c^2$	$0.018 \pm 0.030$	$0.0000 \pm 0.0074$	$0.975 \pm 0.033$	$0.007 \pm 0.012$
$40\text{GeV}/c^2 \leq p < 50\text{GeV}/c^2$	$0.064 \pm 0.044$	$0.000 \pm 0.053$	$0.936 \pm 0.068$	$0.0000 \pm 0.0056$
$0.12 \leq \theta < 0.30$				
$10\text{GeV}/c^2 \leq p < 11\text{GeV}/c^2$	$0.045 \pm 0.023$	$0.110 \pm 0.027$	$0.836 \pm 0.032$	$0.0093 \pm 0.0049$
$11\text{GeV}/c^2 \leq p < 12\text{GeV}/c^2$	$0.073 \pm 0.027$	$0.206 \pm 0.043$	$0.700 \pm 0.049$	$0.021 \pm 0.020$
$12\text{GeV}/c^2 \leq p < 13\text{GeV}/c^2$	$0.069 \pm 0.035$	$0.220 \pm 0.043$	$0.684 \pm 0.046$	$0.027 \pm 0.016$
$13\text{GeV}/c^2 \leq p < 15\text{GeV}/c^2$	$0.076 \pm 0.035$	$0.109 \pm 0.038$	$0.814 \pm 0.048$	$0.0 \pm 0.0$
$15\text{GeV}/c^2 \leq p < 17\text{GeV}/c^2$	$0.190 \pm 0.069$	$0.111 \pm 0.056$	$0.699 \pm 0.081$	$0.0 \pm 0.0$
$17\text{GeV}/c^2 \leq p < 19\text{GeV}/c^2$	$0.29 \pm 0.14$	$0.30 \pm 0.16$	$0.41 \pm 0.17$	$0.0 \pm 0.0$
$19\text{GeV}/c^2 \leq p < 22\text{GeV}/c^2$	$0.34 \pm 0.16$	$0.0 \pm 0.0$	$0.66 \pm 0.16$	$0.0 \pm 0.0$

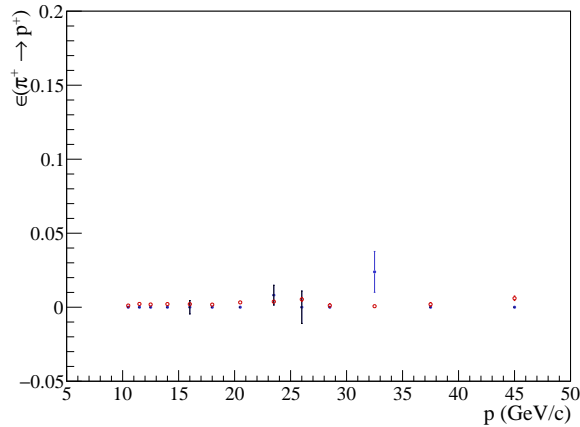
## C Comparison of RICH efficiencies in 2011 and 2012



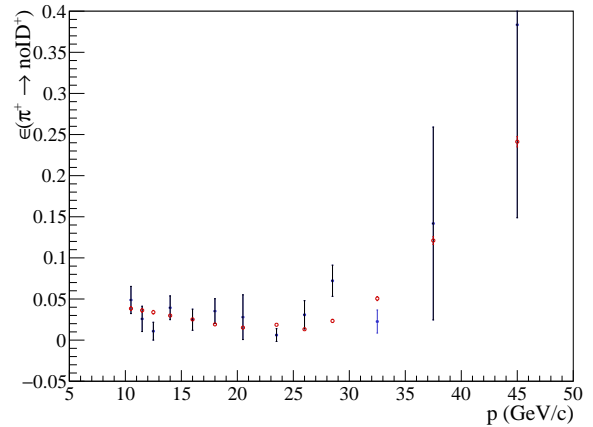
(a) *Pion*



(b) *Kaon*



(c) *Proton*



(d) *No identification*

**Figure 33:** Comparison of the probability to identify positively charged pions with angles between 0.0 and 0.01 rad.

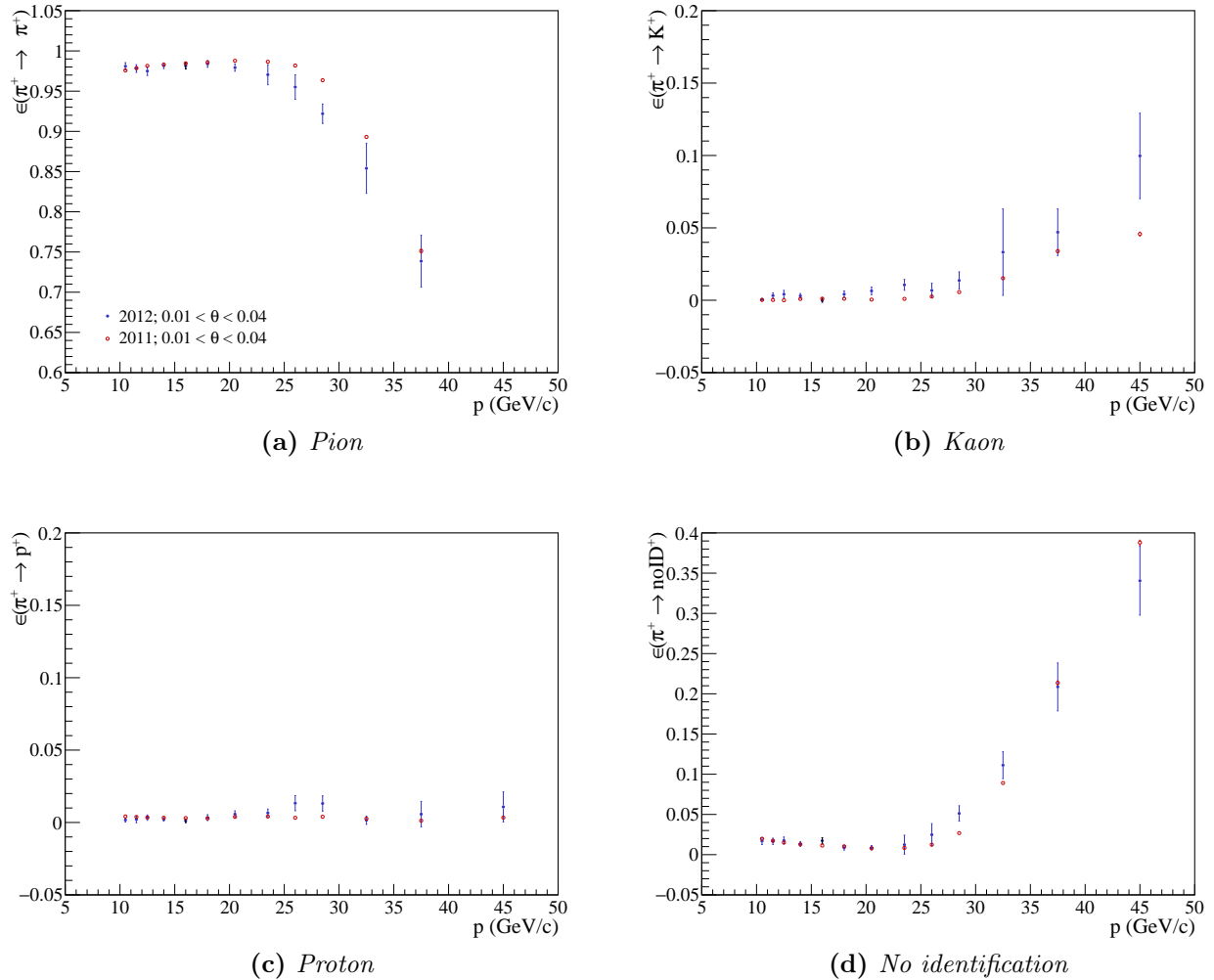
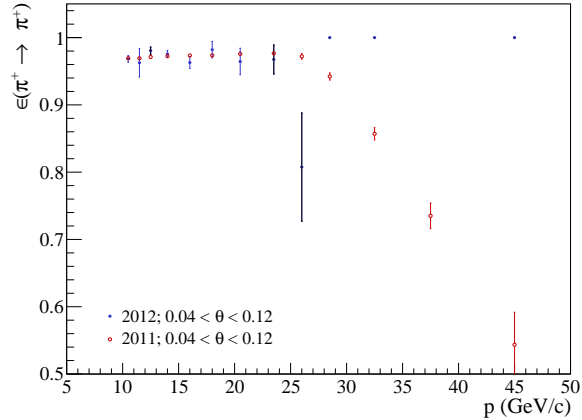
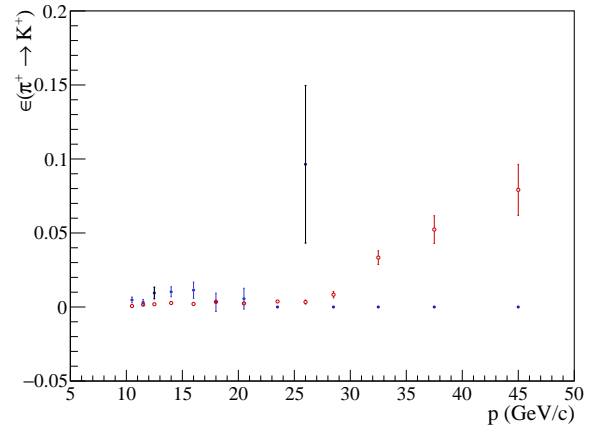


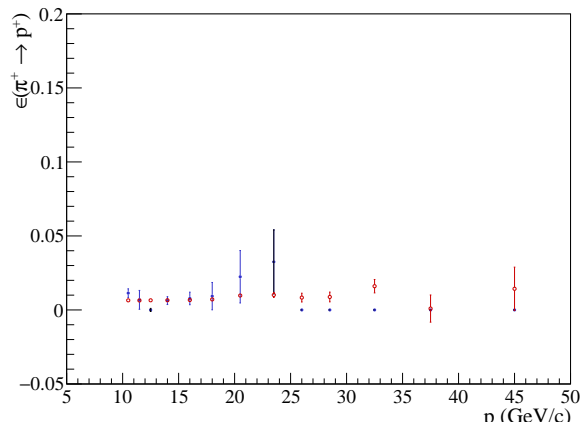
**Figure 34:** Comparison of the probability to identify positively charged pions with angles between 0.01 and 0.04 rad.



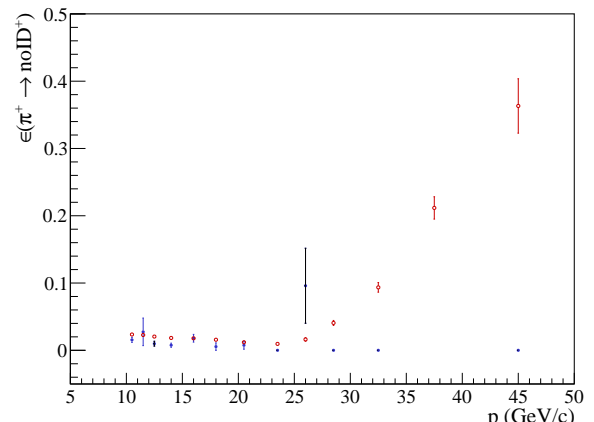
(a) *Pion*



(b) *Kaon*

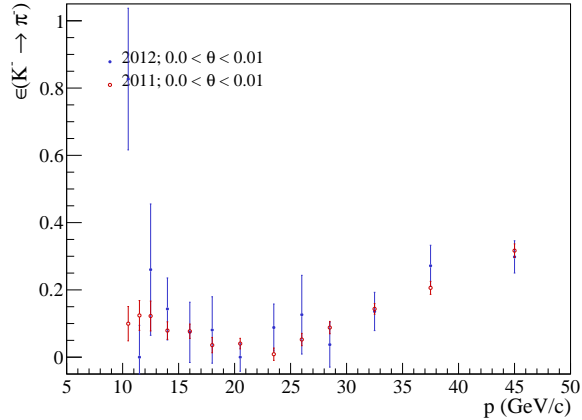


(c) *Proton*

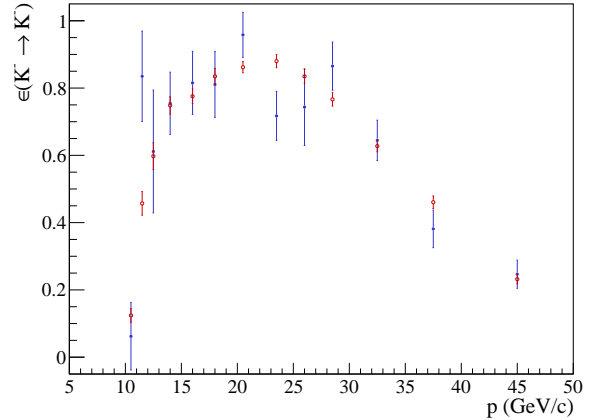


(d) *No identification*

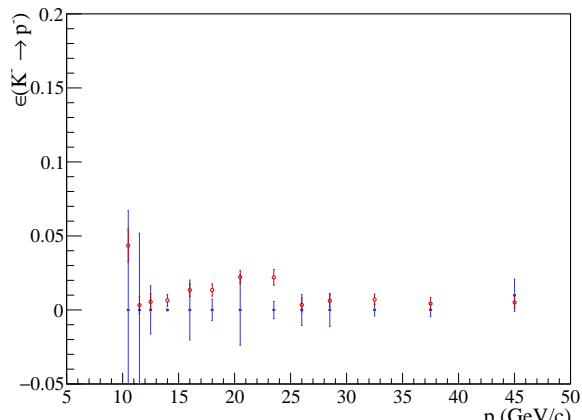
**Figure 35:** Comparison of the probability to identify positively charged pions with angles between 0.04 and 0.12 rad.



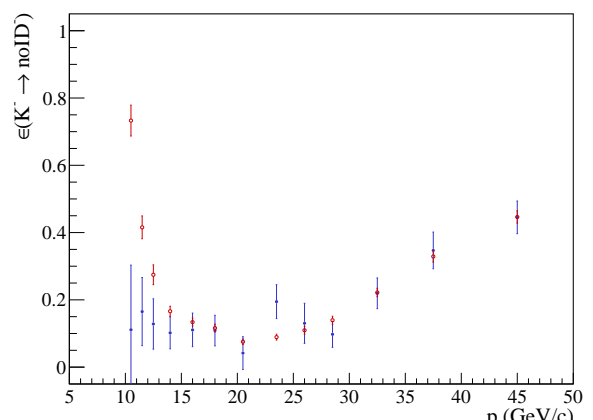
(a) *Pion*



(b) *Kaon*

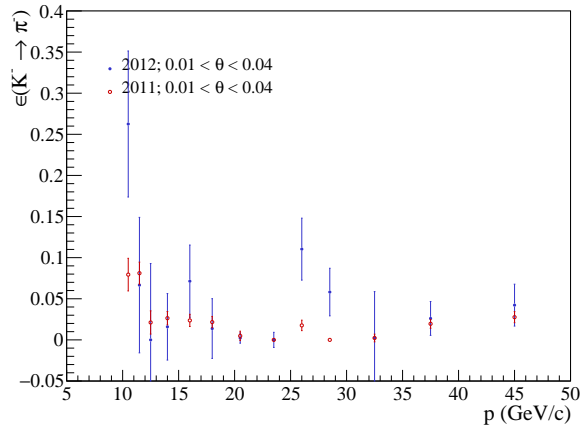


(c) *Proton*

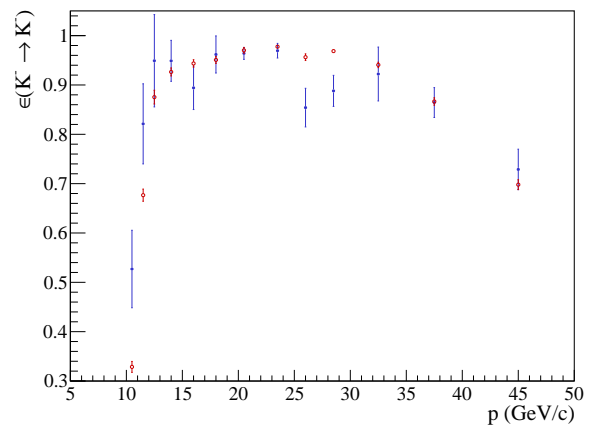


(d) *No identification*

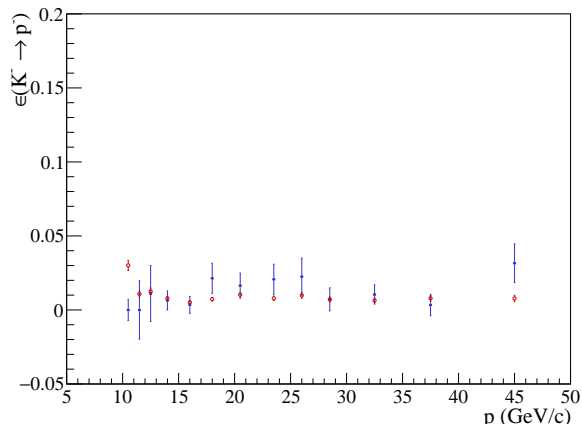
**Figure 36:** Comparison of the probability to identify negatively charged kaons with angles between 0.0 and 0.01 rad.



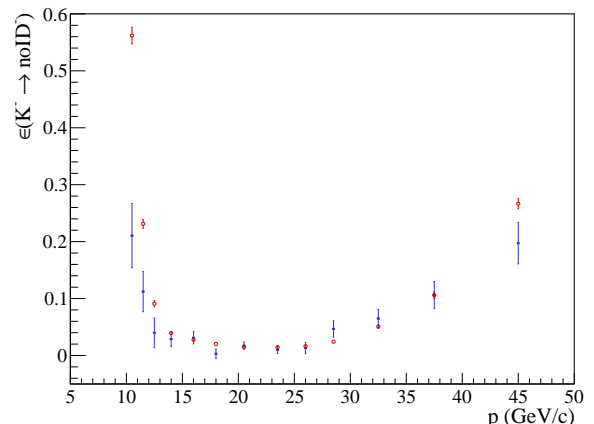
(a) *Pion*



(b) *Kaon*

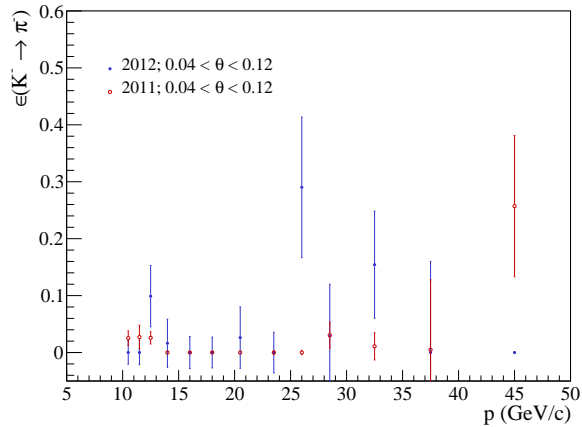


(c) *Proton*

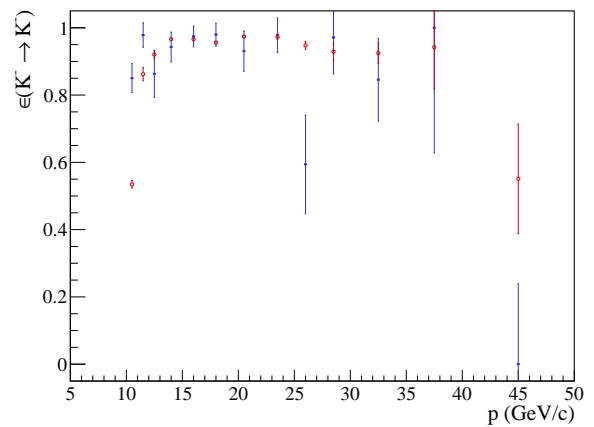


(d) *No identification*

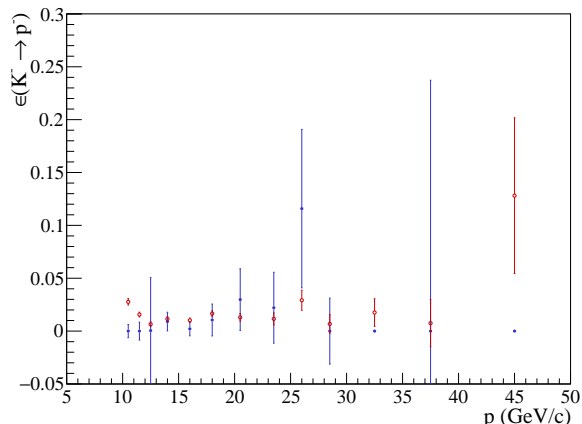
**Figure 37:** Comparison of the probability to identify negatively charged kaons with angles between 0.01 and 0.04 rad.



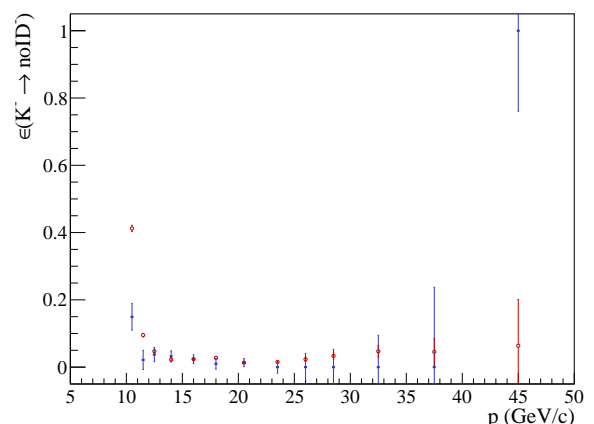
(a) *Pion*



(b) *Kaon*

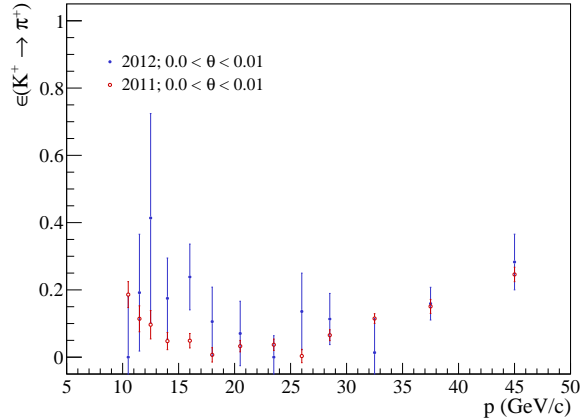


(c) *Proton*

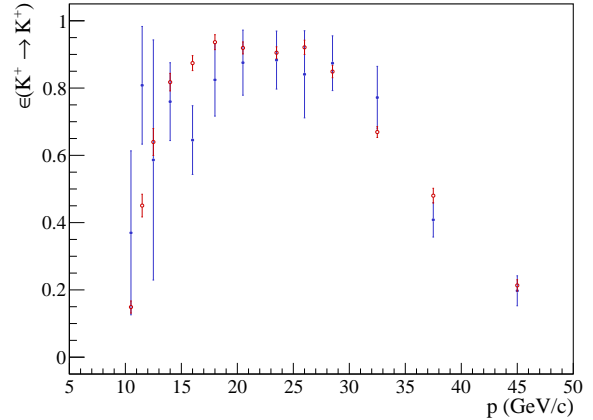


(d) *No identification*

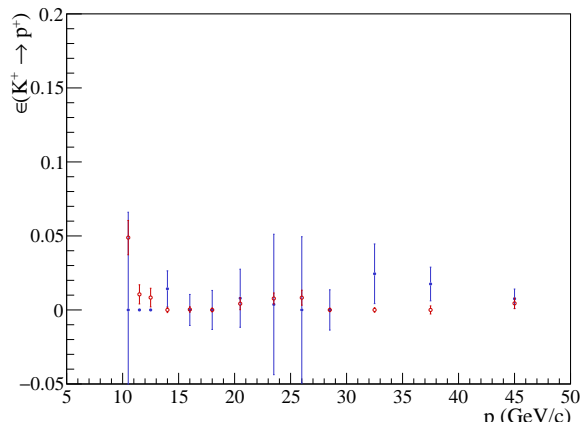
**Figure 38:** Comparison of the probability to identify negatively charged kaons with angles between 0.04 and 0.12 rad.



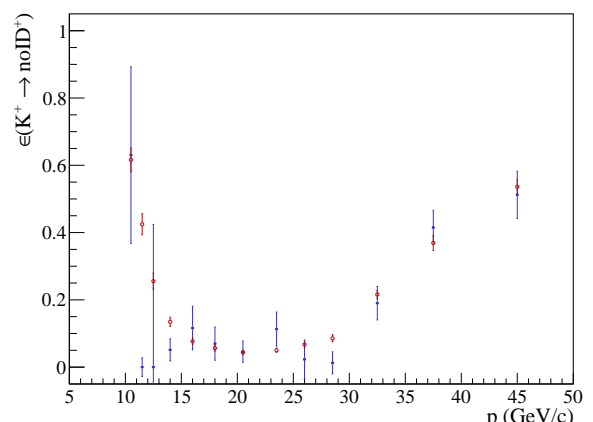
(a) *Pion*



(b) *Kaon*



(c) *Proton*



(d) *No identification*

**Figure 39:** Comparison of the probability to identify positively charged kaons with angles between 0.0 and 0.01 rad.

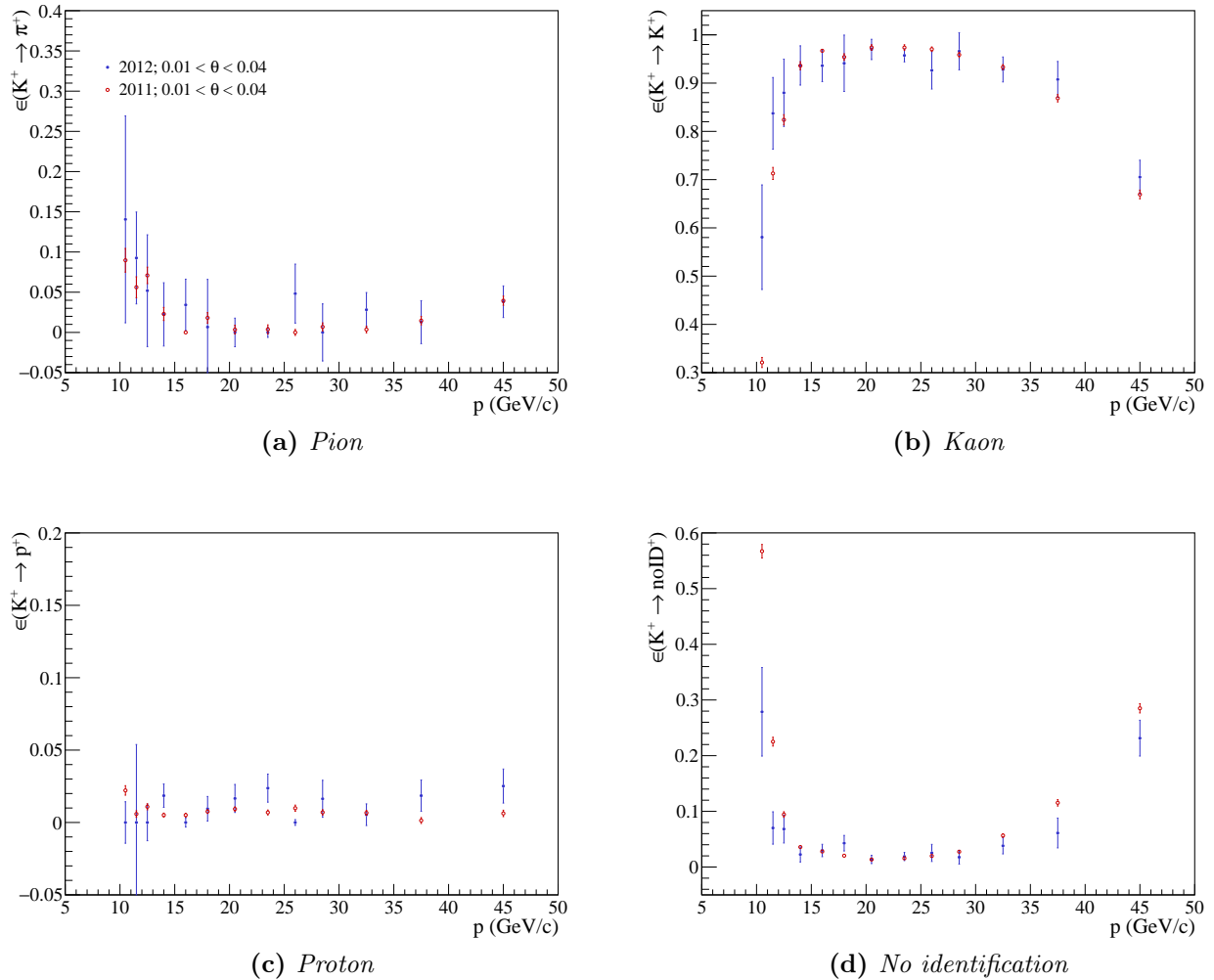
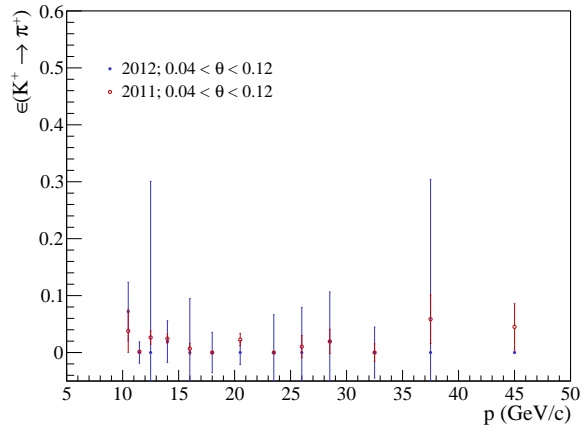
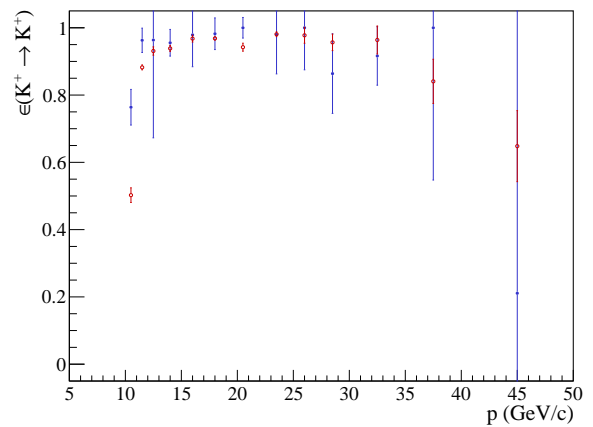


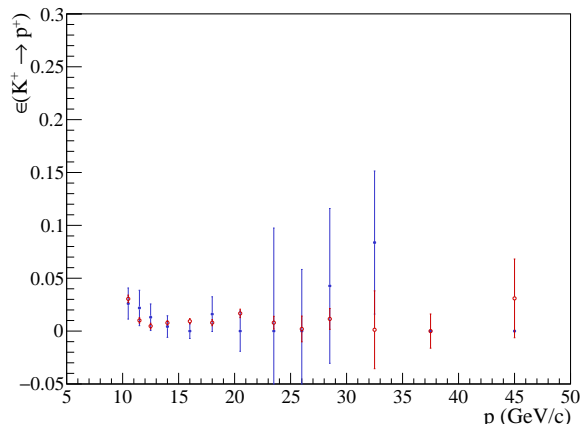
**Figure 40:** Comparison of the probability to identify positively charged kaons with angles between 0.01 and 0.04 rad.



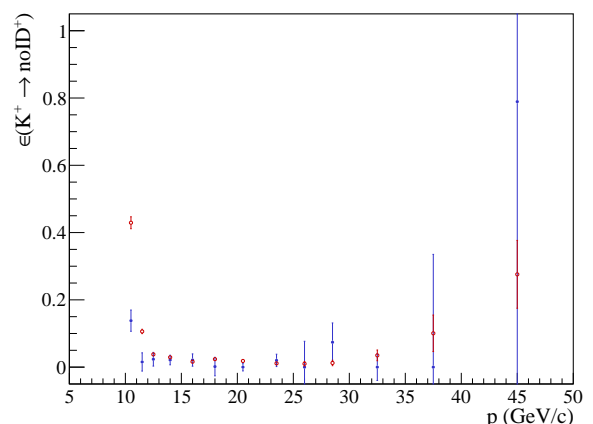
(a) *Pion*



(b) *Kaon*



(c) *Proton*



(d) *No identification*

**Figure 41:** Comparison of the probability to identify positively charged kaons with angles between 0.04 and 0.12 rad.

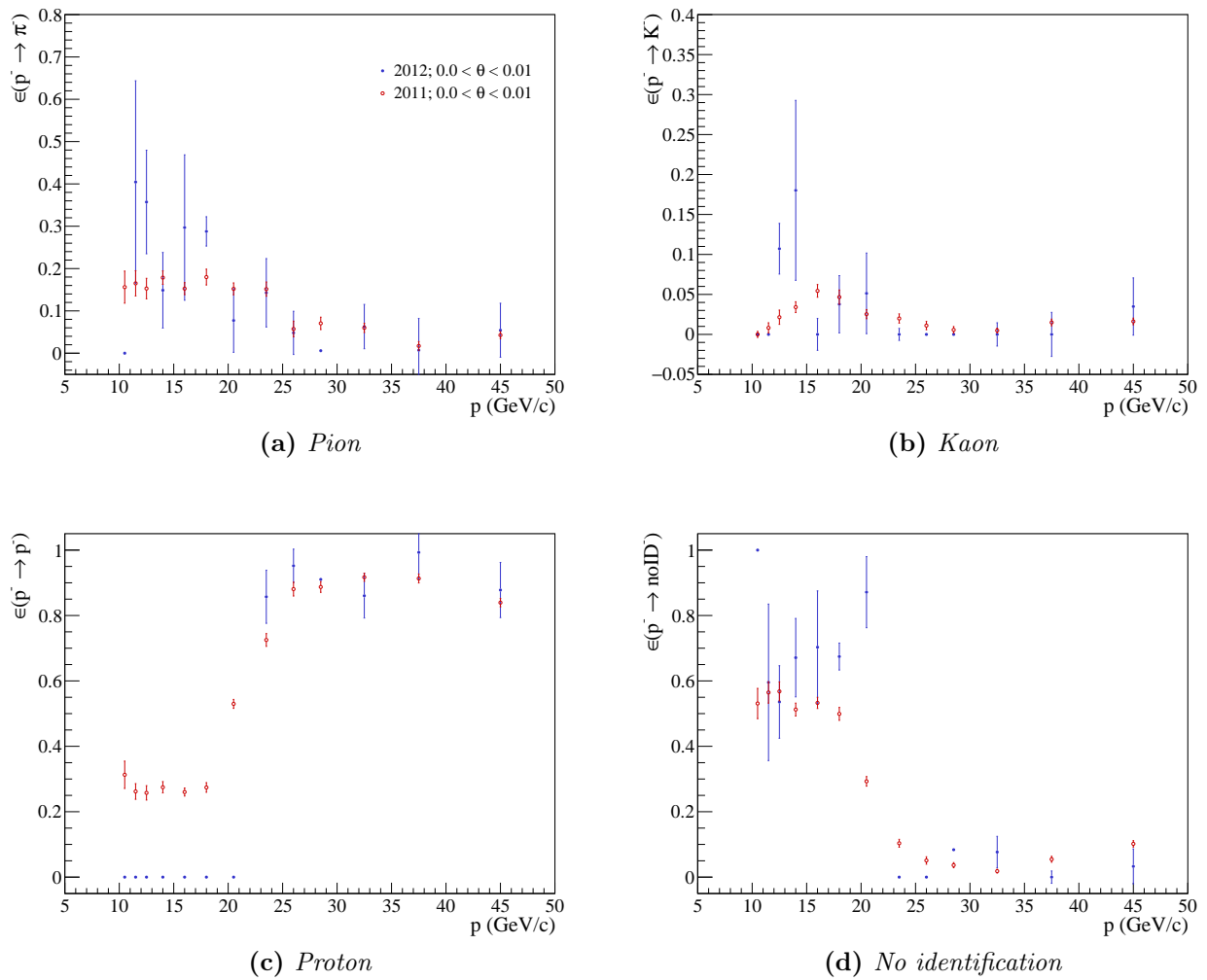
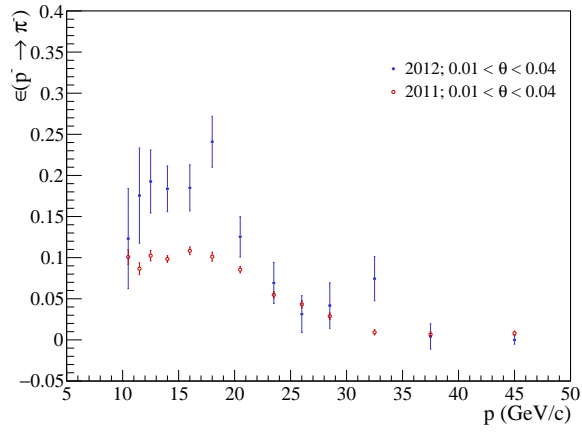
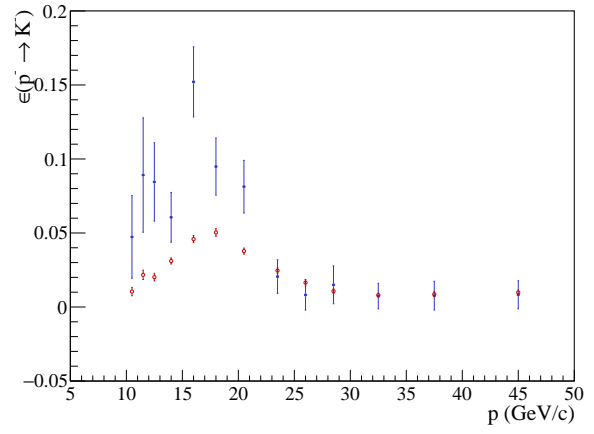


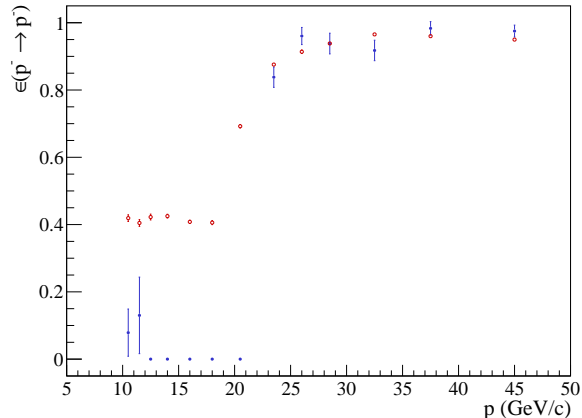
**Figure 42:** Comparison of the probability to identify antiprotons with angles between 0.0 and 0.01 rad.



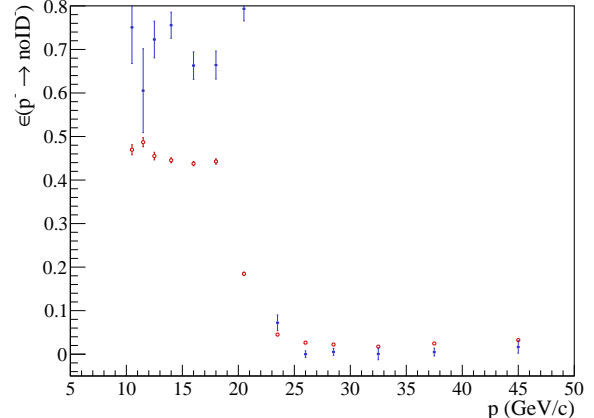
(a) *Pion*



(b) *Kaon*

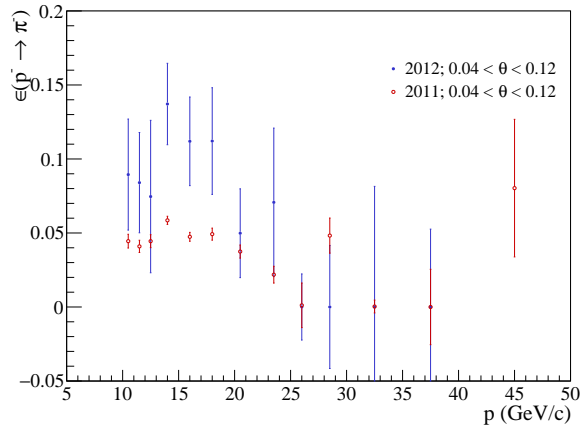


(c) *Proton*

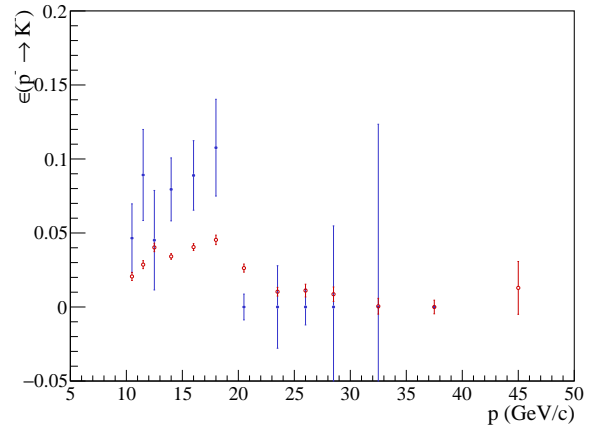


(d) *No identification*

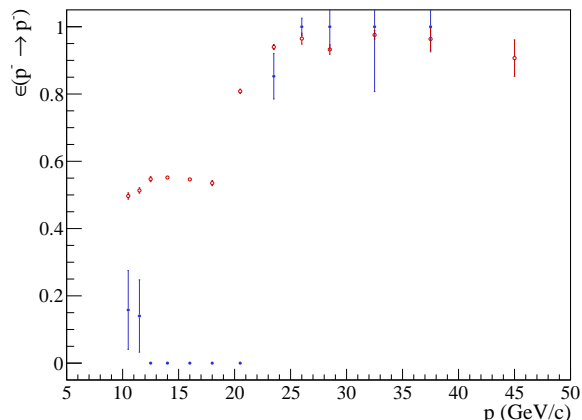
**Figure 43:** Comparison of the probability to identify antiprotons with angles between 0.01 and 0.04 rad.



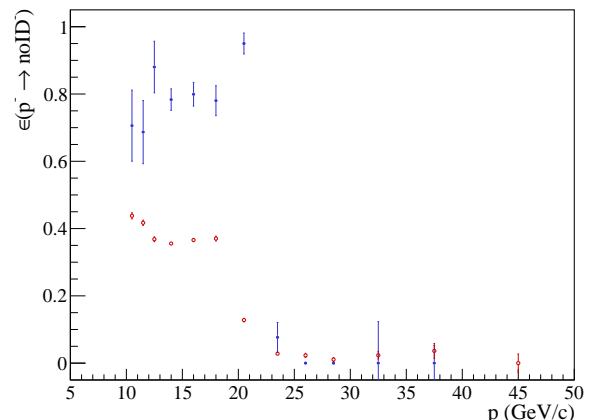
(a) *Pion*



(b) *Kaon*



(c) *Proton*



(d) *No identification*

**Figure 44:** Comparison of the probability to identify antiprotons with angles between 0.04 and 0.12 rad.

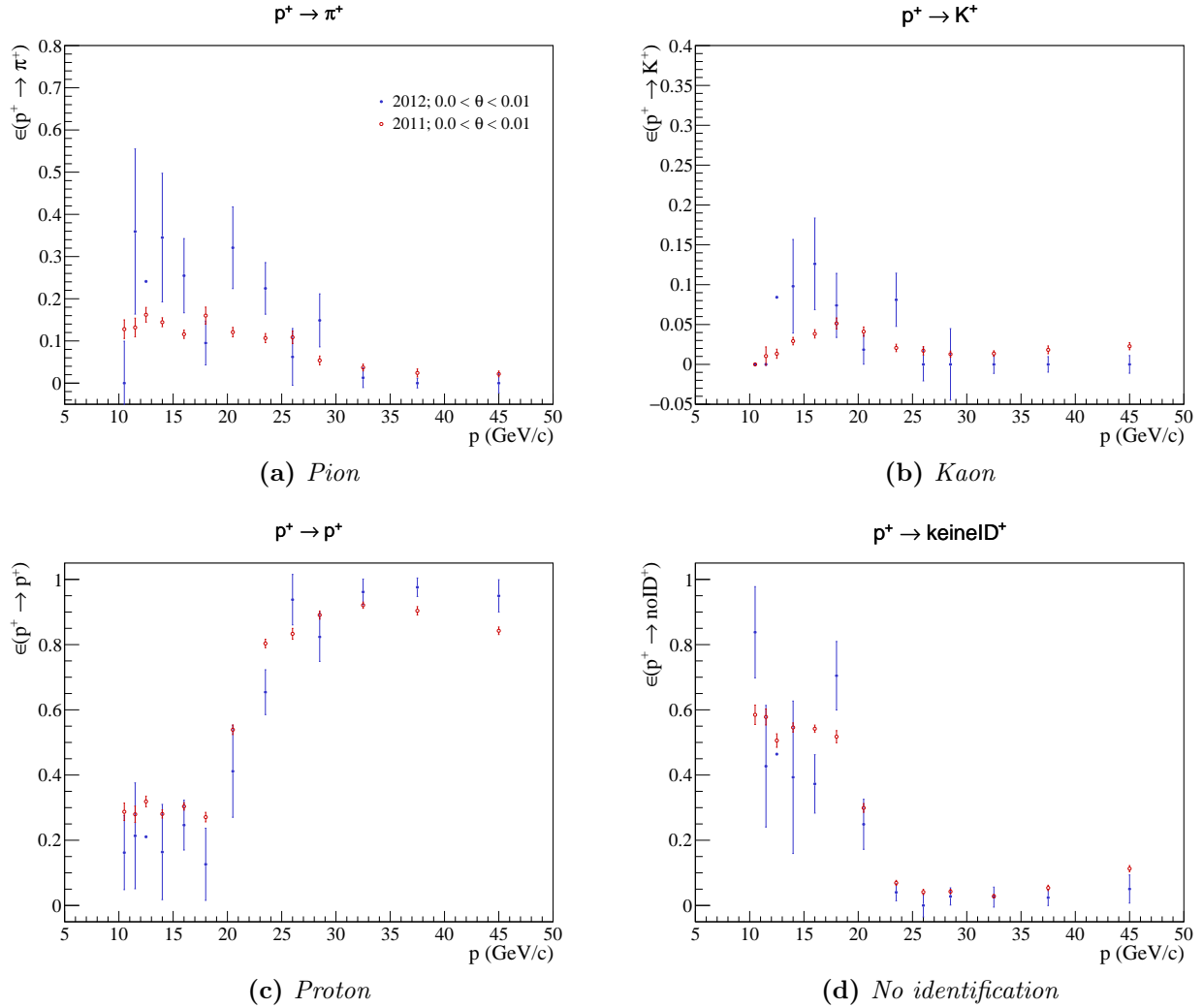


**Figure 45:** Comparison of the probability to identify protons with angles between 0.0 and 0.01 rad.

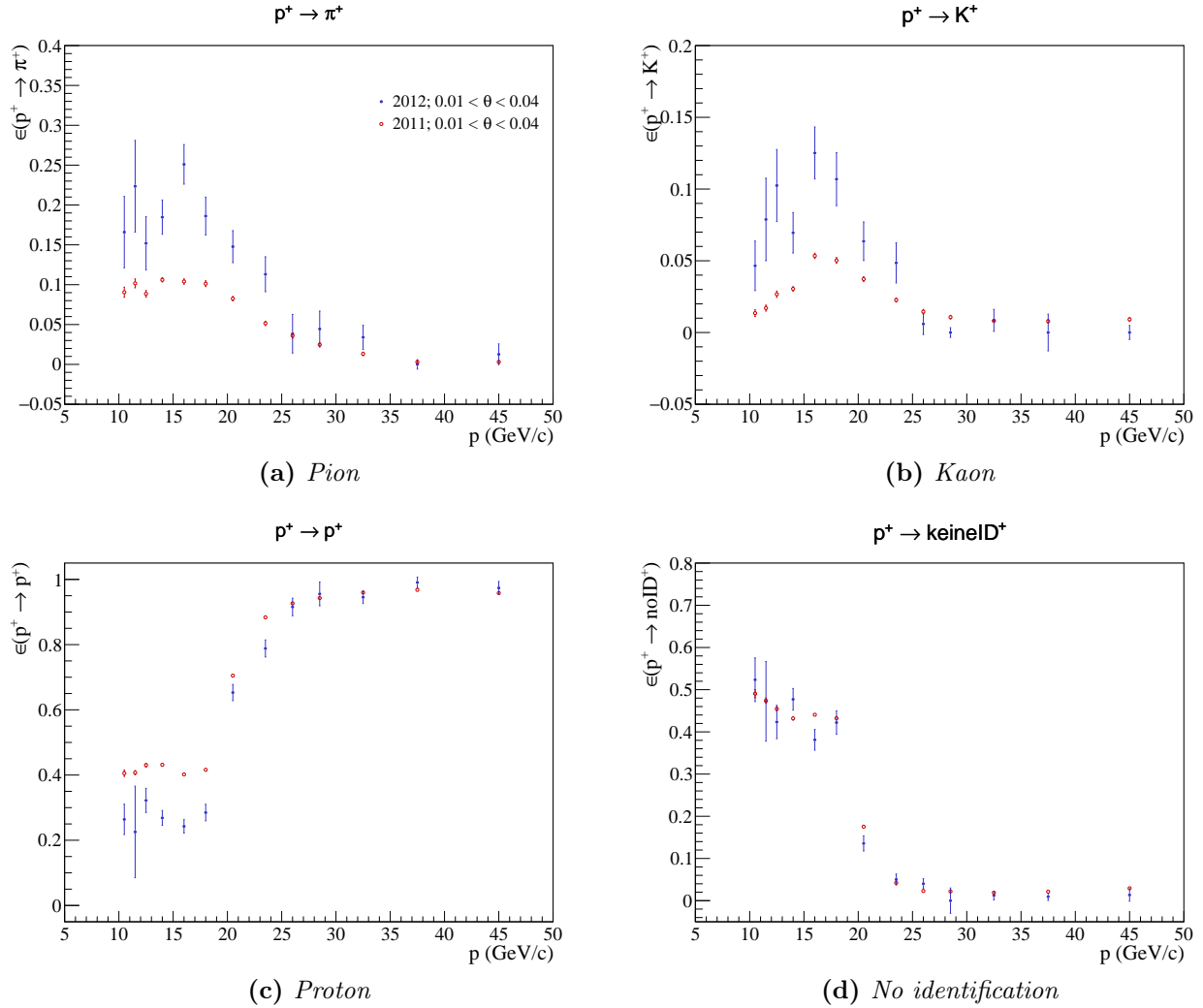


**Figure 46:** Comparison of the probability to identify protons with angles between 0.01 and 0.04 rad.

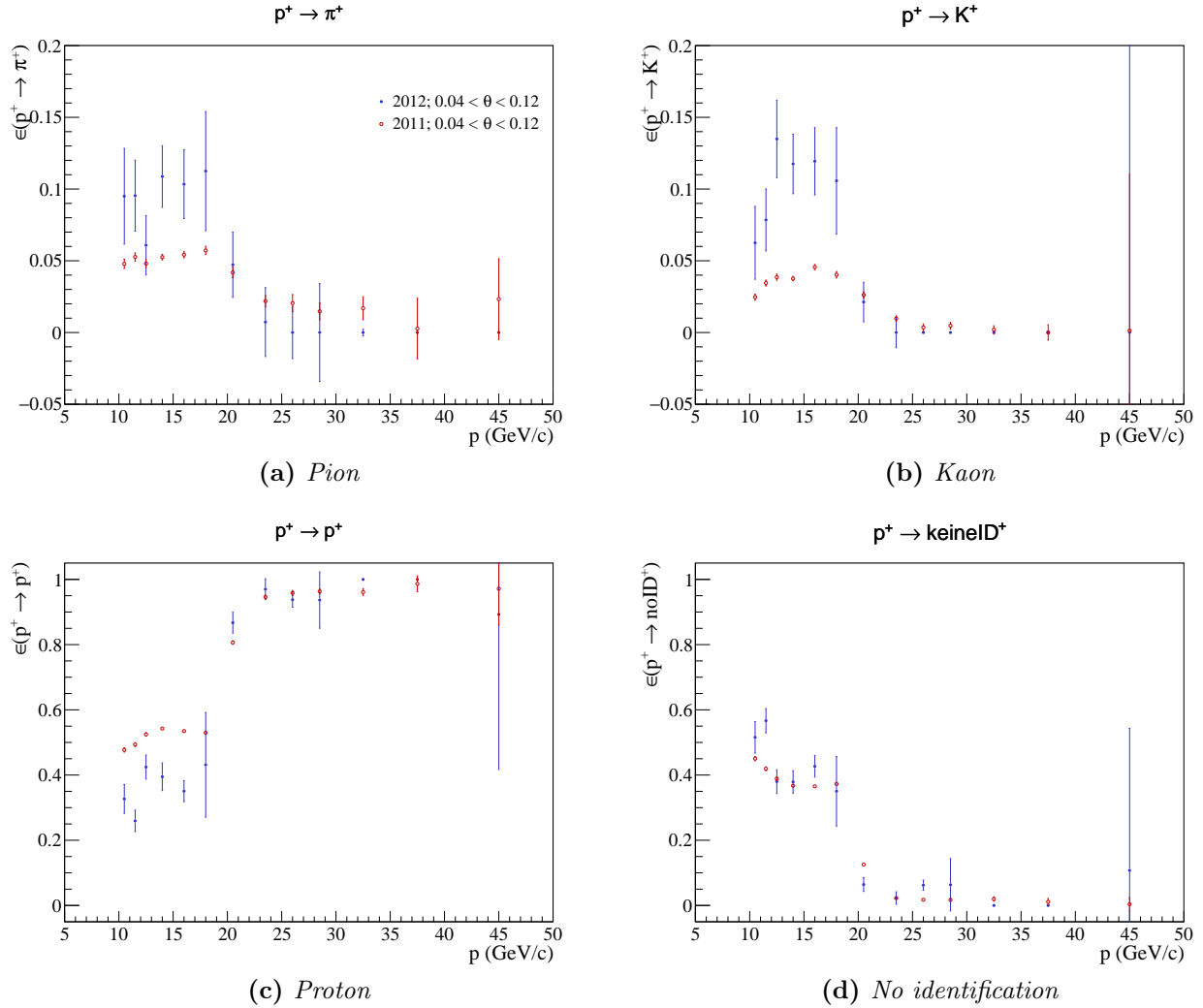


**Figure 47:** Comparison of the probability to identify protons with angles between 0.04 and 0.12 rad.